Monitoring the impact of droughts on vegetation in Australia using MetOp ASCAT Dynamic Vegetation Parameters

B.J. Walraven

Civil Engineering and Geosciences

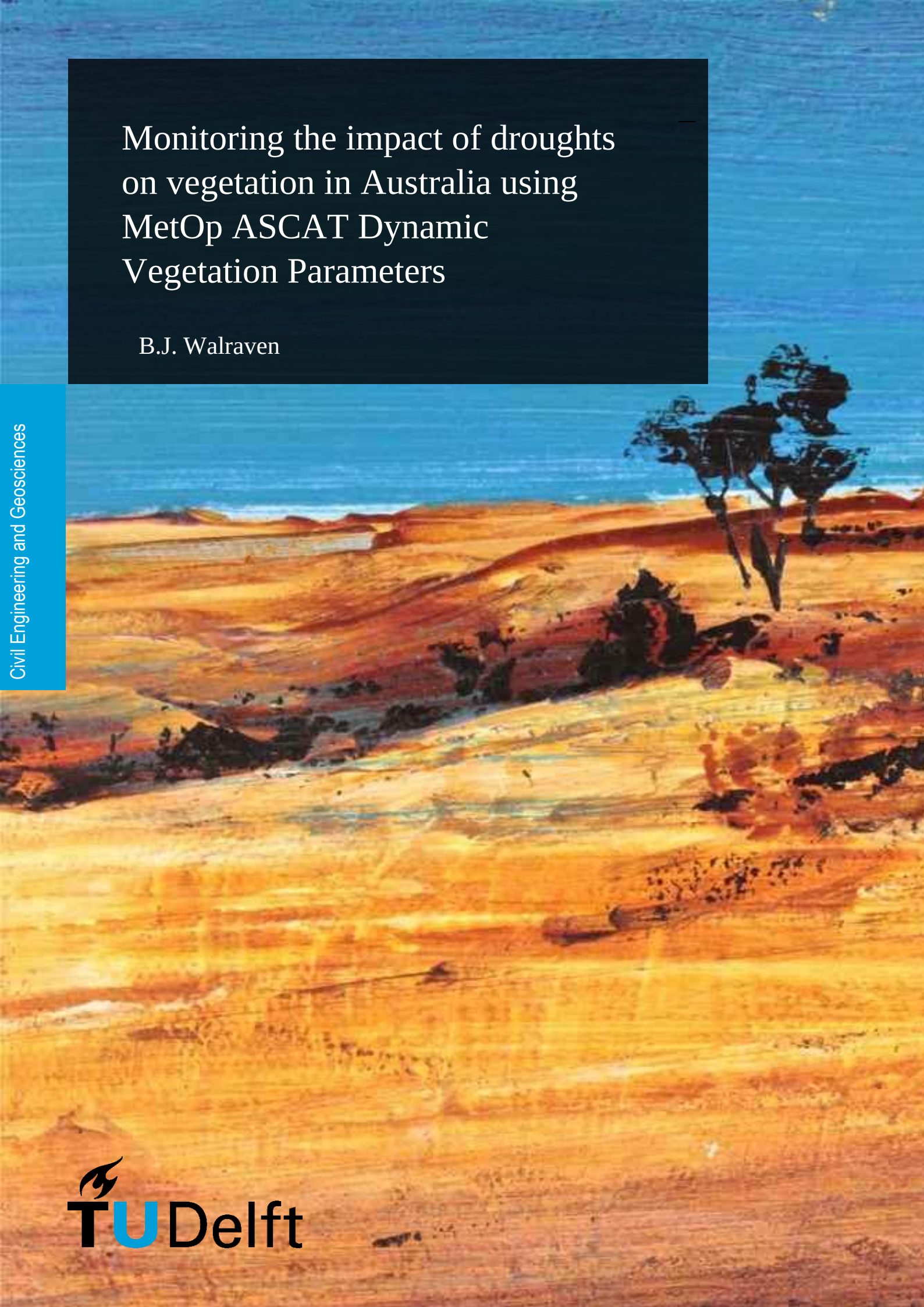

TU Delft

Monitoring the impact of droughts on vegetation in Australia using MetOp ASCAT Dynamic Vegetation Parameters

by

B. J. Walraven

to obtain the degree of Master of Science
at the Faculty of Civil Engineering & Geosciences,
Delft University of Technology

Date:	February 16, 2021	
Student number:	4165438	
Thesis committee:	Prof. Dr. ir. S. (Susan) Steele-Dunne,	TU Delft, chair
	Dr. M. (Markus) Hrachowitz,	TU Delft
	Dr. S. L. M. (Stef) Lhermitte,	TU Delft

Cover page: Debi Riley. Outback Landscape Acrylics Cobalt Sky
https://debiriley.com/2015/03/04/acrylics-cobalt-sky-landscape/

TU Delft

Abstract

Droughts are considered to be one of the most damaging, yet least understood, natural hazards of all. Despite their prevalence, a thorough understanding of them lacks because they are such complex phenomena, and their manifestation can differ depending on the region they occur in. Monitoring hydrological variables and processes is imperative for a good understanding of how droughts develop and persist.

Backscatter from ASCAT and previous scatterometers has long been used for soil moisture retrieval. The first and second order derivative, slope and curvature respectively, of the backscatter - incidence angle relation in the TU Wien Soil Moisture Retrieval algorithm are used to correct for vegetation effects. Recently, new developments to this algorithm have allowed to account for interannual variations in the slope and curvature. This has given rise to the potential of monitoring vegetation directly with slope and curvature, rather than only using it to correct for vegetation effects in soil moisture retrieval. The long data record of ASCAT and previous scatterometers combined has the potential to provide valuable information for drought monitoring.

This study investigates if ASCAT could be used as a self-contained dataset in drought monitoring. The spatial variability, the seasonal cycle, and the drought response of backscatter, slope and curvature across different vegetation types in Australia is assessed. Simulated surface- and root zone soil moisture, LAI and GPP from the land surface model ISBA are used to aid in the interpretation of the ASCAT signal.

The results from this study show that backscatter, slope and curvature can adequately capture vegetation dynamics in times of drought across dry semi-arid grasslands and croplands. Over these regions the soil moisture and vegetation anomalies observed with ASCAT and simulated in ISBA correspond well. Considerable information into the vegetatin dynamics can be gained from analyzing the backscatter - incidence angle relationship. Especially the ability to monitor drought in crops with a coarse spatial resolution is promising for future applications.

It proved more difficult to accurately capture the propagation from a soil moisture anomaly into vegetation anomaly across forests and mixed vegetation with grasses and trees. The first reason for this is the increased attenuation of the signal by vegetation, which hampers accurate measurements of soil moisture content. The second reason is that it is more difficult to separate the soil moisture and vegetation effects due to the fact that less is known about the scattering mechanisms induced by vegetation structure and moisture distribution.

Overall the results support earlier findings the slope can be used as a measure of vegetation wet biomass and confirm that curvature is also a valuable source of information that gives insight into the relative contribution from surface or volumetric scattering to total backscatter. These relations have been shown to also adequately describe vegetation dynamics in times of drought.

Acknowledgements

This thesis marks the end of my time as a student of the water management department here at TU Delft. It was through my bachelor's thesis that my interest for hydrology expanded. The kind people that roam the 4th floor and the strong emphasis on research in this field of study have led me to discover and enjoy working on topics ranging from hill slope hydrology to modelling polders. All for which I am very grateful.
What was still missing from that list was remote sensing. Throughout this thesis I have thoroughly enjoyed diving into the science of droughts and vegetation monitoring with radar, so much so that I would consider pursuing a career in it. I have a couple of people to thank for that.

First of all I would like to thank Susan for introducing me to remote sensing and making me part of the select group that gets excited when they hear the words slope or curvature. Your knowledge and enthusiasm for the topic are contagious. To Stef and Markus I am thankful for their guidance and refreshing questions that led me to think outside the box.

A special thanks to my parents for their support in many different ways, their patience, and their words of encouragement. Mom, I know, I can't give it more than my best. Thanks also to the two not so anonymous reviewers Floor and Jansen, you have improved the readability of this report. Finally a huge thank you to my wife Roos who's support was vital, literally, in these last few months. Babe, you're the best.

B. J. Walraven
Delft, February 2021

Le savant n'étudie pas la nature parce que cela est utile; il l'étudie parce qu'il y prend plaisir et il y prend plaisir parce qu'elle est belle.
- Henri Poincaré

Contents

List of Figures

List of Symbols and abbreviations

Symbols

σ^o	Backscatter coefficient	[dB]
σ^o_{40}	Normalized backscatter at 40°	[dB]
σ'	Slope	[dB/deg]
σ''	Curvature	[dB/deg^2]
θ	Incidence angle	[deg]

Abbreviations

ASCAT	Advanced Scatterometer
BOM	Australian Bureau of Meteorology
DOY	Day of year
DVP	Dynamic vegetation parameters
ESCAT	European Remote Sensing (ERS) Scatterometer
EUMETSAT	European Organisation for the Exploitation of Meteorological Satellites
GPI	Grid point index on WARP5 grid
GPP	Gross Primary Production
ISBA	Land surface model Interaction-Sol-Biosphère-Atmosphère from Météo France
LAI	Leaf Area Index
MetOp	Meteorological Operational satellite
RD	Rainfall Deciles
ROI	Region of Interest
rzsm	Root zone soil moisture
ssm	Surface soil moisture
SWI	Soil Water Index
SH	Southern Hemisphere
TUW SMR	TU Wien Soil Moisture Retrieval Algorithm

1 Introduction

Droughts are considered to be one of the most damaging, yet least understood, natural hazards of all (Wilhite, 2000). Unlike other natural hazards droughts are characterised by a slow and creeping onset, extensive duration, and often far-reaching geographical extent. Moreover, damage done by droughts accumulates slowly over a considerable amount of time, and may even linger far past the end of the drought (Wilhite, 2000). This causes droughts to have profound impacts on the environment, society, and the economy, with secondary 'spinoff' effects further increasing their impact (Sheffield and Wood, 2011; Wood et al., 2015).

This is especially the case for Australia where droughts are a natural and recurrent climate feature (Kiem et al., 2016). The fairly recent 'Millenium Drought' lasted from the late 1990's to mid-2010 and heavily impacted Australia's most populous and important agricultural region. At its worst the drought lead to an estimated drop of A$7.4 billion in agricultural production in a year, good for more than 1.6% of Australia's GDP (Heberger, 2012). The droughts in Australia often also contribute to the occurrence of bushfires with the recent 2019 Black Summer fires as one of the worst in history. More than 17 million ha of land burned, destroying over 3000 houses and costing the lives of 33 people, as well as affecting the public health through intense air pollution (Richards et al., 2020).

Droughts are, however, not limited to regions with a similar climate to Australia, but can occur virtually anywhere. They are a natural climate feature which makes their recurrence inevitable (Wilhite, 2000). Despite the fact that droughts are so prevalent, a thorough understanding of them lacks because they are such complex phenomena, and their characteristics make it difficult to monitor them accurately.

1.1. Drought monitoring

Monitoring of hydrological variables and processes is imperative for a good understanding of how droughts develop and persist (Crocetti et al., 2020; Tallaksen and Van Lanen, 2004). Traditionally observations have relied on site-based measurements, but these are scarce over the large spatial scales that are of interest for drought monitoring and analysis (Sheffield and Wood, 2011). For this reason research has often favored the use of land surface models forced by climate observations, since these are generally more available than variables of the terrestrial hydrological cycle (Sheffield et al., 2009). Many soil moisture drought indices are in fact based on estimated values from climatic variables or hydrological modelling (Carrão et al., 2016). In their review of drought indices Keyantash and Dracup (2002) even found the computed soil moisture from a model that performs a water balance assessment over the soil column, to be superior to other soil moisture drought indices.

However, towards the end of the 20th century a major shift took place, concurrent with advances in remote sensing, from site-based to remote sensing-based indices(West et al., 2019). Together with the evidence that land-atmosphere feedback mechanisms play a large role in the persistence and propagation of droughts, this has made direct observation of vegetation and soil moisture very relevant for drought monitoring (Herrera Estrada et al., 2017).

Even though a drought is often triggered by a precipitation deficit, the direct impacts of a meteorological drought are typically limited (West et al., 2019). Soil moisture is often the first component in the hydrological system to be affected. In general soil moisture is a particularly useful drought indicator because it is roughly an aggregate of the available water from the balance precipitation, evaporation, and runoff (Martínez-Fernández et al., 2015; Sheffield et al., 2009). The top layers of the soil reflect recent precipitation conditions and are highly correlated to meteorological droughts. The root zone soil moisture, on the other hand, is the governing factor of the state of vegetation, and since plant growth is one of the first to be affected by a drought a soil moisture deficit is often a good early indicator of a vegetation anomaly. This makes soil moisture perhaps also the most important variable to monitor since the biggest economic losses, national food security and social stability are related to (a reduction) in crop production (Liu et al., 2016; Tallaksen and Van Lanen, 2004).

The impact of droughts on vegetation health can also be monitored directly. Vegetation water stress is typically assessed using passive multispectral sensors. The most commonly used indices are NDVI, or related indices such as the VHI, NDWI or the EVI (West et al., 2019). These all depend to some extent on photosynthetic activity, vegetation greenness (chlorophyll content) or brightness temperature. The main disadvantage of using these spectral and thermal indices is, however, that these operate at a wavelength that is often hampered by cloud cover, and need sunlight as a natural source of illumination (Jones et al., 2012).

Soil moisture can be successfully retrieved through microwave remote sensing. Microwaves have the advantage to be able to penetrate clouds and operate independent of a natural light source for illumination. Moreover, they are especially suited for measuring soil moisture and vegetation water content due to the dielectric properties of materials in the microwave region of the EM spectrum, which depend largely on water content. Recognizing this potential of microwaves and the key position of soil moisture in global energy distribution, the terrestrial hydrological cycle, as well as its importance in a wide range of applications, SMOS (Soil Moisture and Ocean Salinity) and SMAP (Soil Moisture Active Passive) were launched in 2009 and 2015 respectively (Scipal et al., 2002). These missions, dedicated specifically to the retrieval of soil moisture, measure passively at L-band (0.39 - 1.55 GHz) because the microwave signal is less sensitive to vegetation, and the penetration depth into the soil is larger for longer wavelengths. Though passive microwave measurements can be used for vegetation applications as well, the understanding of vegetation signals in these measurements is weak, such that often a model like the Water Cloud model, or a large set of input parameters is needed to describe vegetation properties (Crocetti et al., 2020; Konings et al., 2019). In addition, these missions often have a coarse spatial resolution, which is not a big problem for drought studies, but their limited data record make it less ideal for drought analysis since a long historical dataset is often needed to form the basis for a calculation of drought indices.

Incidentally the first operational global, near real time, soil moisture product is derived from active C-band scatterometer data (Bartalis et al., 2007). Already soon after the launch of the European Scatterometer (ESCAT) onboard the ERS 1 in 1991, operating at ~5.3 GHz (C-band), it was found that over land the radar backscatter is sensitive to soil moisture, and to some extent to vegetation cover (Frison and Mougin, 1996; Wagner et al., 1999; Woodhouse, 2005). Though in general C-band is seen as sub-optimal for soil moisture retrieval because of its shorter wavelength, scatterometers are originally designed to monitor the speed and direction of ocean winds and can therefore very precisely evaluate σ^o over the surfaces being observed (Frison et al., 2016). This high radiometric accuracy has often been overlooked, but several studies have shown that it allows for sufficiently good soil moisture retrieval compared to L-band instruments (Wagner et al., 2013). Since the launch of ESCAT, its successor, the Advanced Scatterometer (ASCAT) instrument has been launched onboard three different satellites in 2006, 2012, and 2018. Together with ASCAT's planned successor on the METOP Second Generation (SG), set to be launched in 2022, a data record of almost 40 years of backscatter will be available.
The high radiometric accuracy, a temporal resolution of 1-2 days, and the promised data continuity make backscatter from ASCAT ideal for monitoring soil moisture. The current product is used in amongst others the ESA Climate Change Initiave (ESA CCI), and has proven its worth in drought monitoring in multiple studies, either directly or derived as the Soil Water Index (SWI) (Baik et al., 2019; Gouveia et al., 2009). Schroeder et al. (2016) also showed the ability to monitor droughts directly with backscatter by showing consistent spatial and temporal patterns between $\sigma^o{}_{54}$ anomalies

and the U.S. Drought Monitor.

1.2. Dynamic vegetation parameters

The algorithm used to retrieve soil moisture from ASCAT backscatter was developed at TU Wien and is based on a change detection method, which essentially consists of subtracting a reference image, based on a vegetated land surface under dry soil conditions, from the actual backscatter image (Naeimi et al., 2009; Wagner et al., 2007). At the hart of this algorithm is the relationship between backscatter σ^o and incidence angle θ . To account for vegetation effects the multi-incidence angle looking capabilities of ASCAT are exploited. The incidence angle behaviour of σ^o depends on whether volume scattering from vegetation or surface scattering from the soil dominates the total backscatter (Steele-Dunne et al., 2019). The slope (σ') and the curvature (σ'') of the function σ^o (θ) are the so-called 'vegetation parameters' because they are sensitive to vegetation dynamics and surface structure, and as such are used to account for soil and vegetation effects when retrieving soil moisture (Naeimi et al., 2009).
Until recently, to account for noise effects in the measurements, a large number of backscatter observations had to be averaged to ensure robust calculations of $\sigma'$and σ''. Hence, only climatological values of $\sigma'$and σ''were available. However, with twice the number of fan-beam antennas on ASCAT compared to the ERS scatterometer, the data density of observations has increased significantly. This has led to dynamic calculations of $\sigma'$and σ''using a kernel smoother, and hence has allowed to account for interannual variability (Vreugdenhil et al., 2016).

1.3. Recent developments

In light of these new developments, Steele-Dunne et al. (2019) proposed to use the slope and curvature as a source of information about vegetation, rather than to see it as a hindrance in soil moisture retrieval. Steele-Dunne et al. (2019) examined this approach for North American Grasslands and found that the scattering mechanisms are influenced by total vegetation water content, vertical distribution of water within vegetation, and the geometry of the vegetation. More specifically, the slope appeared to be related to vegetation density, or wet biomass, and the curvature to the dominant scattering mechanism related to the vegetation structure. They also found clear seasonal variations, and that soil moisture anomalies resulted in lagged slope and curvature anomalies, suggesting that these dynamic vegetation parameters could be potentially useful in detecting water stress. Petchiappan (2019) built on this and showed that variations in slope and curvature match different land cover types in the Amazon, and that water stress could be observed in the form of negative anomalies, corresponding to recorded drought years. Another study by Pfeil et al. (2020) demonstrated good agreement between the slope signal and the phenology in deciduous broadleaved forest. The peak in slope corresponded with the maximum woody water content, and preceded the increase in leaf area index.

These recent studies have highlighted the possibility of using the dynamic vegetation parameters as a new means of gaining insights into the vegetation water dynamics. This study sets out to further explore the behaviour of slope and curvature, specifically in times of drought, or water stress.

1.4. Research objective

The aim of this research is to assess whether ASCAT can be used to monitor the propagation of a drought from a soil moisture anomaly into a vegetation anomaly.
ASCAT has already proven its worth in soil moisture retrieval and drought assessment, though disentangling vegetation effects from backscatter remains a challenge. A condition for successful retrieval algorithms is that the relationship between measurements and the soil and vegetation is well understood (Mattia et al., 2003). This study focuses more on the dynamic vegetation parameters to determine if these can also adequately capture the vegetation water dynamics in times of droughts.

If ASCAT, as a self-contained dataset, can be used to evaluate both the root causes (i.e. a soil moisture deficit) and the symptoms (a vegetation anomaly) without the need for ancillary datasets or scattering models, this could greatly benefit drought monitoring. Moreover, the long data record could contribute significantly to research into drought onset and persistence.

In a more general sense this study also serves to gain more insight into which physical parameters most strongly influence the dynamic vegetation parameters. At the same time it serves to reinforce the current hypothesis regarding slope and curvature, as there have only been a very limited number of studies on these dynamic vegetation parameters so far.

With these objectives in mind the main research question formulated is:

Can ASCAT be used as a self-contained dataset in drought monitoring?

To adequately analyse the response of ASCAT parameters to droughts, it is necessary to first get a general idea of the distribution of backscatter, slope and curvature across Australia. Subsequently a more indepth understanding of the seasonal cycle across the dominant vegetation types has to be gained, after which it can be assessed how the response of ASCAT parameters change in times of drought. Hence, the following sub questions are investigated to build up to the main conclusions:

1. How does the spatial variability in backscatter, slope and curvature relate to climate and land surface features across Australia?
2. What is the influence of different vegetation types on the seasonal cycle of ASCAT parameters?
3. What is the response of ASCAT parameters to droughts across different vegetation types?

As a reference, to aid in the interpretation of the backscatter, slope and curvature, the land surface model ISBA (Interaction Sol-Biosphère-Atmosphère) from Météo France is used. This model provides surface- and root zone soil moisture, as well as LAI and GPP and serves as a proxy to compare the backscatter and dynamic vegetation parameters with. The droughts in this study are defined based on the root zone soil moisture from ISBA. It may be important to note that the focus of this study is not on identifying droughts, or finding the best drought index. Rather, it looks at the possibility of using a novel data set to monitor vegetation water stress directly, day and night, without the need for ancillary datasets or models.

The choice for Australia as the study site is made in light of previous research on dynamic vegetation parameters. Steele-Dunne et al. (2019) studied grasslands in North America, which exhibit very high seasonal variability. Petchiappan (2019) studied the Amazon rain forest, which has extremely low seasonal variability. Australia is a home to a number of different climate regimes, and as a consequence holds many different land cover types. This allows to confirm the conclusions made for grasslands and forests and extend these to other vegetation types. Moreover, environmental and hydrological data is generally widely available and well documented in Australia, which may be useful in the interpretation of ASCAT data.

1.5. Thesis outline

Chapter 2 gives a brief theoretical overview, which is by far not exhaustive, but should make the reader familiar with the important concepts underlying this study. It covers the threshold level method used to identify drought periods in the root zone soil moisture, and elaborates further on the TU Wien Soil Moisture Retrieval algorithm and the dynamic vegetation parameters.

Chapter 3 provides more information on the datasets used, and describes the study area and the regions of interest in more depth. It also explains the choices that were made in applying the threshold level method.

Chapter 4 visualizes the results. First the seasonal climatologies of the regions of interest are interpreted, then the full time series are shown to analyze the response of backscatter and the dynamic vegetation parameters amidst drought events.

Chapter 5 discusses the results and reflects on them in light of the current developments in monitoring vegetation with backscatter from ASCAT. The conclusions and the implications of this study are given in chapter 6.

2

Theoretical overview

This chapter provides a brief theoretical background to the two main topics explored in subsequent chapters; droughts and scatterometers, specifically ASCAT. If the reader is familiar with the concept of drought, how it is defined, and how it is quantified, section 2.1 can be skipped, though section 2.1.3 elaborates on the theory of the threshold level method used to identify drought events in this study. Section 2.2 is particularly interesting because it discusses the relatively novel TU Wien Soil Moisture Retrieval algorithm and the recent developments concerning the dynamic vegetation parameters, which forms the core of this study.

2.1. Droughts

2.1.1. Defining a drought

One of the major obstacles in drought studies lies in its definition. On the one hand the lack of a universally accepted definition, reflected in the wide range of variables used to describe a drought, can lead to multiple, even contradicting, conclusions. On the other hand there is actually a need for different definitions because a drought impacts so many different sectors in society and can manifest itself differently depending on where in the hydrological system it occurs (Sheffield et al., 2004; Wilhite, 2000). Thus, any definition given will depend on both the objectives of the study, and the nature of the water deficit (Van Loon, 2015). In general terms though, a drought can be defined as "a sustained and regionally extensive deficit of water compared to normal conditions, often with reference to a specific demand" (Tallaksen and Van Lanen, 2004).

Commonly, droughts are classified into three categories based on their disciplinary perspective, which also reflect the hydrological variable used to quantify the drought (Hisdal and Tallaksen, 2000).

- Meteorological drought: refers to a precipitation deficiency over an extensive area, generally for a period of months to years. It can be accompanied by above average temperatures, leading to increased evaporation, and is often the cause of other types of drought.
- Soil moisture drought: is a deficit in soil moisture, predominantly in the root zone, essentially reducing the amount of water available to vegetation. This leads to reduced plant growth and crop production, which in turn can be a local feedback that enhances anomalies in land-atmospheric processes, thus further affecting the drought. When the focus is specifically on cultivated crops, as opposed to natural vegetation, the term agricultural drought is often used.
- Hydrological drought: refers to negative anomalies in surface and subsurface flow, often triggered by a precipitation, or soil moisture, anomaly. A hydrological drought could also be the trigger to a soil moisture drought, depending on the regions characteristics. It often develops more slowly due to the fact that it involves storage in, amongst others, rivers, lakes, reservoirs, or aquifers (Dai, 2011; Van Loon, 2015).

A fourth type, the socio-economic drought, is often also included. However, unlike the three 'envi-

ronmental droughts' it is rather a measure of failure of the water resources to meet the specific water demands of a socio-economic system (Liu et al., 2016).

It may be important to note that a drought is not the same as aridity. Although an arid region, such as large parts of Australia, characterized by extremely low rainfall, may be more susceptible to droughts because it depends on only a few precipitation events, it still represents a (relatively) permanent condition. A drought on the other hand is always a temporary abberation, though perhaps a long lasting one (Wilhite, 2000).

2.1.2. Drought propagation

The different types of drought roughly follow the propagation of a water deficit through the terrestrial part of the hydrological system (Sheffield and Wood, 2011). The onset of a drought is frequently a result of prolonged precipitation deficiency, possibly in combination with higher temperatures. Although the exact science concerning the onset of a drought is still unclear, it is widely accepted that droughts are caused by extremes in climate due to random variability of atmospheric circulation patterns such as El Niño Southern Oscillation (ENSO), the Indian Ocean Dipole (IOD), and the Southern Annular Mode (SAM) (Dai, 2011; Herrera Estrada et al., 2017). Though most droughts are triggered by a rainfall deficit, compared to other types of droughts a meteorological drought has relatively few direct impacts (West et al., 2019). It is, however, often an early indicator of more impactful events.

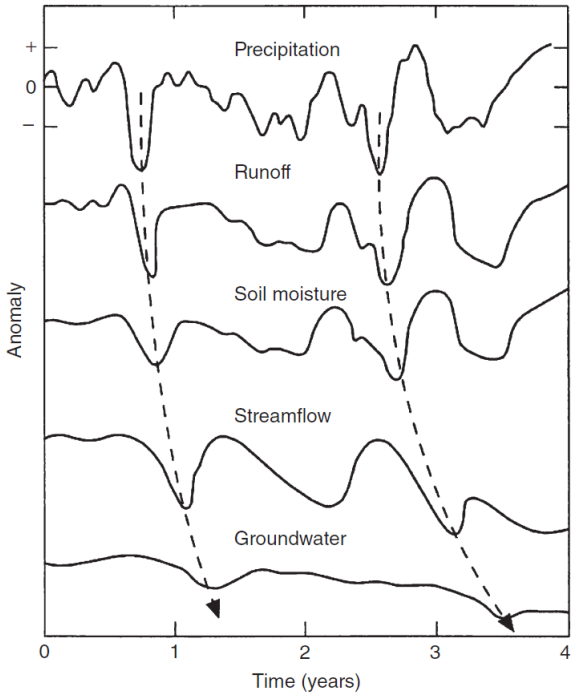

Figure 2.1: Propagation of precipitation anomaly through the terrestrial part of the hydrological cycle (from Van Loon (2015))

As the drought propagates through the hydrological system the drought signal is often delayed and smoothed (see fig. 2.1. It can take months to years, or the drought signal may even be completely attenuated, before it registers in the groundwater (Sheffield and Wood, 2011). However, the recovery from a drought is dictated by the same principles and will also take longer further down the hydrological system (Van Loon, 2015). The speed of propagation and drought recovery is largely dependent on regional characteristics, the capacity of the catchment to store water, and antecedent conditions.

Local land-atmosphere feedbacks can cause droughts to persist for a prolonged period of time (Herrera Estrada et al., 2017). When this happens the precipitation anomaly may propagate into a soil moisture anomaly. Initially evaporation and transpiration from bare soil and plants will increase, partially due to the frequently high temperatures associated with a meteorological drought. If this

situation perseveres and soil moisture levels become too low, a vegetation anomaly will ensue and plants may, depending on their drought coping strategy, whither and die (Sheffield and Wood, 2011). This limits further evaporation and could also limit locally generated precipitation, further reinforcing the drought condition. A hydrological drought may subsequently follow if the soil moisture no longer drains to the groundwater causing reduced streamflow, and runoff is also reduced due to a precipitation deficit (Van Loon, 2015). It is, however, good to remember that even though these drought categories are often studied separately for practical reasons, they are not physically isolated but actually intimately linked (Dracup et al., 1980).
In this study, the primary focus is on soil moisture droughts and the propagation into a vegetation anomaly, because these are the variables that can be monitored with ASCAT.

2.1.3. Quantifying droughts

A drought can occur virtually anywhere around the world but the way it manifests itself can vary strongly depending on the climatic region it occurs in (Dracup et al., 1980). To adequately be able to compare droughts across space and time essential drought characteristics such as duration, magnitude (i.e. the maximum deviation from normal during a drought event), severity (cumulative deficit during the entire drought) and spatial extent, have to be identified (Sheffield and Wood, 2011).

The most common way to express drought characteristics numerically is through indices (Mishra and Singh, 2010). The advantage of standardized drought indices lies in the opportunity to compare droughts across space and time. Like drought definitions, there exist a vast number of indices to quantify droughts. The purpose of monitoring largely defines which index is used and all have their advantages and disadvantages (Heim, 2002; Keyantash and Dracup, 2002; Wanders, 2010). However, the amount of drought indices also highlights the complexity of droughts, and the inability of a single index to adequately capture all the aspects impacted by a drought (Heim, 2002). Moreover, drought indices generally only describe one type of drought, like rainfall deciles (RD) used by the Australian Bureau Of Meteorology (BOM) (Hisdal and Tallaksen, 2000). Standardized drought indices are often also not directly based on the time series of the drought variable but rather on a distribution fitted to the data (e.g. the Standard Precipitation Index, SPI), or on a water balance computation (e.g. Palmer Drought Severity Index, PDSI) (Van Loon, 2015).

Threshold level method

In this study preference is given to the threshold level method. The main advantage of this method is that it stays close to the actual time series and is ideal for monitoring drought propagation through the terrestrial hydrological cycle. This section covers the theoretical concepts of the threshold level approach, largely based on the work of van Loon (2013). Chapter 3.3.3 elaborates on the subjective choices that have to be made to quantify the exact drought characteristics in this study.

In the threshold level method a site is considered to be in drought if the variable measured is below a predefined threshold. The drought ends once the threshold is exceeded again (Van Loon, 2015; Yevjevich, 1969). Each drought event can then be characterised by its duration or some measure of severity (see fig. 2.2) (van Loon, 2013). The transparency with which drought characteristics can be identified allows for easy comparison with other (hydrological) variables. The method was originally intended, and is primarily used, for hydrological droughts, but has also been applied to soil moisture (Borgomeo et al., 2015; Sheffield et al., 2009; van Loon, 2013). Even though for state variables like soil moisture the severity (area under the curve) of a drought is physically meaningless, it still gives a good indication of the total deficit during a drought, and makes comparison with other variables possible (Van Loon et al., 2014). In this study, where soil moisture, backscatter, and vegetation parameters are compared this is a great benefit. Alternatively, a more suitable measure of the drought severity for state variables is the magnitude, the maximum deviation d_{max} from from threshold during a drought event of T time steps, defined as:

$$d_{max} = max(d_1(t), ..., d_T(t)) \tag{2.1}$$

The propagation of a drought through a catchment strongly depends on regional characteristics like soil and vegetation (Van Loon and Van Lanen, 2012). Therefore, to be able to quantify drought characteristics and identify a water deficit the threshold chosen should reflect a certain regional bias (Wilhite, 2000). The threshold can be a fixed threshold or a variable threshold. Preference is often given

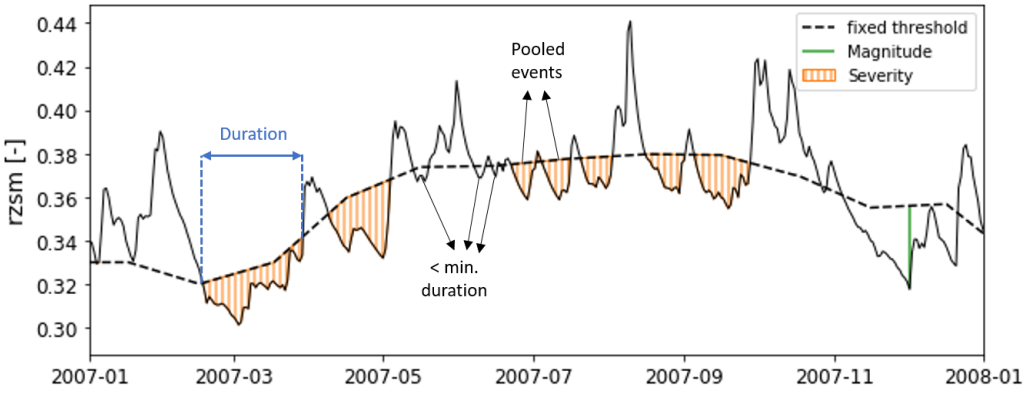

Figure 2.2: Drought characteristics explained (own work). Magnitude is the max. deviation from threshold. Severity is the cumulative deficit of an event. Droughts that fall within the inter-event period are pooled and droughts with short duration are not considered.

to a variable threshold because a fixed threshold would mean that seasonal periods of low soil moisture content would wrongly be marked as a drought (Van Loon and Van Lanen, 2012). Moreover, a variable threshold also shows deficiencies in the wet season that could lead to drought in the next dry season.

Defining a suitable threshold is a crucial, yet subjective, step in the threshold level method. Ideally the threshold should reflect the water demand in a region, but since this is often difficult to quantify it is frequently derived from flow duration curves (for hydrological droughts), and will depend on the flow regime (Van Loon, 2015). An area with a time series containing many zero values, for example, may require a specific threshold to avoid too many non-drought years. For perennial and intermittent streams a threshold ranging between the 70th and 95th percentile is frequently used(Fleig et al., 2006). A 70th percentile would lead to more events with longer durations and higher deficit volumes, whereas the opposite would be true for thresholds based on the 95th percentile (Hisdal et al., 2004; van Loon, 2013). This range has also been applied to droughts in soil moisture. For state variables like soil moisture the flow duration curve translates to the proportion of time a specified soil moisture level is equalled or exceeded during the record period (Hisdal and Tallaksen, 2000).

The threshold also varies depending on whether it is based on a daily, monthly or seasonal duration curve. Together with the length and time resolution of the data record this will influence the number and length of the drought events (Fleig et al., 2006; Vidal et al., 2010). For short time series a low threshold can be problematic because a certain number of events are required for a suitable calculation of percentiles, and when the time resolution used is short in comparison with the droughts two other problems can arise. 1) Minor droughts skew the drought distribution and disturbs extreme value analysis. 2) Mutually dependent droughts interrupt what is actually one long event with short excess periods, causing multiple drought events (Fleig et al., 2006).

To deal with short droughts a minimum drought duration can be set. This is once again quite arbitrary, but should logically reflect the purpose of the study and the regional characteristics. To pool dependent droughts together the inter-event time criterion, t_c, can be used. This approach defines two mutually dependent droughts as one long drought if the the number of days between the droughts τ_i is less than the predefined t_c (see fig. 2.2). The duration (d) of the drought event is then defined as:

$$d_{pooled} = d_i + d_{i+1} + \tau_i \qquad [T] \tag{2.2}$$

The deficit volume (v) is defined as the sum of the individual deficits, without the excess volume from the inter-event period, though this could be included depending on the study purpose (Fleig et al., 2006).

$$v_{pooled} = v_i + v_{i+1} \qquad [L^3] \tag{2.3}$$

Another way of dealing with mutually dependent droughts is to use the moving-average procedure, which smooths the time series. Even though this eliminates both short duration droughts and pools

mutually dependent droughts, the disadvantage is that the deficit volume also changes as a result. Alternatively, the moving average can be used to to identify only the pooled duration, with the deficit still being calculated from original time series (Fleig et al., 2006). In this study the minimum duration and inter-event time criterion are used to remove and combine drought events respectively, because these don't require manipulating the original time series.

2.2. Scatterometry and soil moisture retrieval

Scatterometers are radars that provide very accurate measurements of the backscatter coefficient of the observed surface, usually over a wide range of incidence angles (Woodhouse, 2005). As an active system, scatterometers transmit a continuous series of microwave pulses, and measure the power of the proportion of the signal that is reflected back by the surface in the direction of the incident wave after scattering. The received power depends on instrument properties (power transmitted P_t, antenna gain G, wavelength λ), the distance to the surface (R), and the footprint, the area over which the measurement is made (A). Naturally, it also depends on the properties of the illuminated surface, captured in the backscattering coefficient, σ^o (Woodhouse, 2005).

Since the objective of monitoring is to gain information about the surface, the radar equation (2.4) is used to convert the received power measurements to σ^o , commonly expressed in decibels $[dB]$ (Wagner, 1998).

$$P_r = \frac{\lambda^2 G^2 P_t A}{(4\pi)^3 R^4} \sigma^o \tag{2.4}$$

Dielectric constant
The backscattering coefficient σ^o is dependent on the interaction between microwaves and the (vegetated) surface, governed by the dielectric properties of the surface materials and their geometrical structure. The dielectric constant is a measure of how well a material polarizes in an electric field and strongly affects the reflective and emissive properties of the material. Especially in the low-frequency microwave region of 1-10 GHz the dielectric constant of water ($\sim$80) differs significantly from that of soil and air ($\sim$4 and 1 respectively) (Woodhouse, 2005). A higher dielectric constant will result in higher backscattering of the incident wave and, consequently, a lower penetration depth as shown in figure 2.3a. As such, a higher σ^o is often related to higher moisture content in soil or vegetation.

Scattering
The amount of energy redirected in the direction of the incident wave is the result of either direct surface scattering, volume scattering, multiple scattering, or a combination of them. Surface scattering generally occurs at the air-soil boundary and is determined by the dielectric properties of the upper few centimetres of soil, and by incidence angle and surface roughness relative to the wavelength (Wagner, 1998). As shown in figure 2.3a a smooth surface will typically reflect a focused narrow beam in the forward direction, whereas a rough surface scatters more diffusely, increasing the component of the wave scattered in the incident direction, thus increasing σ^o . Surface scattering can also occur at the top of a vegetation canopy due to high vegetation water content.

Volume scattering refers to scattering caused by dielectric discontinuities of discrete elements with a significant cross section compared to the wavelength in an otherwise homogeneous dielectric medium (Ulaby and Long, 2014). Forest canopies are often considered volume scatterers as each individual scattering element, a trunk, branches or leaves, may scatter in a particular direction but the combined result has no preferential direction (see fig. 2.3b). For this reason, backscattering as a result of volume scattering will tend to show less dependence on the incidence angle (Rees, 2013).

Multiple scattering refers to multiple interactions of a signal between the soil and the vegetation, or between vegetation components (Konings et al., 2019). Nr. 3 and 4 in figure 2.3b give an idea of this scattering mechanism (though it is by far not limited to these). Across forests multiple scattering can occur between bare twigs and branches that are high in water content, while at the same time attenuating the signal from the underlying surface (Pfeil et al., 2020). In croplands multiple scattering can be strongly influenced by the geometrical arrangement and 3D structure of the vegetation (Veloso et al., 2017). Similarly, Steele-Dunne et al. (2019) observed ground-bounce terms, and the attenuation thereof, from scattering from vertical constituents in grasslands. Multiple scattering can contribute significantly to the total backscatter, especially over surfaces where the signal is not rapidly attenuated by vegetation.

2.2.1. The Advanced Scatterometer (ASCAT) instrument

ASCAT is a scatterometer operating at a frequency of 5.3 GHz (C-band) on board EUMETSAT's Meteorological Operational (MetOp) -A, -B, and -C satellites, launched in 2006, 2012, and 2018, respectively.

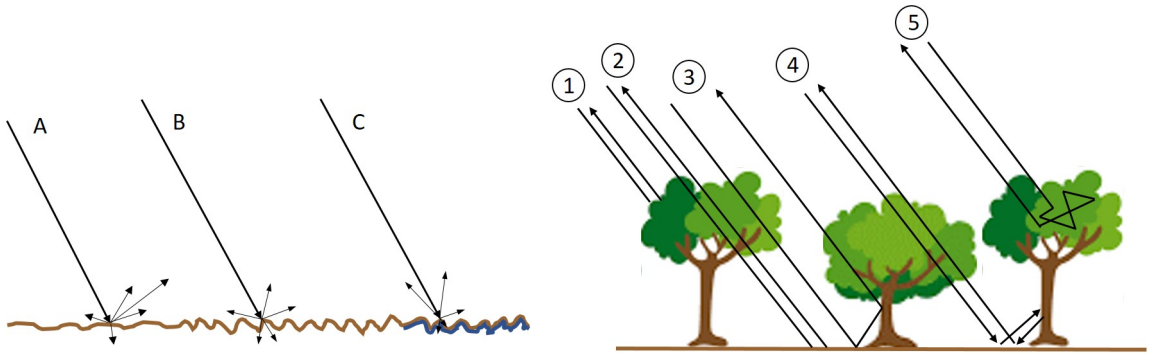

(a) Scattering over bare soil (b) Scattering over vegetated surface

Figure 2.3: (a) A: relatively smooth surface. B: rough surface. C: wet soil.
(b) 1: Surface scattering from top of canopy. 2: Surface scattering from underlying soil (fig. 2.3a) 3: Ground-vegetation (and vice versa) scattering 4: Ground-vegetation-ground scattering 5: Volume scattering from canopy.

These satellites fly in a near-polar, sun-synchronous orbit at an altitude of 817 km, completing an orbit in approximately 100 minutes, so 14 orbits a day (Wagner et al., 2013). The satellites cross the equator around 9:30 and 21:30 local time for descending and ascending overpasses and have an in-orbit separation of half an orbital period, about 50 min (Hahn et al., 2017). Though the revisit times of the satellites is 29 days, it only takes 3 days to achieve full global coverage. With only one satellite a daily coverage of 82% can already be achieved, but with gaps around the equator. This spatial irregularity also causes an irregular temporal coverage (Wagner et al., 2013). Therefore, the backscatter product from ASCAT is aggregated into 10 day intervals, or dekads.

The ASCAT instrument builds on the succes of the European Scatterometer (ESCAT) which flew on board the ERS1/2 from 1991-2011. Like the ERS1/2 scatterometer ASCAT is a fixed fan beam scatterometer, but with two instead of one, sets of three fan-beam side ways looking antennas. The three antennas on each side, referred to as fore, mid and aft beams, are oriented at 45°, 90°, and 135°with respect to the satellite track. Each set of antenna triplets illuminates a 550 km swath, with a satellite track of about 360 km separating the swaths (Figa-Saldaña et al., 2002). The incidence angles of the fore and aft beam range from 34°- 65°and for the mid beam range from 25°- 55°, see figure 2.4.

This ability to measure at multiple incidence angles forms the basis for the TU Wien Soil Moisture Retrieval algorithm.

2.2.2. TU Wien Soil Moisture Retrieval Algorithm

Originally scatterometers were only intended to measure wind speed and direction over oceans, with no services foreseen over land. However, early studies by Frison and Mougin (1996) already showed high agreement between backscatter and global vegetation index maps. Later, Wagner et al. (1999) and Woodhouse and Hoekman (2000) provided evidence that scatterometer data could possibly be used for soil moisture monitoring.

Generally a wavelength of 5.7 cm (C-band) is considered sub-optimal for soil moisture retrieval compared to longer wavelengths like L-band, which are less sensitive to surface roughness and have a deeper penetration through vegetation (Wagner et al., 2007). What is often overlooked, however, is the high radiometric accuracy of scatterometers like ASCAT. Scatterometers are designed to make very accurate estimates of σ^o by taking the average of the power received at the antenna of a large number of 'looks' so that the variance in P_r becomes very small, but the average remains unchanged, resulting in a high signal to noise ratio (Frison et al., 2016). The high radiometric accuracy does come at the cost of spatial resolution, which for ASCAT is 25 km.

The potential to monitor soil moisture with C-band scatterometry led to the development of the TU Wien Soil Moisture Retrieval algorithm (TUW SMR). At C-band the effects of surface roughness generally dominate over soil moisture, and disentangling these effects in the backscattered signal remains a major challenge (Scipal et al., 2002). Typically semi-emperical backscattering models, like the Water Cloud Model, are used. However, if instead of looking at the spatial signal pattern the temporal pat-

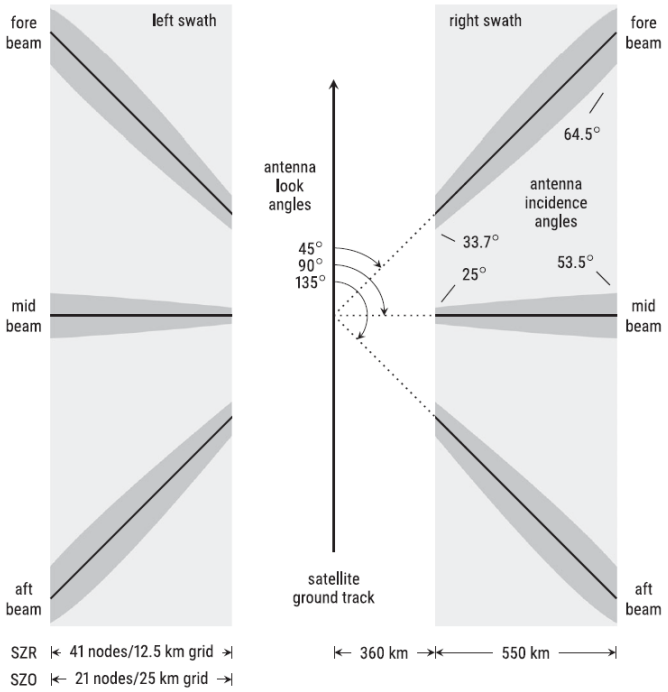

Figure 2.4: Specifications of the ASCAT instrument onboard MetOp-A, B and C (from Hahn et al. (2017))

terns are investigated, the effect of soil moisture becomes apparent because the temporal effects in soil moisture dominate that of vegetation phenology, while surface roughness can be taken as a constant, as illustrated in figure 2.5 (Scipal et al., 2002). This so called 'change detection method' forms the basis of the TUW SMR. One disadvantage is that this is a lumped approach where soil moisture and vegetation are all still lumped together (Wagner et al., 2013).

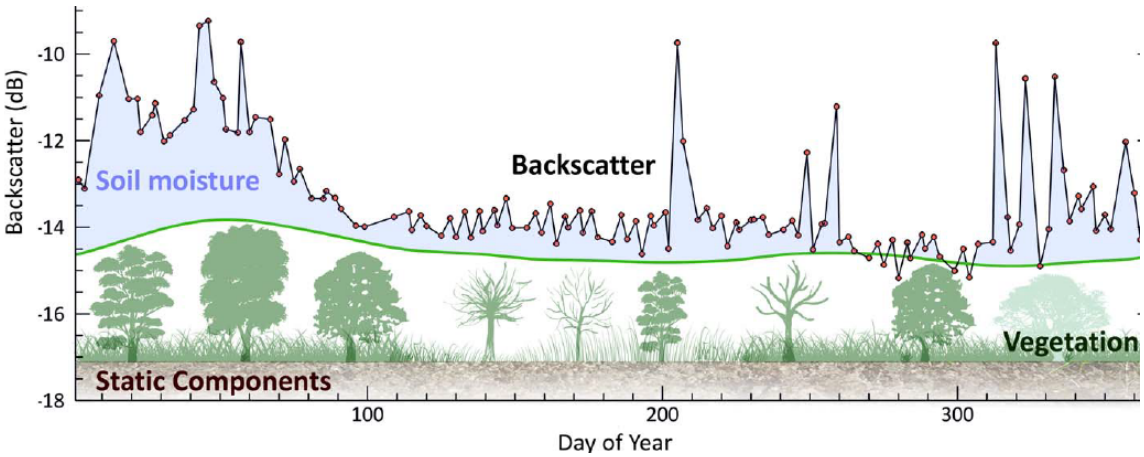

Figure 2.5: Time series of one year with evident differences in temporal signal patterns between soil moisture, vegetation phenology and surface roughness for a point in Queensland, Australia (from Vreugdenhil et al. (2016))

At the core of the algorithm is the relationship between incidence angle θ and backscatter σ^o . In general, the overall level of backscattering is determined by the surface properties, such as the dielectric constant, or moisture content. The dependence of backscatter on incidence angle is largely governed by the scattering mechanism; whether the total backscatter is dominated by surface scattering or volume scattering from vegetation (Rees, 2013; Steele-Dunne et al., 2019). At higher incidence the backscatter is more sensitive to vegetation as the contribution from the soil surface becomes very small due to most of the signal being attenuated by the vegetation. As can be seen in figure 2.6 over dense vegetation the backscatter is influenced less by the incidence angle as a result of volume scat-

tering. Visually, this is associated with a rotation in of the $\sigma^o - \theta$ curve.

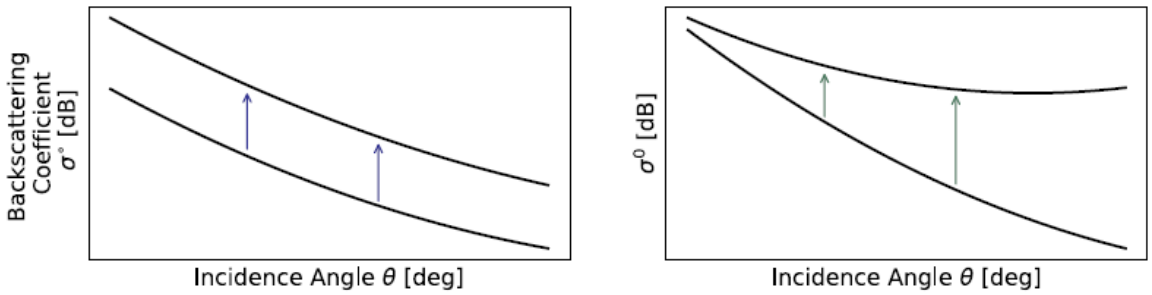

Figure 2.6: The two panels show the σ^o - θ relation changes with increasing soil moisture and vegetation (from Steele-Dunne et al. (2019))

In the dB domain the relation between σ^o and θ can be modeled by a linear function (eq. 2.5).

$$\sigma^o(\theta) = \sigma^o(\theta_r) + \sigma'(\theta_r) \cdot (\theta - \theta_r) \qquad [dB/deg] \tag{2.5}$$

However, towards the higher incidence angles the backscatter signal tends to flatten out. In order to accurately describe this behaviour the linear function can be expanded into a second order Taylor polynomial around a reference angle θ_r (Wagner et al., 1999).

$$\sigma^o(\theta) = \sigma^o(\theta_r) + \sigma'(\theta_r) \cdot (\theta - \theta_r) + \frac{1}{2}\sigma''(\theta_r) \cdot (\theta - \theta_r)^2 \qquad [dB/deg] \tag{2.6}$$

The slope (σ') and the curvature (σ") of the function $\sigma^o(\theta)$ are used to normalize all backscatter measurements to a single reference angle θ_r. Equation 2.6 can be rearranged into equation 2.7 to remove the incidence angle dependence on backscatter and make different backscatter observations comparable at a single reference angle, which in the TUW SMR algorithm is 40° (Hahn et al., 2017).

$$\sigma^o(\theta_r) = \sigma^o(\theta) - \sigma'(\theta_r) \cdot (\theta - \theta_r) + \frac{1}{2}\sigma''(\theta_r) \cdot (\theta - \theta_r)^2 \qquad [dB/deg] \tag{2.7}$$

The parameters $\sigma'$and $\sigma''$are also known as the vegetation parameters because they are estimated to correct for vegetation effects in soil moisture retrieval. While σ^o_{40} is mainly controlled by surface soil moisture, $\sigma'$is related to wet biomass, and $\sigma''$is used to describe the backscatter signal at higher incidence angle where the σ^o - θ curve tends to flatten out due to volume scattering (see fig. 2.6) (Hahn et al., 2017).

2.2.3. Dynamic Vegetation Parameters

The slope and curvature are estimated from the simultaneously observed backscatter at different incidence angles, so called backscatter triplets. A backscatter triplet consists of the backscatter signal measured by the fore (f), mid (m) and aft (a) antenna, of which the fore and aft beam measure at the same incidence angle. This allows for an instantaneous computation of the so called local slope, which is only valid near the respective incidence angle (see eq. 2.8) (Hahn et al., 2017). However, the local slope values are typically noisy measurements so a large number of local slopes distributed over the entire incidence angle range must be combined (Naeimi et al., 2009). Until recently several years of local slope data was used to produce a seasonal climatology of slope and curvature.

$$\sigma'\left(\frac{\theta_{mid} - \theta_{a/f}}{2}\right) = \frac{\sigma^o_{mid}(\theta_{mid}) - \sigma^o_{a/f}(\theta_{a/f})}{\theta_{mid} - \theta_{a/f}} \qquad [dB/deg] \tag{2.8}$$

However, recently Melzer (2013) demonstrated the possibility to calculate $\sigma'$and σ''dynamically, which allows to take interannual variations into account. Melzer (2013) uses a Kernel Smoother approach whereby the slope and curvature are estimated from local slopes within a 42 day window around a

particular day. An Epanechnikov kernel with $\lambda = 21$ is used to give more weight to local slopes closer in time. Hahn et al. (2017) found that using a kernel window of 42 days yielded a good trade-off between bias and variance in the calculation of daily slope values.

In light of this new development, Steele-Dunne et al. (2019) suggested to use σ' and σ'' as information on vegetation phenology and water dynamics instead of only using it to correct for vegetation in soil moisture retrieval. They confirmed that slope is not so much related to vegetation greenness but more to the seasonal dynamics in wet biomass of the vegetation and found that curvature also holds information about vegetation. They showed that, in grasslands, curvature is dependent on the relative dominance of direct scattering over ground-bounce contribution, which in turn depends on the vegetation water content and geometry (Steele-Dunne et al., 2019).
This study sets out to investigate whether slope and curvature can provide the same information over other types of vegetation, and whether they are also able to describe the vegetation water dynamics during periods of water stress.

3

Data & Methods

This chapter gives more information on the datasets used, particularly from the land surface model. The study area and regions of interest are described in detail in section 3.2. Section 3.3 covers the methods, including the application of the threshold level method in this specific study.

3.1. Datasets

3.1.1. ASCAT

The three ASCAT datasets, normalized (40°) backscatter σ^o_{40} , slope σ', and curvature σ'', are provided on the discrete global WARP5 (Soil Water Retrieval Package) 0.25°x 0.25°grid. The datasets span 13 years, from 2007 - 2019. The slope and curvature are calculated at daily time steps using the TUW SMR algorithm and kernel smoother as explained in section 2.2.2. The temporal resolution of the backscatter is more irregular because the constellation of the three MetOp satellites provides observations every one to three days (Figa-Saldaña et al., 2002). Therefore the backscatter data is aggregated into 10 day intervals (dekads).

3.1.2. Land surface model ISBA

The variables soil moisture, LAI and GPP are obtained from the land surface model ISBA, which stands for Interaction Sol-Biosphère-Atmosphère and is part of the surface modelling platform SURFEX, developed by Météo-France. SURFEX (SURface EXternalisée) merges the surface variables from several land and ocean surface models to be coupled with atmospheric models for numerical weather prediction purposes (Moigne, 2018). Within SURFEX, the ISBA scheme computes the exchange of energy and water between the soil, vegetation and atmosphere. The ISBA version that is currently used is ISBA-A-gs, a CO_2 responsive module that simulates photosynthesis and the associated net CO_2 assimilation (A_n), and stomatal conductance (g_s). Through the simulation of these water vapour fluxes and the diurnal carbon cycle daily LAI and biomass values can be produced. The ISBA-A-gs version also includes the effect of soil moisture stress on vegetation represented by one of two drought coping mechanisms, namely reducing evaporation through stomatal regulation (drought-avoiding), or applying a more efficient root water uptake or a more rapid growing cycle (drought-tolerant) (Moigne, 2018).
For this study ECMWF's ERA5 climate reanalysis dataset is used as atmospheric forcing in ISBA to generate the soil moisture, LAI and GPP datasets at a spatial resolution of 0.25°x 0.25°, consistent with ASCAT. All ISBA datasets also span from 2007 - 2019 and have a daily time resolution.

Soil Moisture
The soil moisture in ISBA is calculated using a 'force-restore' method for heat and water content in which capillary rises act as a restore term to bring the near surface soil moisture in equilibrium with the root zone soil moisture after transpiration (Calvet and Noilhan, 2000). The distribution of roots is generally taken to be uniform through the root depth, which can be specified, or is taken as a constant based on vegetation type (Moigne, 2018). In this study simulated soil moisture $[m^3\ m^{-3}]$ is provided

at different depths (0.01m, 0.04m, 0.1m, 0.2m, 0.4m, 0.6m, 0.8m and 1m). This is consistent with the Soil Water Index (SWI) which has been successfully used in conjunction with ISBA before (Albergel et al., 2008). The SWI is one of the products offered by the Copernicus Global Land Service, and simulates the infiltration process from ASCAT derived surface soil moisture down to 1m depth using an exponential function . Nevertheless, using a single static root zone depth of 1m for vegetation ranging from croplands to forests definitely has its limitations. These are discussed further in chapter 5. For the purpose of this study the top two layers (0.04m), and the deeper layers are aggregated separately using a depth weighted average to represent surface soil moisture and root zone soil moisture, respectively. The reason for this distinction is that the C-band signal from ASCAT has a soil penetration depth in the order of 0-5cm. Thus when analyzing ASCAT backscatter it is better to compare it to the faster reacting top two surface soil layers than to the often slower reacting lower layers that also contain more 'memory' of antecedent conditions. To analyse the vegetation's response to soil moisture shortage the root zone soil moisture is more useful because that is where the vegetation draws it water from. For most trees, however, this happens at depths much greater than 1m (Robinson et al., 2006).

Leaf Area Index
Leaf Area Index (LAI) $[m^2\ m^{-2}]$ is the ratio of total upper leaf surface of vegetation to the surface area of land on which the vegetation grows. In ISBA-A-gs LAI is a prognostic variable derived from leaf biomass, in contrast to the standard ISBA scheme where LAI is a prescribed surface parameter.

Gross Primary Production
Gross Primary Production (GPP) $[t\ C\ ha^{-1}\ y^{-1}]$ is a measure of the raw carbon uptake in vegetation through photosynthesis. As such, it is a measure of the accumulation of biomass.

ISBA vegetation type
The land surface parameters used in SURFEX come from the ECOCLIMAP database, which combines land cover maps and satellite information. Each of the SURFEX grid cells is divided into four tiles; town, vegetation, sea, and lake. For the ISBA scheme the vegetation tile is split into 12 different patches, listed in table 3.1. These patches are the vegetation types used as land cover in this study. Each grid cell is made up of a fraction of these 12 patches. Fig. 3.1 shows a map of the vegetation types with the highest fraction per grid cell.

ISBA vegetation type	**abbreviation**
bare soil	NO
bare rock	ROCK
permanent snow	SNOW
deciduous broadleaved	TREE
needleleaved	CONI
evergreen broadleaved	EVER
C3 crops	C3
C4 crops	C4
irrigated crops	IRR
temperate grassland	GRAS
tropical grassland	TROG
wetlands, parks and gardens	PARK

Table 3.1: ISBA vegetation types

3.1.3. Data preparation
Since the ISBA surface and rootzone soil moisture are frequently compared to backscatter, for both practical reasons and to resemble the backscatter time series better, the soil moisture time series are aggregated into dekads. The dekads are grouped from day 1-10, 11-20, and 21 to the last day of the month. The time signature of the dekads is always the last day of the 10 day interval.

To make the comparison between LAI and GPP, and the dynamic vegetation parameters more convenient, the LAI and GPP time series are also smoothed using an Epanechnikov kernel with a half window (λ) of 21 days. This especially makes a difference for GPP, which otherwise has a high frequency signal, but also the LAI signal is now smoothed over 42 days. The Epanechnikov kernel in equation 3.1 weighs all values within the interval of $|(d-d_0)/\lambda| \leq 1$ according to their distance to the current day of year d_0 (Hahn et al., 2017).

$$k(d_0, d) = \frac{3}{4} \cdot \left(1 - \left(\frac{d - d_0}{\lambda}\right)^2\right), \tag{3.1}$$

with d ranging from [-21, 21].

3.2. Study area

The study area contains mainland Australia and Tasmania, and extends from from 112°E - 155°E, and 10°S - 44°S. Based on the same 0.25°x 0.25°WARP5 grid as ASCAT, which roughly translates to 25km x 25km, this comes down to 11135 grid points (or grid point indices, gpis) over land. Figure 3.1 shows the dominant vegetation types in the study area. Almost half of the gridpoints are dominated by bare soil (5187 gpis). The four other prevalent dominant vegetation types are tropical grasslands (3907 gpis), C3 crops (905 gpis), evergreen broadleaf forests (653 gpis) and temperate grasslands (459 gpis). The dominance is relative to the other vegetation types in a grid point so for a heterogeneous grid point the absolute cover fraction of the dominant vegetation type can still be quite low. Figure 3.2 shows the cover fraction of each of the vegetation types.

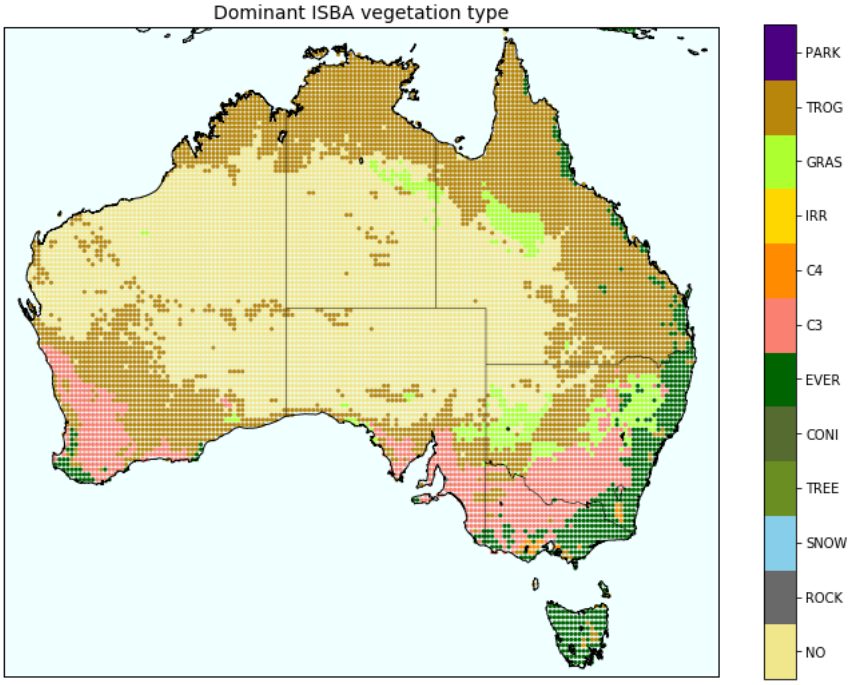

Figure 3.1: ISBA vegetation type with the highest fraction per grid cell

Droughts are considered a natural part of Australia's highly variable hydroclimate (Kiem et al., 2016). Due to its location between the Indian, Antarctic and Pacific Ocean, Australia is particularly sensitivity to large scale climate modes such like the El Nino Southern Oscillation (ENSO), the Indian Ocean Dipole (IOD), and the Southern Annular Mode (SAM) (BoM, 2021; Vreugdenhil et al., 2017). Though the focus of this study is not on the science of the origin of droughts, for an accurate interpretation of backscatter, slope, and curvature signals it is important to be aware of the wide range of climate conditions in Australia that determine the energy distribution, and thus in part the occurrence of droughts (Tallaksen and Van Lanen, 2004).

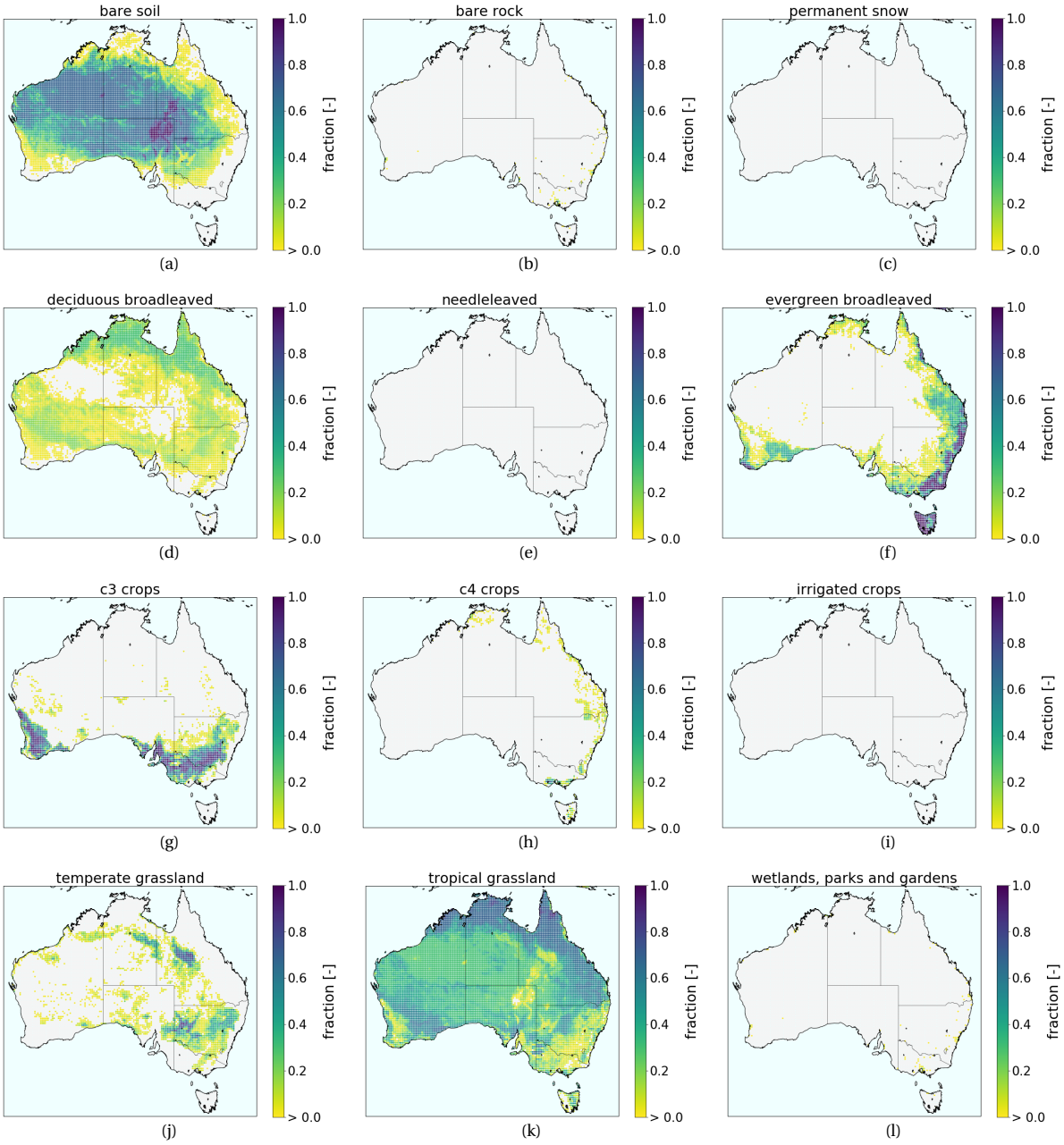

Figure 3.2: Fractions per grid point of each of the 12 ISBA vegetation types

Figure 3.3 shows a climate classification of Australia based on the Köppen Geiger climate classes, which are divided according to precipitation and temperature data. Much of central Australia is dominated by a dry arid climate. The southwest and east have a temperate climate with predominantly warm summers, and the north(east) is characterized by a monsoonal tropical climate. The resemblance of spatial patterns between the climate classes in figure 3.3 and the dominant vegetation types in figure 3.1 acknowledge the strong influence of climate on vegetation, and to some extent, vice-versa.

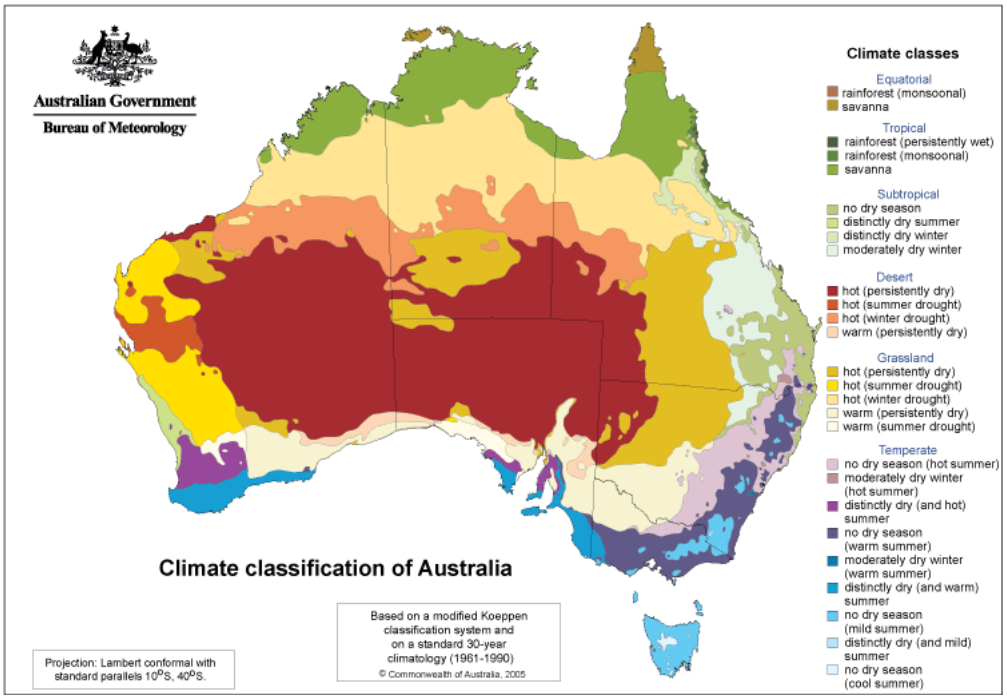

Figure 3.3: Climate classification of Australia based on the Köppen Geiger Climate Classes from the Australian Bureau of Meteorology (BOM) (from (*Bureau of Meteorology - Climate Classifications Maps* 2021))

3.2.1. Regions of interest

Several regions of interest are defined, primarily based on a high fraction of one of the ISBA vegetation types. These regions of interest are chosen to facilitate the interpretation of backscatter, slope and curvature across an otherwise very heterogenous, in terms of vegetation types, study area. To further differentiate within the vegetation types the bioregions from the Interim Biogeographic Regionalisation of Australia (IBRA 7.0) were used. These correspond in large to the ecoregions from Olson et al. (2001), used succesfully by Steele-Dunne et al. (2019) and Petchiappan (2019) to differentiate the behaviour of ASCAT parameters within one land cover type. Similarly to Olson et al. (2001), IBRA7 classifies distinct bioregions based on common climate, geology, landform, species and native vegetation, and is slightly more detailed and tailored to Australia [1].
Three main criteria used to determine the regions of interest (ROIs) were:

1. homogeneous vegetation type. Grid points with a cover fraction < 80% were excluded (for GRAS and TROG < 70% was used, otherwise the second criteria could not be met)
2. large enough number of grid points. The ROIs had to be large enough for a drought signal to be actually considered a drought. Approximately 25000km^2, or 40 grid points, is used by Andreadis et al. (2005), and used as the minimum number to qualify as an ROI in this study.
3. contiguous grid points. The grid points within an ROI had to be relatively contiguous so if a drought occurred, it most likely affected all the points in the ROI.

Finally, a manual revision of the slope time series was done to remove outliers within each ROI. Grid points near the coast for example can show a highly divergent temporal signal due to the high fraction of water present.

Identifying ROIs is important because droughts manifest themselves differently from region to region. Moreover, backscatter data from ASCAT has been shown to be sensitive to vegetation type, thus for an accurate interpretation of σ^o_{40} and the dynamic vegetation parameters it is imperative to have a firm knowledge of the land surface. Spatial averaging over the ROIs is performed after climatology and anomalies have been calculated for each individual grid point.

[1] https://www.environment.gov.au/land/nrs/science/ibra

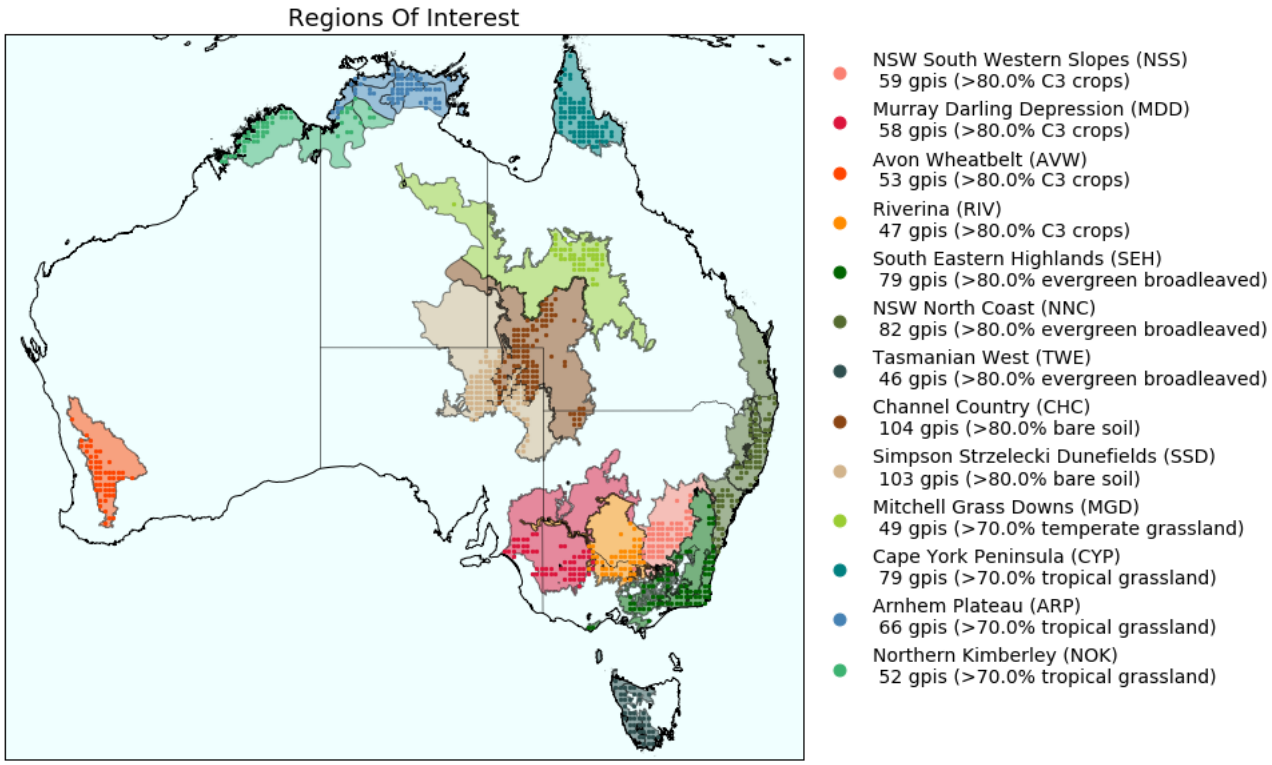

Figure 3.4: The ROIs delineated by the IBRA7 bioregions. The dominant (>70% or >80%) ISBA vegetation type is given in brackets.

All the information below about the ROIs is obtained from Woinarski and Mockrin (2020), Bastin (2008) and the overview of bioregions from the State of New South Wales (*Bioregion Overviews* 2016). For some ROIs an image is included to give an appreciation of the types of vegetation in these regions. The vegetation images are all from the Australian National Botanic Gardens' collection (*Vegetation Photos in the ANBG Collection* 2012).

The region of interest within vegetation type C3 crops are:

Avon Wheatbelt (AVW): the AVW makes up most of the Wheatbelt in Western Australia, an important economic region which exports more than 80 percent of its produce. Practically all of the native savanna vegetation has been cleared for wheat and barley cultivation, and sheep rearing. It has a temperate climate where yields depend strongly on winter rains, as spring rainfall is generally unreliable. Both wheat and barley are winter crops, meaning they are sown in SH-autumn and harvested in spring or summer.

Murray Darling Depression (MDD): part of the economically important wheat-sheep zone. The native mallee woodlands in this region have been extensively cleared for cereal cropping and pasture. Both the Murray and the Darling river flow through this region, and the landscape consists of undulating plains with lakes, swamps and depressions. It has a warm semi-arid climate with annual rainfall ranging from 200-400mm.

Riverina (RIV): part of the wheat-sheep zone. Most of the original eucalypt vegetation has been cleared for wheat cropping and sheep pastures. This region is strongly marked by the presence of the presence of several large rivers creating alluvial fans, floodplains and river channels. It has a dry semi-arid climate with hot summers and cool winters. The highest level rainfall occurs in May and September. Rainfall in winter is more consistent than rainfall from summers which come from thunderstorms. Mean annual rainfall ranges from 250mm in the north to 600 in the south.

NSW South Western Slopes (NSS): also part of the wheat-sheep zone. The native vegetation has been

heavily cleared for cereal cropping and pasture. The grid points are located in the foothills and ranges to the west of the Great Dividing Range. The region is dominated by a sub-humid climate with hot summers and no dry season. Rainfall is distributed with high mean annual rainfall (1200mm) in the east and lower values to the west (400mm).

The region of interest within vegetation type evergreen broadleaved forest are:

NSW North Coast (NNC): This region borders the coast to the east, and the Great Divididing Range to the west. From east to west the topography changes from coastal sand barriers, to foothills, to steep slopes. Vegetation changes accordingly and is dominated by temperate rainforests in the east and eucalypt communities on the slopes. The mean annual rainfall ranges from 600-3000mm, increasing land inwards, while the mean annual temperature decreases from 8-20°C along this gradient. This ROI also has some points in the Sydney Basin and South East Queensland.

Figure 3.5: Eucalypt forest with rain forest understory, VIC. Typical Australian wet sclerophyll forests are similar. Compared to rain forests these canopies are less dense.

South Eastern Highlands (SEH): This ROI has points in the South Eastern Highlands and the South Eastern Corner IBRA7 bioregions. It is characterized by a temperate climate with warm summers and no dry season. Mean annual temperature ranges from 6-16°C and annual rainfall ranges form 500-1500mm, with the wetter regions near the coast. Grid points are located on both sides of the Great Dividing Range. Its diverse topography and climate is reflected in the diversity of vegetation communities, though the majority is made up by eucalypt forest and wet sclerophyll forests, with some temperate rain forest.

Tasmanian West (TWE): this ROI is heavily dominated by rain forests at a large range of elevations. The terrain is rugged with a chain from north to south along the east side of the region. It has temperate climate with mild winters and cool summers. Rainfall is heaviest in winter and no strong seasonality exists.

The region of interest within vegetation type temperate grasslands are:

Mitchell Grass Downs (MGD): all grid points lie in the northern Queensland part of the bioregion. It consists mostly of treeless plains dominated by Mitchell tussock grasslands. MGD has a dry semiarid climate, influenced by SH-summer monsoons to the north. Average annual rainfall is around 300mm.

Figure 3.6: Mitchell Tussock Grasslands, Queensland

The region of interest within vegetation type tropical grasslands are:

Cape York Peninsula (CYP): CYP is dominated by eucalyptus and melaleuca woodland, with some rain forest to the east. Its climate is strongly monsoonal with most rains falling in the SH-summer. Summers are hot and humid and the annual rainfall gradient decreases from 2400mm to 800mm from north to south.

Arnhem Plateau (ARP): the grid points are spread over several bioregions with a similar climate and vegetation cover. Towards the west a sandstone massif dominates the otherwise flat topography. Veg-

etation communities include heathlands, hummock grasslands, open eucalyptus woodlands, and patches of monsoon forest. The tropical monsoonal climate has a distinct wet and dry season with high temperatures throughout the year. Almost all of the approximate 1200mm rain falls in the wet season between November and March, leaving a nearly rain free period for the rest of the year. **North-**

(a) Melaleuca woodland with grass understory, northern Queensland (b) Open eucalypt woodlands, northern Queensland

Figure 3.7: Open woodlands in ISBA vegetation type Tropical Grasslands

ern Kimberley (NOK): the vegetation in this region is characterised by open eucalyptus woodlands with canopy heights between 5-15m and understories of tall grass savanna. The vegetation varies strongly from the rugged coastal areas to the plateaus more inland. A strong seasonal monsoonal climate makes for a short wet season from October to March and a long, nearly rain free dry season for the rest of the year. Mean annual rainfall ranges from 1400mm in the north to 600mm in the south-west.

The region of interest within cover type bare soil are:

Simpson Strzelecki Dunefields (SSD): the SSD is very arid and has an unpredictable rainfall of 150-200mm annually, which usually falls during summer storms. It comprises long linear dunefields and sandplains, and some saltpans. The little vegetation that occurs is predominantly made up of acacia and chenopod shrublands.

(a) Acacia shrublands and sand dunes in the Simpson Desert (b) Chenopod shrublands in Channel Country

Figure 3.8: Vegetation types in Australian deserts; ISBA vegetation type is bare soil

Channel Country (CHC): CHC is characterised by multiple river channels that drain to Lake Eyre and vast braided flood and alluvial plains. It is characterised by an arid climate with very dry hot summers and short dry winters. Although rainfall is persistently low and erratic (approx. 150mm per year), extensive flooding from the north can lead to considerable pasture growth. Vegetation then includes ephemeral grass and herbs, mulga, Mitchell grass and some eucalypt.

3.3. Methods

3.3.1. Spatial patterns

Backscatter data from scatterometers is known to be useful in discriminating main vegetation regions. It is also sensitive to water bodies, and the relief and moisture content of the soil surface (Wagner et al., 1999). Hence, for a first indication of the distribution of σ^o_{40} , $\sigma'$and σ''values across the whole of Australia, and to give an idea of how the values in the ROIs correspond to the rest of the country, maps of the mean and range of the 13 year long ASCAT datasets are made.

Thereafter the focus is on the ROIs. Scatterplots of mean vs. range are shown first to appreciate the difference between the ROIs in different vegetation types. Each marker represents an individual gridpoint in an ROI.

3.3.2. Seasonal climatology

To analyse the seasonal climatologies of each ROI the time series of all the variables is decomposed manually into two additive components:

Observed time series (O) = Seasonal climatology (S) + Anomalies (R)

The climatology is calculated by taking the average of the entire time series (2007-2019) for each day of the year, or each dekad. Since the climatology is based on only 13 years of data it is important to keep in mind that the seasonal climatologies may be skewed compared to an actual climatology based on 30+ years of data. The seasonal climatologies are presented in three panels: 1) soil moisture related variables (σ^o_{40} , ISBA rzsm & ssm), 2) vegetation related variables (σ', LAI & GPP), 3) ASCAT parameters (σ^o_{40} , σ' & σ'').

To give more insight into the scattering mechanisms that drive the seasonal cycle of ASCAT parameters the σ^o - θ relation is plotted, with some key moments highlighted.

3.3.3. Drought response

In this study the simulated root zone soil moisture from ISBA is used as the variable to define droughts. As stated before soil moisture is generally a good indicator of droughts as it is roughly an aggregate of the available water from the balance precipitation, evaporation, and runoff (Sheffield et al., 2009). Moreover, the root zone soil moisture determines the available water for plant growth, and since most of the vegetation growth in Australia is water limited (Nemani et al., 2003), that makes root zone soil moisture anomalies a good representation of droughts.

The full time series of all ASCAT and ISBA parameters are studied to analyze the response of backscatter, slope and curvature in and around droughts. The droughts are primarily used to identify the periods of extreme root zone soil moisture deficit, and not to study the individual drought characteristics. The anomalies in root zone soil moisture and other variables prior to, and after the drought event, are just as important. For the propagation of drought in this context the exact magnitude and accuracy of a drought event is less relevant compared to the relative magnitude of the droughts to each other within the time series.

The droughts are defined using the threshold level method because it stays close to the original time series, and the quantification of drought characteristics is very transparent which makes it ideal for studying drought propagation. The choices made in the application of the threshold level method are discussed below.

In the results the drought events in the time series are highlighted. Since the seasonality of the droughts is important because it can determine the impact on the available moisture content the next season, the highlighted droughts have slightly different colors depending on whether they occur in SH-summer or SH-winter. This is determined based on whether at least 50% of the drought days falls between Oct. - Mar. or Apr. - Sep. respectively.

The anomalies prior to, and following a drought event are equally important when studying the drought response in ASCAT parameters. Anomalies here are defined as the observed time series minus the seasonal climatology. In this case the anomalies contain both long term trends and short term residuals, and in general in this study no further differentiation is made between the two because determining which part belongs to which component is rather subjective. However, occasionally in the

presence of a clear long term trend in the observed data series the *statsmodels.tsa.seasonal.seasonal_decompose* package in Python is used to appreciate the different long and short term components in the anomalies better. This package calculates the long term trend using a centred rolling average with a window of 365 days. Because the window is centred the first (last) six months of the time series, that would otherwise be empty, are extrapolated using the first (last) year of the trend. The observed time series then consists of the following three additive components:

Observed time series (O) = Seasonal climatology (S) + Trend (T) + Anomalies (R)

Identifying drought events

Chapter 2.1 covers the theoretical concepts of the threshold level approach, and this section elaborates on the (*italicized*) subjective choices that have to be made to quantify the drought characteristics for this study.

Since the analyses in this study are based on ROIs, the average soil moisture profile of all grid points in the region is used to identify whether a ROI is in drought or not. That is also why the ROIs consist of spatially contiguous grid points.

A *variable* threshold is used so as to take seasonal variations into account. It is a *monthly* threshold, which allows for seasonal variation to be apparent while ignoring the high variability of daily values. As mentioned before the soil moisture is often presented in dekads in this study, but the monthly threshold value is based on the monthly duration curves using daily soil moisture data because this leads to more data points in a month and thus a more accurate determination of the monthly threshold. In this study this monthly threshold is derived from the *80th percentile*, meaning a value is chosen that is exceeded 80% of the time in a specific month (see fig. 3.9). This is a reasonable threshold, used before to define droughts in soil moisture (van Loon, 2013). However, it remains a subjective choice, and the effect of this choice on the distribution of drought characteristics can be found in appendix A.

Based on twelve monthly duration curves a threshold is defined for each month of the year, and applied to the entire time series, as seen in figure 3.9. To prevent unnatural droughts characteristics due to a 'staircase' pattern, the threshold is *smoothed using a centred moving average of 30 days* (see fig. 3.10).

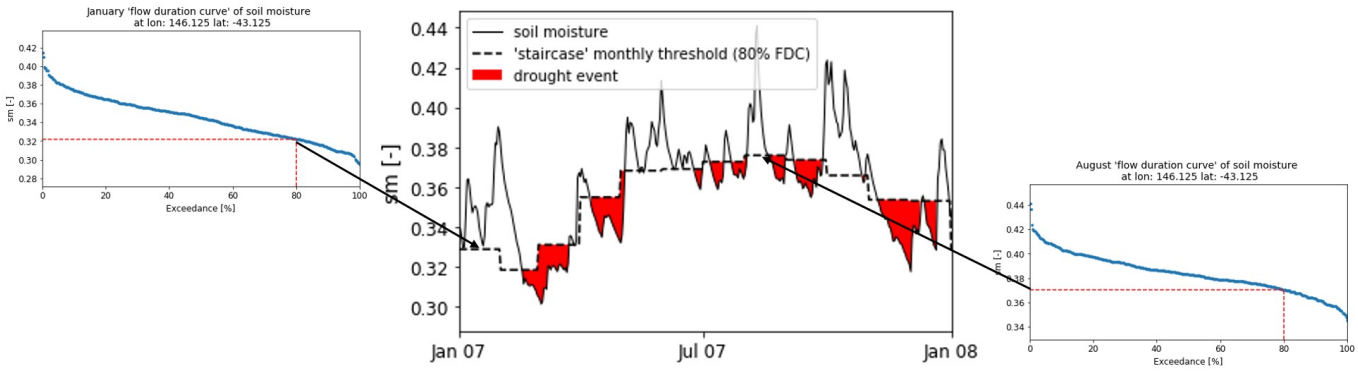

Figure 3.9: Monthly probability of exceedance curves for the months Jan. and Aug. for of a point in Western Tasmania (lon:146.125, lat:-43.125). The 80th percentile is used to define monthly threshold values. Discrete monthly threshold values lead to a 'staircase' pattern which creates unrealistic drought events

Finally short dependent droughts are pooled together, and minor droughts are removed. Pooling is based on the inter-event time criterion, as described in chapter 2.1. Since this is quite a subjective parameter the influence of different inter-event times on deficit characteristics is tested, and the results are shown in appendix A. In this study an *inter-event time of 10 days* is used, concurrent with van Loon (2013). It is quite a conservative number, but a good trade off between minimizing the occurrence of dependent droughts and including too long periods of high moisture content. Minor droughts with a duration shorter than *20 days* have been excluded. Though this is a fairly high number it has been shown that minor droughts can have durations up to 20 days (van Loon, 2013). Also, by applying a minor duration larger than the pooling criteria, individual drought days just within the inter-event time that form artificial drought events are not taken into account. Moreover, the objective here is to

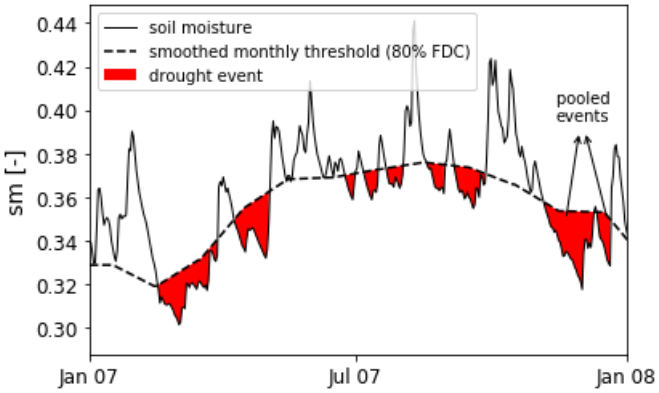

Figure 3.10: Same grid point in Tasmania as in fig. 3.9. Smoothing the 'staircase' pattern using a 30 day moving average leads to much more realistic drought even characteristics. Mutually dependent drought events within the inter-event time period are pooled.

study drought propagation, and not the distribution of drought characteristics, which is why short droughts are less relevant.

The spatial distribution of droughts identified here are visually compared to historic drought events from the Australian Bureau of Meteorology (BOM) to see if they roughly agree. The comparison can be found in appendix A. The spatial pattern will never be exactly the same because the BOM uses rainfall deciles (RD) to define droughts. However, what is most important is that no known major historical droughts are not absent from the time series because this would hamper the accurate interpretation of drought response in observed ASCAT parameters.

3.3.4. Burnt area detection

To assess whether ASCAT dynamic vegetation parameters can also be used to identify burnt areas, as they should be sensitive to such big and sudden changes in vegetation water dynamics, the time series of σ^o_{40} , σ', and σ'' for single grid points are examined. As an example, a single grid point is shown to illustrate the results. The current burnt area information is obtained from the MODIS burnt area product (MCD64A1)[2].

[2]https://modis-fire.umd.edu/

4

Results

The results first cover the variability in σ^o_{40} , σ' and σ'' across the whole of Australia to give an impression of how this relates to the climate, the distribution of vegetation, and other land surface variables. Then the mean and ranges of the ROIs are reviewed to see how these compare to each other. Section 4.2 zooms in further on one ROI per ISBA vegetation type to show what the regular seasonal cycle looks like. With this in mind, section 4.3 shows the entire time series of all the variables for that ROI so that an analysis of the response of ASCAT parameters in and around a drought can be made.

4.1. Spatial patterns

Figures 4.1 shows the spatial distribution of mean and range of backscatter, slope and curvature for all 13 years of data. The backscatter mean (fig. 4.1a) is highest along the eastern and northern coast, congruent with the high rainfall zones and generally woody vegetation, and decreases land inwards. The patch of high mean backscatter in the west is over the Hamersley ranges in Pilbara, where vegetation is a mix of tropical grasslands and bare soil. The lowest mean backscatter is found in the Simpson desert, the lightest patch in the middle of figure 4.1a, north-west of Cameron Corner.

Comparing the mean slope (fig. 4.1b) to the bioregions in figure 3.4 (e.g. the orange Avon Wheatbelt in Western Australia) the croplands in the wheat-sheep zone (AVW, MDD, RIV, NSS) are clearly distinguishable with their low mean slope compared to surrounding higher rainfall zones. The temperate grasslands (MGD) and bare soil (SSD, CHC) have even lower mean slope values. These are also the regions with the highest range in slope and backscatter (see fig. 4.1d & 4.1e) suggesting a relatively clear seasonal cycle, as would be expected in the grass and croplands.

The high range of the ASCAT parameters in the Simpson Desert may be a result of occasional flash floods from the north that drain to Lake Eyre (the gridpoints with a range of ±12 dB south of Simpson Desert). Vegetation in this arid region will respond quickly changing the land cover from bare soil to vegetated for a short while. It could also indicate enhanced volume scattering from deeper soil layers, common for very dry soils.

The spatial pattern of the range in slope and curvature is quite similar. The generally arid regions with a high slope range are dominated by grass-like vegetation, including crops. Curvature is most sensitive to this type of vegetation as the relative contribution of either ground bounce or direct scattering from vertical plant constituents is more pronounced than over bare soil or evergreen forests.

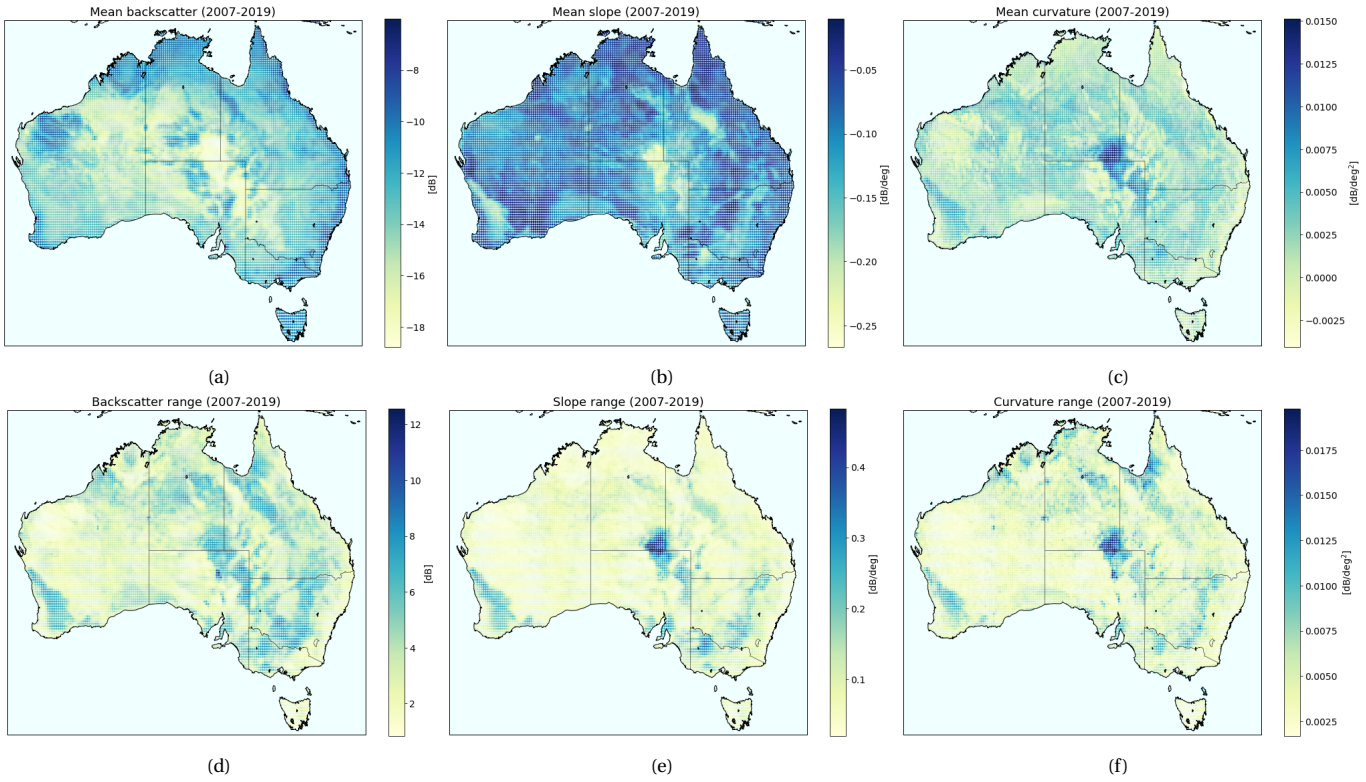

Figure 4.1: Mean and range of ASCAT parameters from 2007-2019

Figure 4.2 zooms in on the ROIs and shows the distribution of the mean and range of backscatter, slope and curvature for individual grid points in each ROI. The arid desert regions (SSD, CHC) clearly have the lowest backscatter values, and the tropical grasslands (CYP, ARP, NOK, blueish points) and evergreen forests (SEH, NNC, TWE, darkgreen points) have the highest mean backscatter, which is a result of high annual rainfall and subsequent soil moisture content.

Tropical grasslands and evergreen forest also have similar slope values, where the range across tropical grasslands is even lower than for forests. This is likely the effect of the high presence of trees in the ISBA vegetation type tropical grasslands (see section 3.2.1) and the fact that tropical vegetation usually exhibits less seasonality than vegetation in temperate climates, where the evergreen forests ROIs are located. For the range in backscatter, however, the inverse is true as the tropical grassland ROIs in the north of Australia have a more pronounced soil moisture seasonality due to monsoonal rainfalls, whereas the soil moisture in the more temperate climate of evergreen forests is likely to be more constant.

The distinction between evergreen forests and tropical grasslands is more evident in the curvature. The fraction of the dominant ISBA vegetation type in tropical grasslands on average is lower than in evergreen forests (0.75 and 0.95 resp.), which means the vegetation cover in CYP, ARP, and NOK is more heterogeneous. More specifically, they contain a higher fraction of grasslands (see figure 3.2), which generally have a higher curvature values than forests.

The curvature of the Mitchell Grass Downs (light green fig. 4.2c) is even more positive, as are the croplands, which mainly consist of winter crops and some grazing pastures. Both the mean and range of the backscatter over the MGD is also similar to the croplands. The MGD slope, on the other hand, resembles the sparser vegetated arid bare soil ROIs, which is not surprising considering that more densely vegetated croplands are likely to have a higher biomass and vegetation water content, which is what drives the slope.

The distinct variation between dominant ISBA vegetation types, and particularly between translucent (crops and grasses) and non transparent (forests and bushes) vegetation is consistent with ear-

lier studies where scatterometer data is used to discriminate between regions with different dominant vegetation types (Wagner et al., 1999).

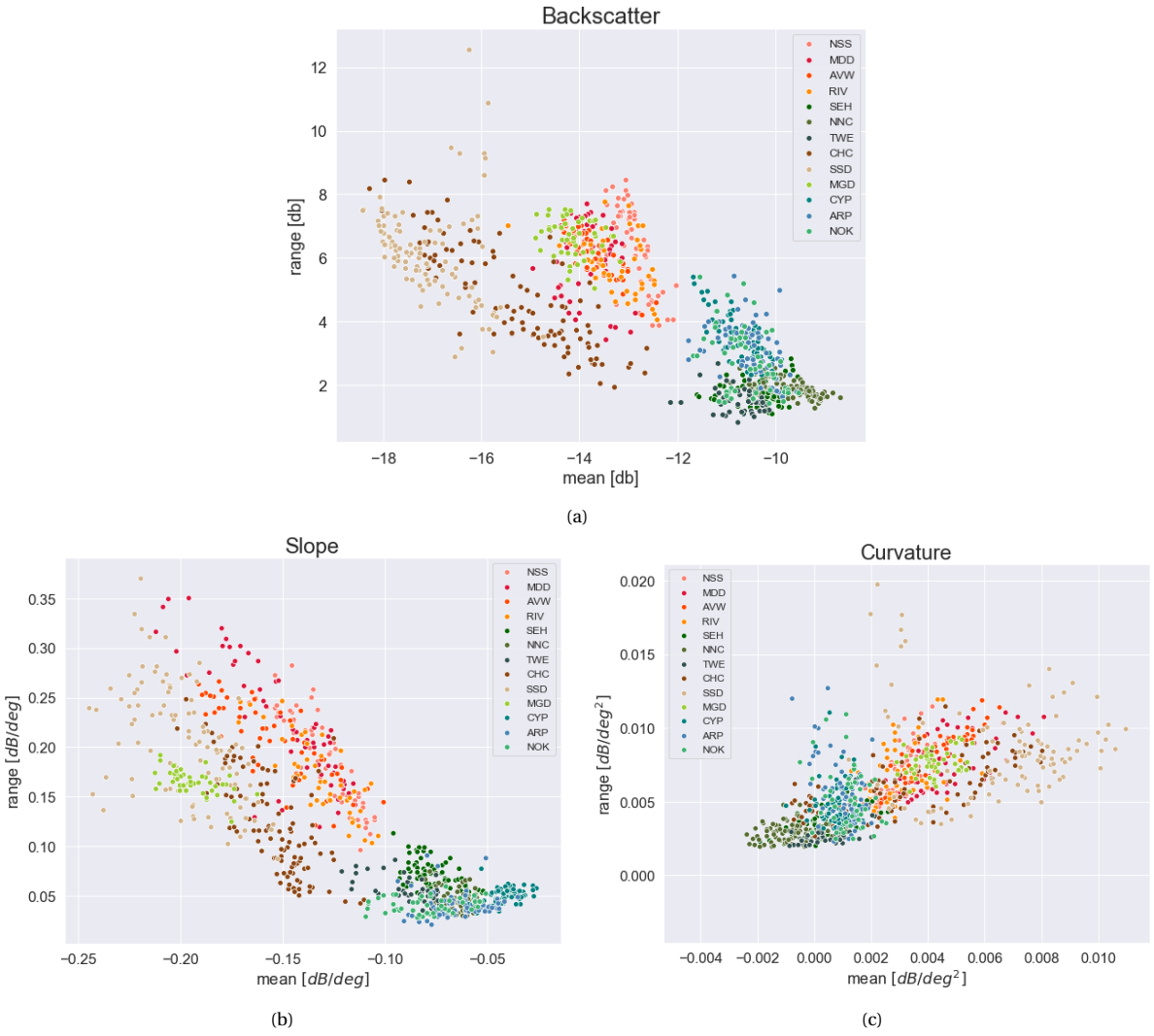

(a)

(b)

(c)

Figure 4.2: Mean and range of ASCAT parameters for each grid point in the ROIs. Red/orange are croplands, darkgreens are forests, tan/brown are bare soil, light greens are temperate grasslands, and blueish are tropical grasslands.

4.2. Seasonal climatology

Having looked at the difference in distribution of mean and ranges across the different vegetation types, this section describes the seasonal cycles of σ^o_{40} , σ' and σ''. Since ROIs within a vegetation type often resemble each other only one ROI per dominant vegetation type is evaluated here. Figures of the additional ROIs can be found in appendix B. The figures of the seasonal cycles are accompanied with a σ^o - θ plot with some key dates highlighted to better explain the change in ASCAT parameters throughout the year.

4.2.1. C3 crops

Figure 4.3a shows the seasonal climatology of the Murray Darling Depression. It has a distinct wet season, approximately from day 120-300. The σ^o_{40} signature is very similar to the surface soil moisture, with the exception of a small peak in σ^o_{40} around day 300. This peak coincides with the peak in slope, meaning that the σ^o_{40} value has a large contribution from vegetation water content, which is why it deviates from the soil moisture signal.

The vegetation (middle panel fig. 4.3a) peaks in the SH-spring, slightly after the soil moisture peaks, as expected for predominantly winter crops. During the growing season slope follows the same pattern as LAI and GPP, but lags slightly behind. This is likely due to the fact that ISBA simulates the annual cycle of crops in the same way it does natural vegetation and does not take into account exact harvesting dates, whereas slope is calculated from observed backscatter (Moigne, 2018). Interesting to note is that prior to the growing season the slope dips considerably, which is a feature not seen in LAI or GPP.

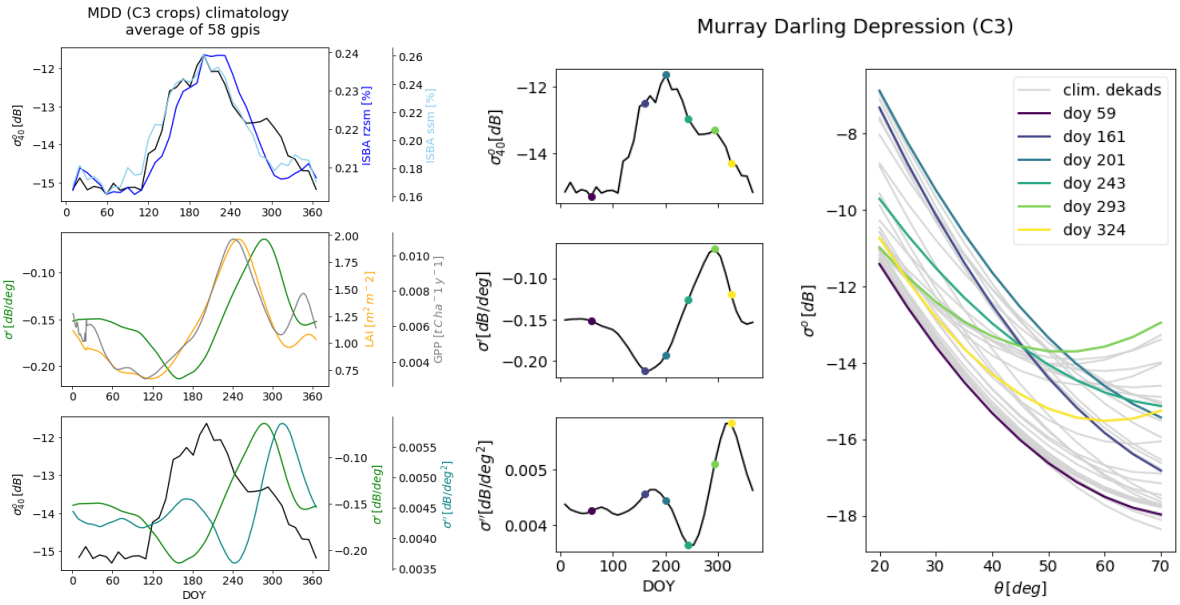

(a) Top panel: soil moisture related variables. Middle panel: vegetation related variables. Bottom panel: ASCAT parameters.

(b) Climatology of σ^o_{40} , σ' and σ'' with key dates highlighted in the σ^o - θ curve. Each line represents a dekad.

Figure 4.3: Seasonal climatologies across the Murray Darling Depression, one of the C3 cropland ROIs.

The similar seasonal cycle and lag between σ'' and σ' can be explained by their sensitivity to the phenology and changes in vegetation structure of winter crops like wheat and barley. During the tillering phase, as the plants start to emerge, around doy 160, backscatter is still dominated by direct scattering from soil moisture (Mattia et al., 2003). Hence the steep dark blue curve with high σ^o values in figure 4.3b. As the wet biomass increases, which is in large due to stem elongation, the slope increases and the σ^o - θ curve flattens as the soil return signal is increasingly attenuated at lower incidence angles, and volume scattering starts to dominate. Around doy 290 the biomass is at its peak, at the formation of the heads. The backscatter minimum around 50°at this point (light green line fig. 4.3b) is the result of a change in dominant scattering mechanisms. At lower incidence angles scattering involving

a ground bounce term is dominant. However, as the incidence angle increases, this ground bounce term becomes insignificant due to the vertically polarized waves that couple with the vertical structure of the wheat stalks (Stiles et al., 2000). In addition, direct scattering from the upper portion of the stalk and the grains, which are rich in water content, increases with increasing incidence angles. This leads to a minimum of the σ^o - θ curve around 50°and a curving upwards at higher incidence angles, as was observed by Mattia et al. (2003) and Stiles et al. (2000). After heading, as the vegetation water content decreases, and in this case soil moisture decreases too, the sensitivity to ground scattering from soil moisture increases. This leads to a sharp decrease in backscatter at low incidence angles, whereas the interaction of the microwave signal with the vertical stalks still dominates at higher incidence angles, resulting in the peak in σ''(yellow line fig. 4.3b). The ability to describe the growing season of wheat so neatly with the combined seasonal cycles of slope and curvature at this spatial resolution is encouraging.

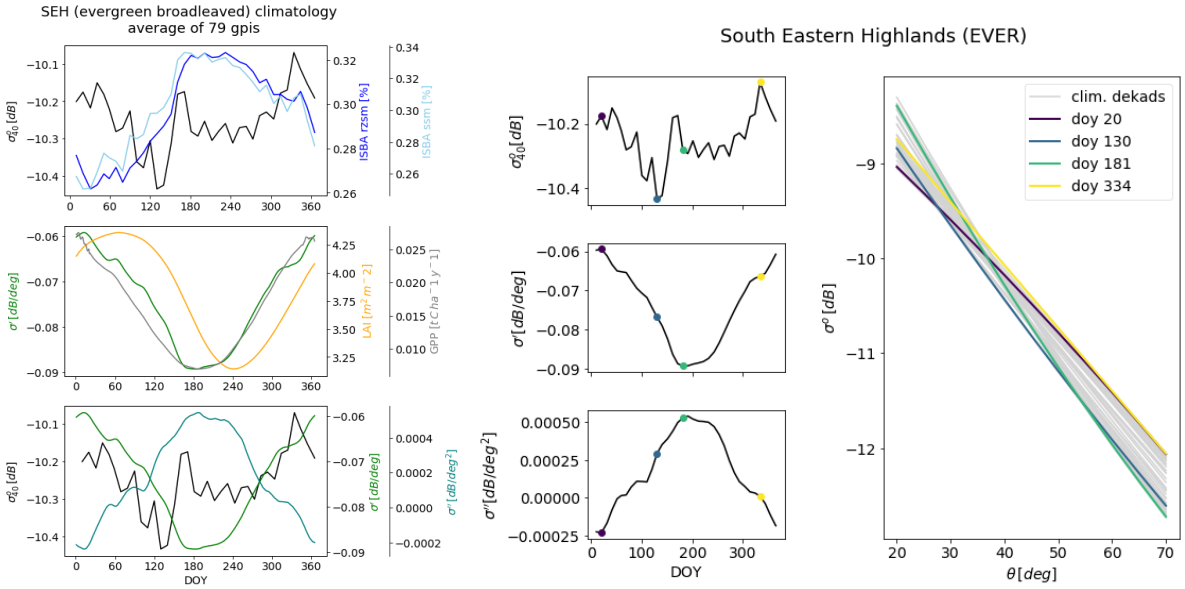

(a) Top panel: soil moisture related variables. Middle panel: vegetation related variables. Bottom panel: ASCAT parameters.

(b) Climatology of σ^o_{40} , $\sigma'$and $\sigma''$with key dates highlighted in the σ^o - θ curve. Each line represents a dekad.

Figure 4.4: Seasonal climatologies across the South Eastern Highlands, one of the evergreen broadleaf forest ROIs.

4.2.2. Evergreen broadleaved forests

Seasonal variations in σ^o_{40} , $\sigma'$and $\sigma''$are generally small over evergreen forests. Figure 4.4a shows that the range in σ^o_{40} climatology is only 0.3dB and its seasonal cycle is also significantly different from root zone and surface soil moisture, which have a more distinct wet season. This dissimilarity is likely due to the fact that over dense forests the microwave signal attenuates before reaching the soil, and the backscatter signal is dominated by vegetation water content, or interception at the top of the forest canopy.

Though there appears to be a clear seasonal cycle in the slope, its magnitude is really small compared to grass-like vegetation. This is evident in the compact and almost linear σ^o - θ curve in figure 4.4b, meaning dominant scattering mechanisms are the same all year long at all incidence angles. This stable backscatter signal is typical for evergreen forests. The limited variation in slope could be attributed to small phenological changes in leafy biomass, whereby the σ^o - θ relation changes from slightly convex to linear throughout the year. Consequently the curvature becomes inversely related to the slope.

The seasonal variations in LAI and GPP are larger than in slope when compared to other vegetation types. This highlights a perhaps trivial point in this study that though the slope is often said to be a measure of vegetation density, it is ultimately a measure of different scattering mechanisms induced by vegetation. Nonetheless, in this case it is apparent that slope is more strongly driven by the

woody water content, which is more closely related to the faster reacting GPP than leaf emergence or vegetation greenness (Vreugdenhil et al., 2017). Hence why the LAI cycle lags behind the slope and GPP.

4.2.3. Temperate grasslands

The Mitchell Grass Downs is a region with relatively low vegetation density, dominated by tussock grasses, which is why backscatter correlates fairly well with soil moisture. It is a dry semi arid region, with a distinct wet season influenced by summer monsoons from the north, and otherwise low backscattter and soil moisture values from doy 120 onwards.

Slope, LAI and GPP all have a very similar seasonal cycle due to the fact that the production of biomass is all in the form of leaf-like structures, with no woody components. The slope, LAI, and GPP also follow the peak in soil moisture much faster than over croplands. This is because in an otherwise dry climate, grasses well tend to bloom rapidly in response to a rainfall event (Jones et al., 2012). The curvature values are all positive too, consistent with what Steele-Dunne et al. (2019) found in North American grasslands, though the signal is not as smooth as over croplands.

Looking at figure 4.5b and comparing the σ^o - θ curve with croplands it is clear that the intra-annual variation, especially at lower incidence angles where direct scattering from the soil dominates, is much smaller across these grasslands. At higher incidence angles, however, the presence of vegetation and consequent volume scattering becomes evident as the dark blue and purple lines, which are clearly higher due to increased soil moisture content, start to curve.

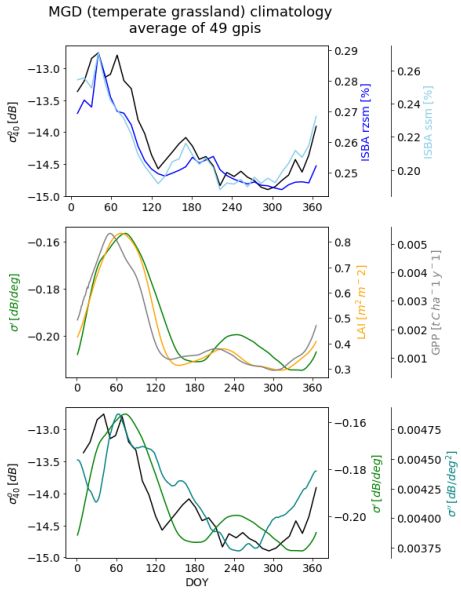

(a) Top panel: soil moisture related variables. Middle panel: vegetation related variables. Bottom panel: ASCAT parameters.

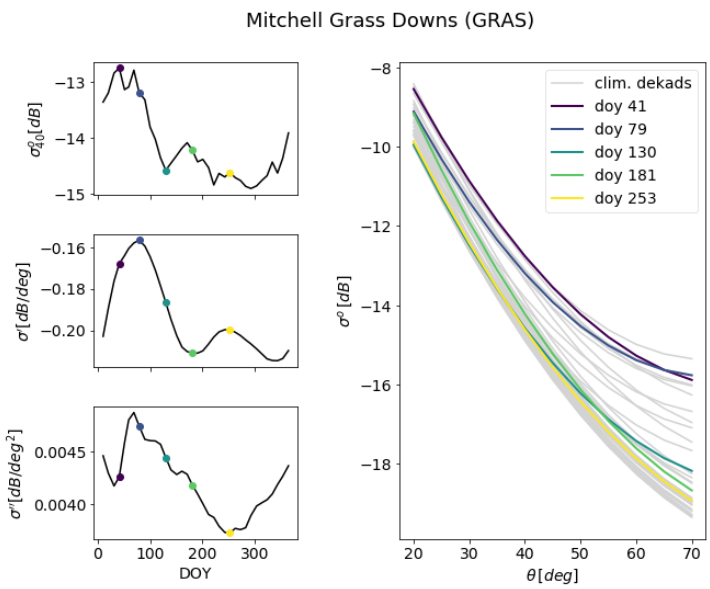

(b) Climatology of σ^o_{40} , σ' and σ'' with key dates highlighted in the σ^o - θ curve. Each line represents a dekad.

Figure 4.5: Seasonal climatologies across the Mitchell Grass Downs, the temperate grassland ROI.

4.2.4. Tropical grasslands

The tropical grasslands are woody savannas in the north of Australia, with a distinct summer monsoon in an otherwise fairly dry climate. The seasonal cycles across the Arnhem Plateau shown in figure 4.6a have high slope values, comparable to evergreen forests, but the timing is inversed due to the wet season occurring in SH-summer instead of winter. The range in the seasonal cycle of σ' is also similar to evergreen forest, indicating that vegetation is stable throughout the year, which can be expected in tropical regions. This is also evident from the σ^o - θ relation in figure 4.6b. Variations are even slightly larger at low incidence angles than at high incidence angles underscoring that fact that changes in the σ^o - θ relation are dominated by changes in soil moisture rather than phenology.

The magnitude of the GPP climatology is similar to evergreen forests but the LAI is lower indicating the foliage is not as dense as over forests. This is further emphasized by high cover fraction of grasses, and the positive curvature. The slight changes in curvature throughout the year from a convex to a concave curve in figure 4.6b could be ascribed to small seasonal fluctuations tree foliage, as a direct result of available plant water. Hence the curvature is also directly out of phase with σ^o_{40} climatology. Nonetheless the mix of grasses and trees makes adequately interpreting the ASCAT signal more challenging.

Finally, looking at appendix B the seasonal signal in curvature is roughly the same for all tropical grassland ROIs, whereas the slope varies more. The opposite is true for evergreen forests.

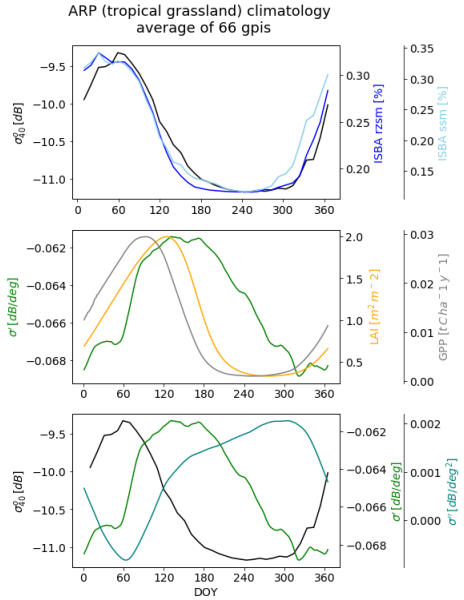

(a) Top panel: soil moisture related variables. Middle panel: vegetation related variables. Bottom panel: ASCAT parameters.

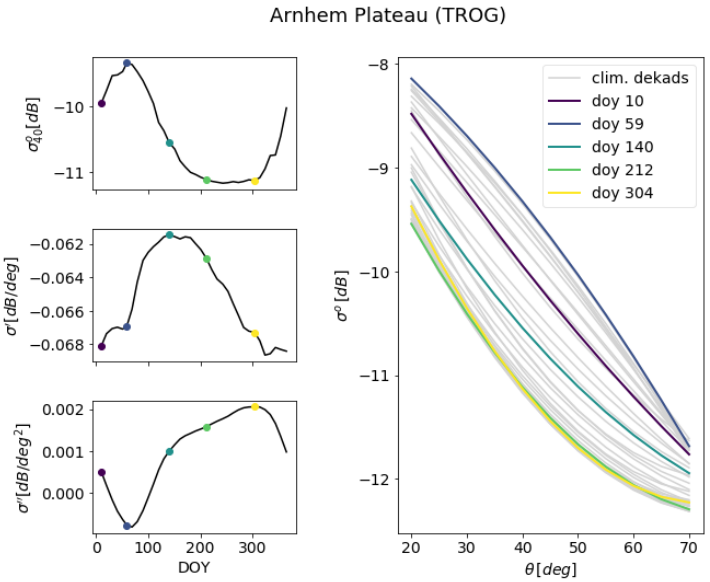

(b) Climatology of σ^o_{40} , σ' and σ'' with key dates highlighted in the σ^o - θ curve. Each line represents a dekad.

Figure 4.6: Seasonal climatologies across the Arnhem Plateau, one of the tropical grassland ROIs.

4.2.5. Bare soil

Though bare soil is technically not a vegetation type it is an abundant land cover type in Australia. The climatological values of the variables from the land surface model in figure 4.7a are indicative of a desert like region, and the σ^o_{40} values are low too. However, the Simpson Desert and to a larger extent Channel Country (see appendix B) are known to experience rare flooding events due to rain prolonged extreme rainfall to the north. Consequently these arid regions can become rapidly vegetated. The small fraction of tropical grassland, as seen in figure 3.2 supports this. However, a seasonal climatology constructed from a relatively short (13 years) time series with prolonged positive or negative anomalies should be interpreted with care, especially if the magnitude of the climatology is small compared to the anomalies, which is the case here. As can be seen in figure 4.7b and the time series in section 4.3 the seasonal cycle is really insignificant. Hence the slope and curvature climatologies are actually a construct of large anomalies in the time series.

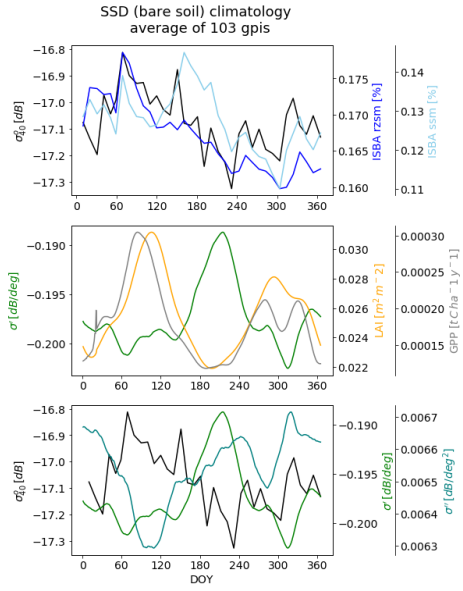

(a) Top panel: soil moisture related variables. Middle panel: vegetation related variables. Bottom panel: ASCAT parameters.

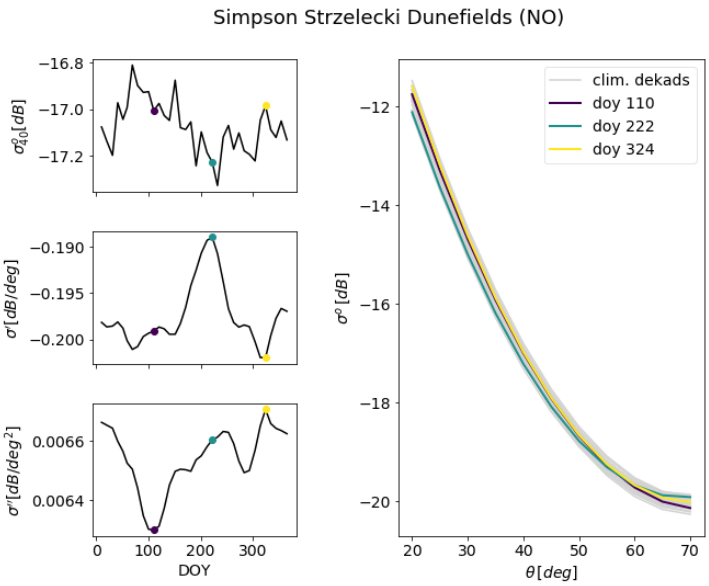

(b) Climatology of σ^o_{40} , σ' and σ'' with key dates highlighted in the σ^o - θ curve. Each line represents a dekad.

Figure 4.7: Seasonal climatologies across the Mitchell Grass Downs, one of the bare soil ROIs.

4.3. Drought response

This section looks at the full time series from 2007-2019 to analyse the response of σ^o_{40} , σ' and σ'' in and around drought events. The results shown here are for the same ROI as in the previous section, and the results for the other ROIs can be found in appendix C. Two types of plots are produced that show the anomalies in two different ways to appreciate the magnitude and the timing of the anomalies. The first (a) shows the anomalies shaded (lightgrey=positive, red=negative) as the difference between the observed. This allows to accurately see when the anomaly takes place in the seasonal cycle, and, for example, how large the impact of this anomaly is on the next season. The second figure (b) shows panels with time series and anomalies of soil moisture related, vegetation related, and ASCAT parameters so that the timing and magnitude of these can be more easily compared amongst each other.

As mentioned in chapter 3.3.3 the drought events are primarily defined to highlight the worst anomalies in ISBA root zone soil moisture in the 13 year data record. Rather than isolating the individual droughts events and studying those, the time series are studied in their entirety because an anomaly in any of the variables, preceding or succeeding the actual drought event, can be equally valuable to interpret the vegetation dynamics. Looking at the entire time series also allows to better appreciate the relative magnitude of the seasonal cycles compared to the anomalies.
The timing of the drought events can also play an important role in whether a soil moisture anomaly propagates into a vegetation anomaly. Hence the drought events in the figures in this section are highlighted slightly different depending on whether they occur in SH-summer or SH-winter.

4.3.1. Drought signal in backscatter

In this chapter the root zone soil moisture from ISBA is used to define droughts. This is because we are interested in the effect a soil moisture deficit has on vegetation, and whether this can be picked up by the dynamic vegetation parameters slope and curvature, and root zone soil moisture determines the available water for plant growth. Appendix A shows that the droughts defined based on ISBA root zone soil moisture visually compare well to the droughts identified by the BOM using rainfall deciles. Multiple studies have also proven the worth of ASCAT in detecting soil moisture droughts, though these have all been based on the surface soil moisture retrieved through the TU Wien Soil Moisture Retrieval algorithm, or on the SWI, which is estimated from this surface soil moisture (Baik et al., 2019; Gouveia et al., 2009). However, Schroeder et al. (2016) also showed the ability to monitor droughts directly with backscatter by showing consistent spatial and temporal patterns between σ^o_{54} anomalies and the U.S. Drought Monitor. The potential to monitor droughts directly with σ^o_{40} is reaffirmed here in figure 4.8.

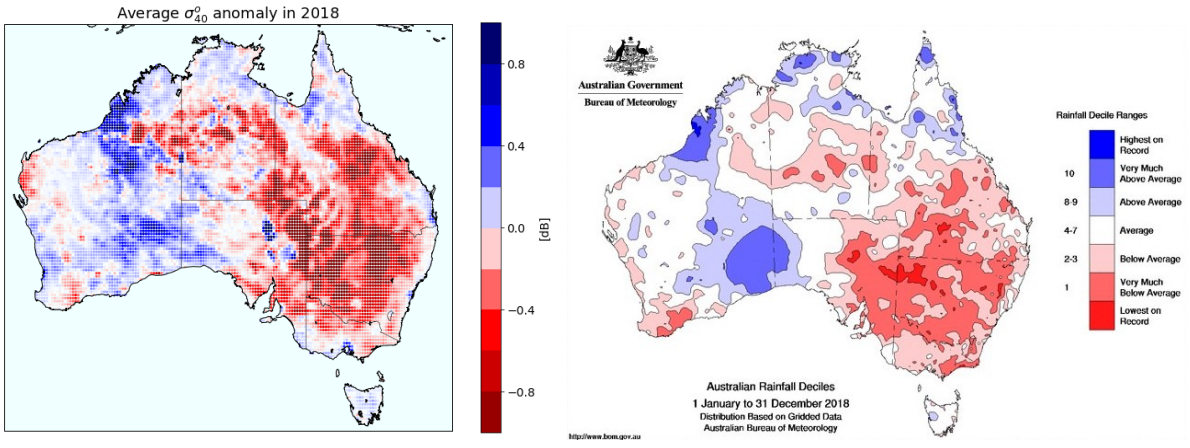

(a) (b)

Figure 4.8: σ^o_{40} anomaly and rainfall deciles from the BOM averaged over 2018

The reason the σ^o_{40} anomalies in figure 4.8 resemble the rainfall deciles so well is that σ^o_{40} , which is largely governed by the soil moisture in the top cm of soil, is a more close and direct representation of antecedent rainfall conditions than the deeper and slower responding root zone soil moisture.

4.3.2. C3 crops

The three longest drought events in the Murray Darling Depression are in 2011, 2013, and 2018 (see fig. 4.10a). The 2011 drought occurs due to a root zone soil moisture deficit in the rising limb of the wet peak. However, the influence on σ' is minimal with no negative anomalies present, even in the next season. The large positive slope anomaly prior to the drought due to unusually high antecedent soil moisture conditions in early 2011 appears to be large enough to bridge the effect of the drought in slope. The mechanisms driving slope appear to have a longer 'memory' than LAI and GPP, which do develop a negative anomaly as soon as the drought starts in 2011. This could perhaps be expected since these are outputs from the same land surface model that simulates soil moisture.

Looking at the slope, LAI and GPP anomalies in figure 4.10b (panel 4) the slope anomalies are slightly lagged behind LAI and GPP, just like their seasonal climatologies. This is also the case for all other C3 crop ROIs in appendix C. As mentioned before, this likely due to the strong anthropogenic influence on croplands, which is not taken into account by ISBA.
The large positive anomaly in LAI and GPP that follows from the unusually high wet season in 2016 also highlights the non-linear relation between σ' and LAI and GPP. Compared to the magnitude of their seasonal cycle the anomaly in LAI and GPP is almost twice as large, whereas for slope the positive anomaly is only half the magnitude of the seasonal cycle (fig. 4.10b, panel 4).

The 2013 and 2018 droughts both occur in the low soil moisture season. Though these have a delayed impact on the slope, figure 4.10b (panel 4) shows that the σ' anomalies are not as large as, for example, after the droughts in end 2014 and 2015. These droughts, which are of shorter duration, cause a larger slope anomaly because they occur in the rising limb of the increase in vegetation biomass. This shows that the seasonality of the drought is equally important in the propagation from a soil moisture to a vegetation anomaly.
Moreover, the fact that a small soil moisture anomaly at the end of 2016, despite a very wet season, propagates into a σ' anomaly, but the drought at the end of 2007 does not underlines the fact that antecedent conditions play a large role in drought propagation. It is likely the vegetation in 2016 is still vulnerable from the deficits in 2015, and has not fully recuperated, despite the large wet season. This also highlights the difficulty in studying individual drought events because the effect of a single drought event cannot be viewed separately from potential anomalies occurring prior to the drought.

Across C3 croplands, positive anomalies in curvature tend to be associated with negative anomalies in slope and backscatter, and vice versa. Thus, in periods of drought the curvature will tend to be even more positive. This is similar to the drought response Steele-Dunne et al. (2019) found across grasslands. Though vegetation density is lower than normal, hence the negative slope anomaly, direct scattering from the vegetation still dominates over the ground bounce term because the soil is so dry. This is illustrated in figure 4.9 which shows the σ^o - θ relation for the dekad when the curvature peaks in the 2015 drought. The orange line still curves at high incidence angles due to volume scattering effects from vegetation, but at lower incidence angles, where direct scattering from the surface dominates, backscatter decreases rapidly with increasing incidence angles because of a dry soil.
The opposite is true for the blue line which is much flatter, and as explained in section 4.2, even curves upward at high incidence angles due to the top of the wheat stalks being full of water. At lower incidence angles scattering from

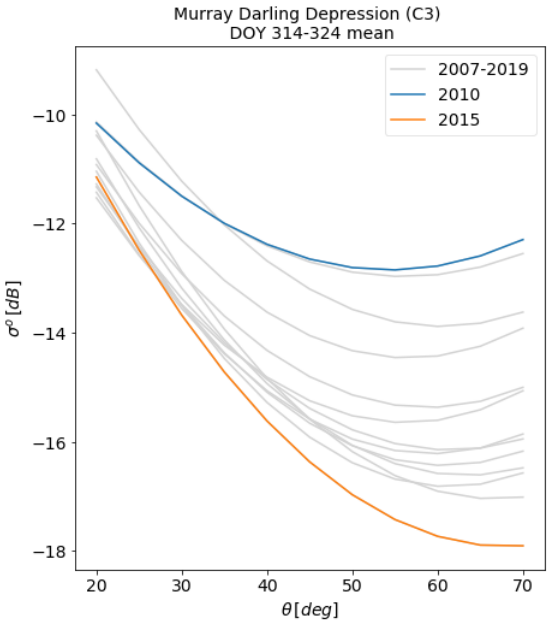

Figure 4.9: σ^o - θ relation for dekad from 10-20 Nov. Orange line is for a dekad in drought in 2015. The blue line is for a dekad with a large positive slope anomaly in 2010.

the underlying soil is also less sensitive to incidence angle because the vegetation is denser, and the soil is wetter.

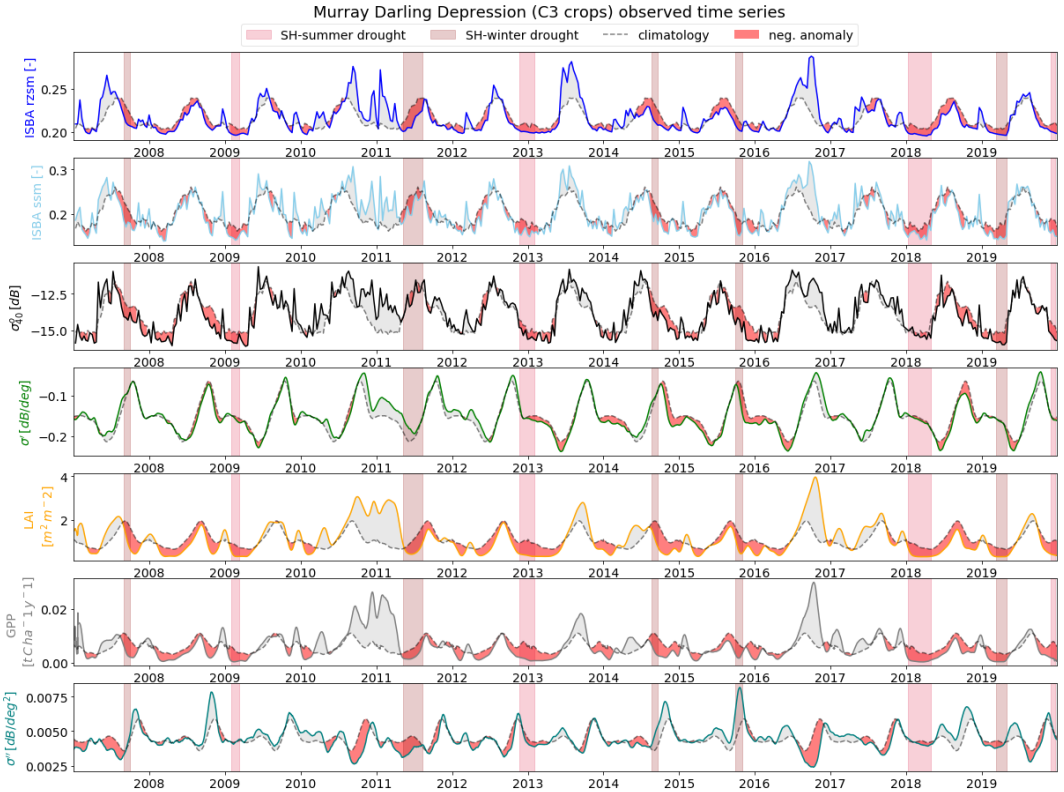

(a)

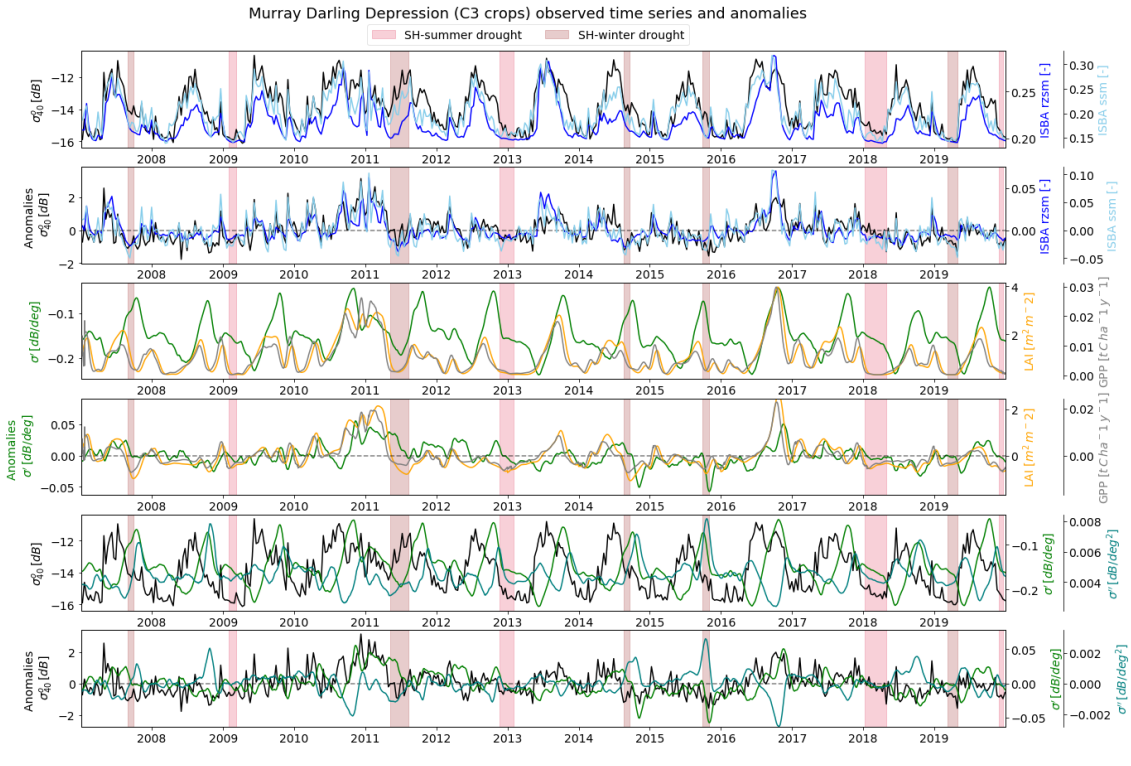

(b)

Figure 4.10: Murray Darling Depression (C3 crops) time series with anomalies and droughts highlighted

4.3.3. Evergreen broadleaved forests

The observed time series across the South Eastern Highlands contain a clear long term trend (see fig. C.4 in appendix C). Usually, in the absence of a clearly visible long term trend, the anomalies in the time series are not further distinguished because separating what are long term and short term anomalies is rather arbitrary. However, when a long term trend is apparent, it can be useful to detrend the time series to better study and compare the anomalies in the different variables.
The figures 4.11a and 4.11b show the time series with the trend removed from the anomalies, and added to the seasonal cycle. The separate long term trend is shown in figure 4.12. The anomalies at the time series edges are perhaps more artificial because of the need to extrapolate the trend in the first and last six months of the time series (see methodology in section 3.3.2). It is good to keep in mind, however, that the actual anomalies are really a sum of both the short and long term variations.

From figure 4.12 it is obvious that all the land surface model variables have roughly the same trend. The trend in σ^o_{40} to some extent also follows the same pattern. Looking at σ^o_{40} in figure 4.11b, that the seasonal cycle is minimal compared to the anomalies, and also less pronounced compared to ISBA root zone and surface soil moisture. As discussed in section 4.2 this is because vegetation cover is fairly stable over evergreen forests, so the backscatter signal is more a measure of interception or dew on top of the canopy, rather than soil moisture. The fact that σ^o_{40} anomalies still align well with the soil moisture anomalies could be the simple result of the simulated soil moisture in ISBA being forced using the ERA5 climate reanalysis, and that over forests the backscatter may be even more directly related to rainfall.

As can be seen in the σ^o - θ curve in section 4.2 the variation in vegetation across evergreen forest is generally really small. Looking at the interannual variation in figure 4.11, the long term σ'trend has a range of ±0.02 dB/deg, similar to the seasonal cycle. In terms of the σ^o - θ relation this translates to minor changes in the slope, possibly as a result of a slightly more or less dense canopies over the years. Looking at the remaining short term anomalies in figure 4.11a these are really high frequency fluctuations, unlikely to be related to the variations in σ^o_{40} as the wet biomass in evergreen forests generally doesn't directly increase after a rainfall event. It is more feasible that these short term fluctuations are a result of the kernel window used to smooth the slope and curvature signal, rather than actual fluctuation in vegetation dynamics. Recently, Steele-Dunne et al. (2021) showed that a shorter kernel window leads to considerably more short term fluctuations, as not enough local slope values are averaged to filter out the measurement noise, which incidentally also led to strongly reduced accuracy in the soil moisture retrieval. Though the effect on the ability of slope and curvature to accurately capture vegetation dynamics using different kernel windows remained mixed across broadleaf forests, Steele-Dunne et al. (2021) suggested that using smoother dynamic vegetation parameters yielded better results in the soil moisture retrieval algorithm. This means that in the case of this ROI the interannual variations, captured in the long term trend, are most interesting to study vegetation anomalies.

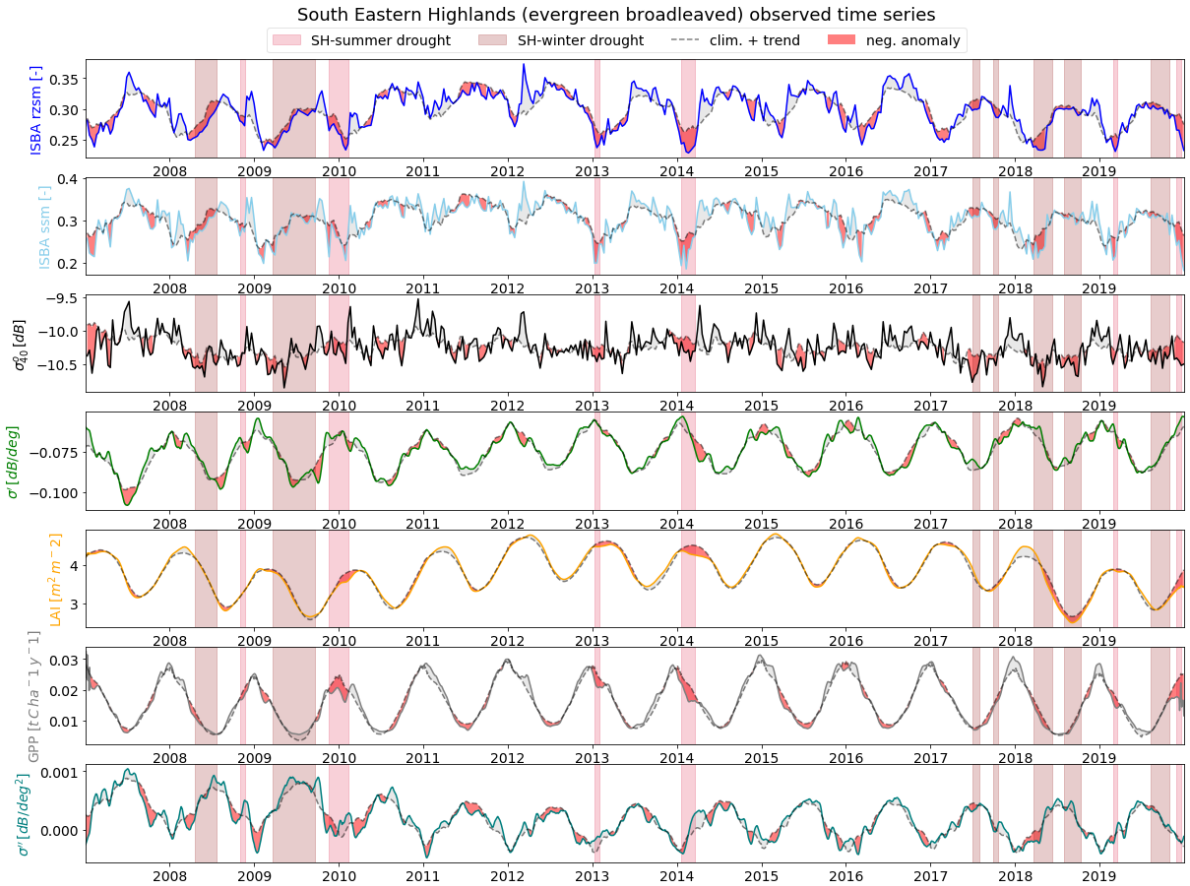

(a)

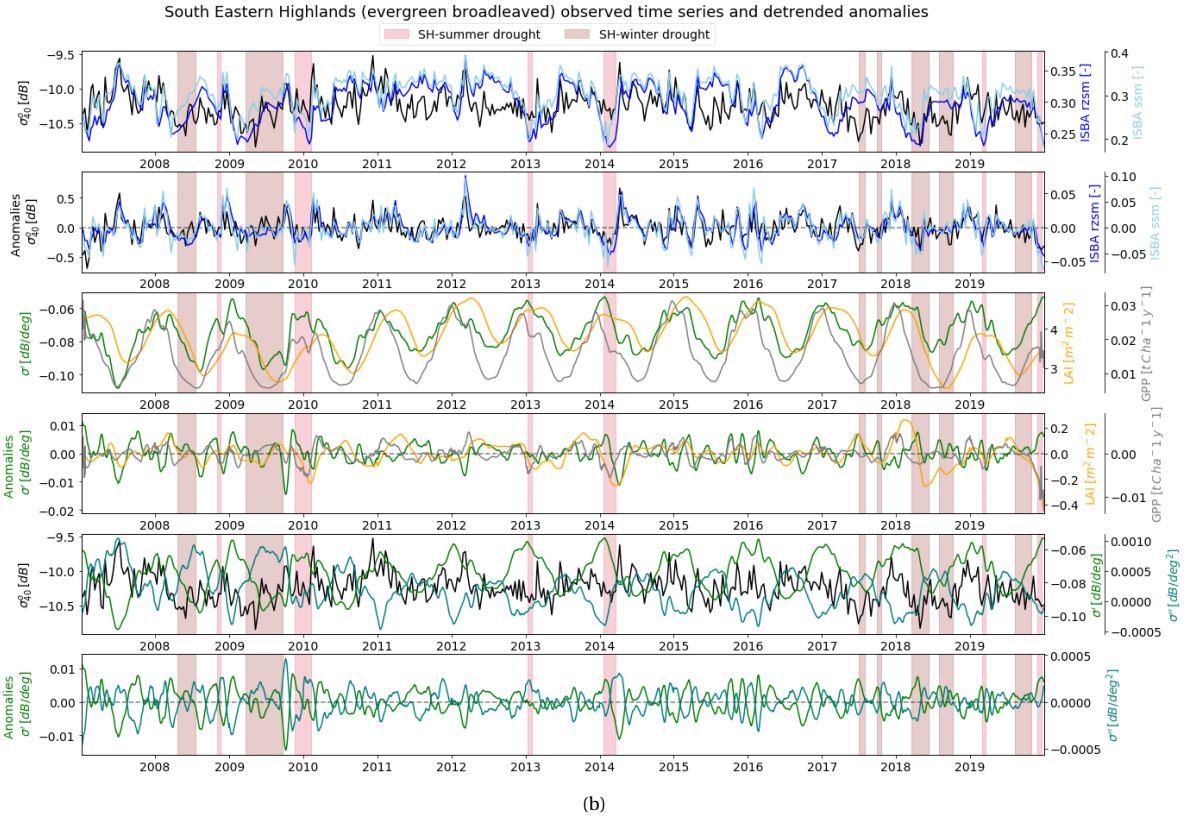

(b)

Figure 4.11: South Eastern Highlands (evergreen broadleaved forests) time series with the long term trend removed from the anomalies and added to the seasonal cycle

The difference in long term trend between LAI and GPP, and σ' and σ'' could possibly be the result of how the simulated root zone is defined in ISBA. As mentioned in chapter 3.1 the simulated root zone is only 1m deep, and has a uniform root distribution. However, Eucalyptus trees, which make up large portions of the forest, are known to have rooting depths that easily exceed 10m (Robinson et al., 2006). This can make a considerable difference in the vegetation's reaction to changes in soil moisture content. Looking at figure 4.12 LAI and GPP start to increase as soon as the root zone soil moisture starts to increase, whereas the rise in σ' is delayed until 2011. The dip in root zone soil moisture at the end of 2012 has clearly propagated to LAI and GPP, but is much more smoothed out in σ', and finally the strong decline in LAI and GPP from 2018 onwards is barely visible in σ' and σ''. This is consistent with the notion that vegetation with a shallower root zone depth as simulated in ISBA will react much faster to soil moisture deficits than the observed forest. The slower reaction of Eucalyptus trees with a deep rooting depth can also explain why the σ' deficits are concentrated in 2007-2011 (see fig. C.4a). This is towards the end of the Millenium Drought, which affected most of southeast Australia from 2000-2010, and it is probable that towards the end of such a drought, even vegetation with deep rooting depths will be impacted significantly.

The difference in long term trends also makes it difficult to compare anomalies between variables, and difficult to follow the drought propagation from soil moisture to vegetation anomalies. The droughts in ISBA root zone soil moisture are all clearly concentrated in two periods (2009-2011 and 2018-2020) because of the simple fact that the other 8 years have a higher than usual soil moisture value. This is the drawback of using relatively short time series of 13 years to define droughts. The anomalies are easily overemphasized because they cannot be viewed in light of more historical records.

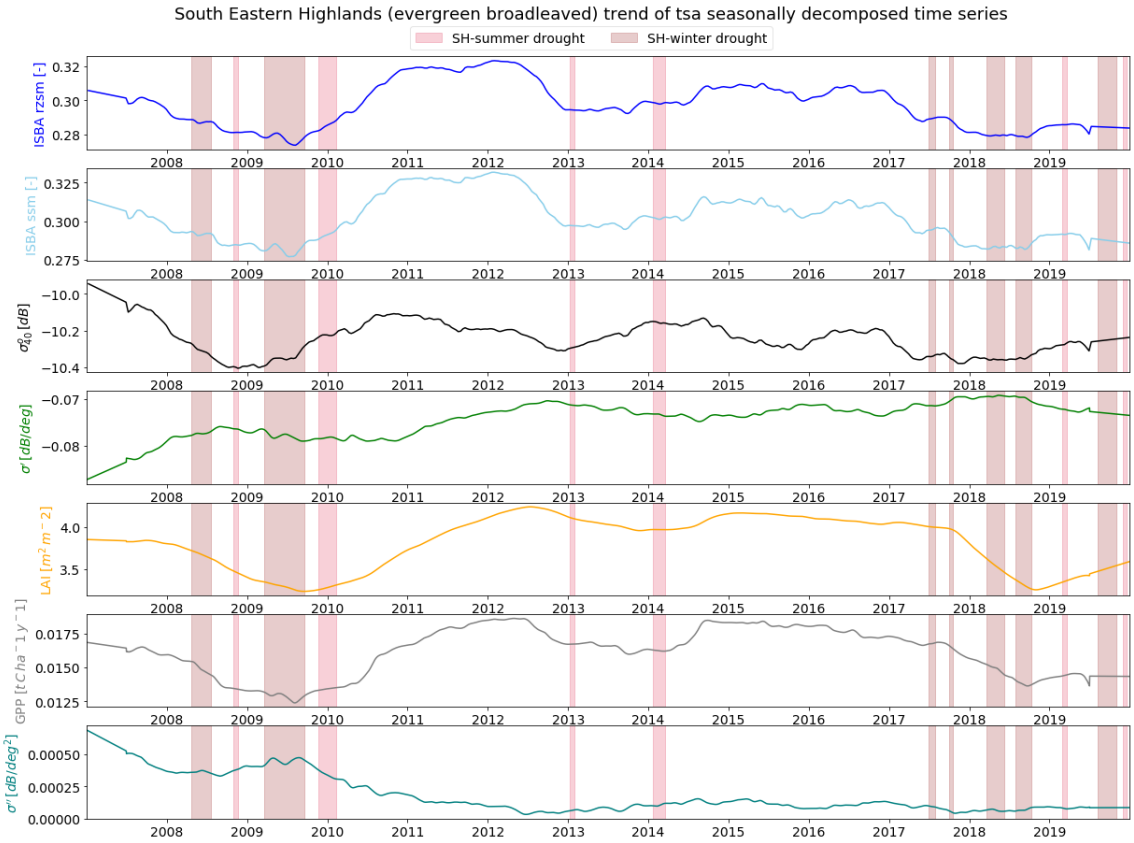

Figure 4.12: South Eastern Highlands (evergreen broadleaved forests) long term trend

4.3.4. Temperate grasslands

The Mitchell Grass Downs experience three major droughts, in 2013, 2015, and 2017. In most of the other years there also appears to be a consistent negative anomaly in the dry season in both soil moisture and vegetation parameters. This is because two 'out-of-season' wet peaks in 2007 and 2016 increase the climatological values of the dry season.

The negative anomalies in σ^o_{40} correspond well with the defined drought periods, and with ISBA soil moisture anomalies in general (see fig. 4.14a). This high sensitivity to soil moisture can be explained by less hindrance due to lower vegetation density compared to other vegetation types (e.g. slope ±-0.2 $[dB/deg]$ and LAI ±0.5 $[m^2m^{-2}]$). Looking at figure 4.14b (panel 5 & 6) the σ' time series and anomalies are also very similar to the σ^o_{40} , especially during the drought periods. This is because in (semi-) arid regions vegetation tends to respond rapidly to precipitation pulses (Jones et al., 2012). For herbaceous vegetation the accumulation of biomass and greening occur at roughly the same time, so the LAI and GPP anomalies are both similar to slope, with no consistent lag between observed and simulated paremeters due to anthropogenic influences like sowing dates. Thus, the strong dependence and rapid response of slope to changes in backscatter make σ^o_{40} and σ' relatively good indicators of drought propagation from soil moisture to vegetation anomalies.

At first sight the σ'' time series in figure 4.14b does not appear to have a consistent relationship with σ'. In 2009 and 2012, for example, the slope anomaly is largely positive all year long, but the curvature anomaly is for the most part negative in 2009, and positive in 2012. However, when looking at the combination of σ' and σ'' in the σ^o - θ relationship, the curvature gives insight into the dominant scattering mechanism, which is determined by the abundance of vegetation, which is in line with the findings of Steele-Dunne et al. (2019) in North American grasslands.
Looking at figure 4.14a, 2009, and especially 2012, are years with positive σ^o_{40} and σ' anomalies, indicative of high soil moisture content and vegetation density. The minimal difference between these two years in figure 4.13, beside higher σ^o values, is the curving at higher incidence angles. Hence, the presumably slightly higher vegetation water content that leads to stronger volume scattering at higher incidence angles in 2012 is enough to make the difference between a positive and negative curvature anomaly.

In contrast, in the drought events of 2015 and 2017 both years experience low backscatter values and low slope values as a result of dry soil with little vegetation. This is also evident from figure 4.13 where 2015 and 2017 are the lowest, and steepest curves. In 2015 the σ^o - θ line is practically linear, which is not surprising considering it's the third consecutive year with below average soil moisture conditions. Now comparing the year 2017 with 2009 it is apparent that, though at higher incidence angles the curves are fairly similar, at lower incidence angles the 2017 line is much steeper. This indicates strong dominance of surface scattering at most incidence angles. The slight curving at higher incidence angles could be due to the presence of some vegetation as a result of the positive slope anomaly in 2016, considering tussock Mitchell grasses are generally quite drought tolerant. Thus, looking at curvature values alone, 2012 and 2017 seem similar, but looking at them in combination with backscatter and slope values reveal the dominance of direct surface scattering in a dry and sparsely vegetated 2017, and more volume scattering in a wetter, more densely vegetated, 2012.

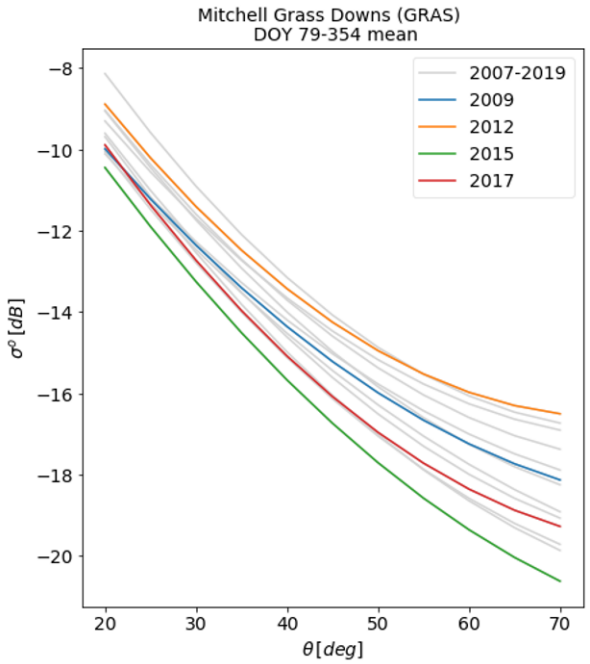

Figure 4.13: σ^o - θ relation averaged over the period of 20 Mar. - 20 Dec., corresponding to the duration of the 2015 drought event

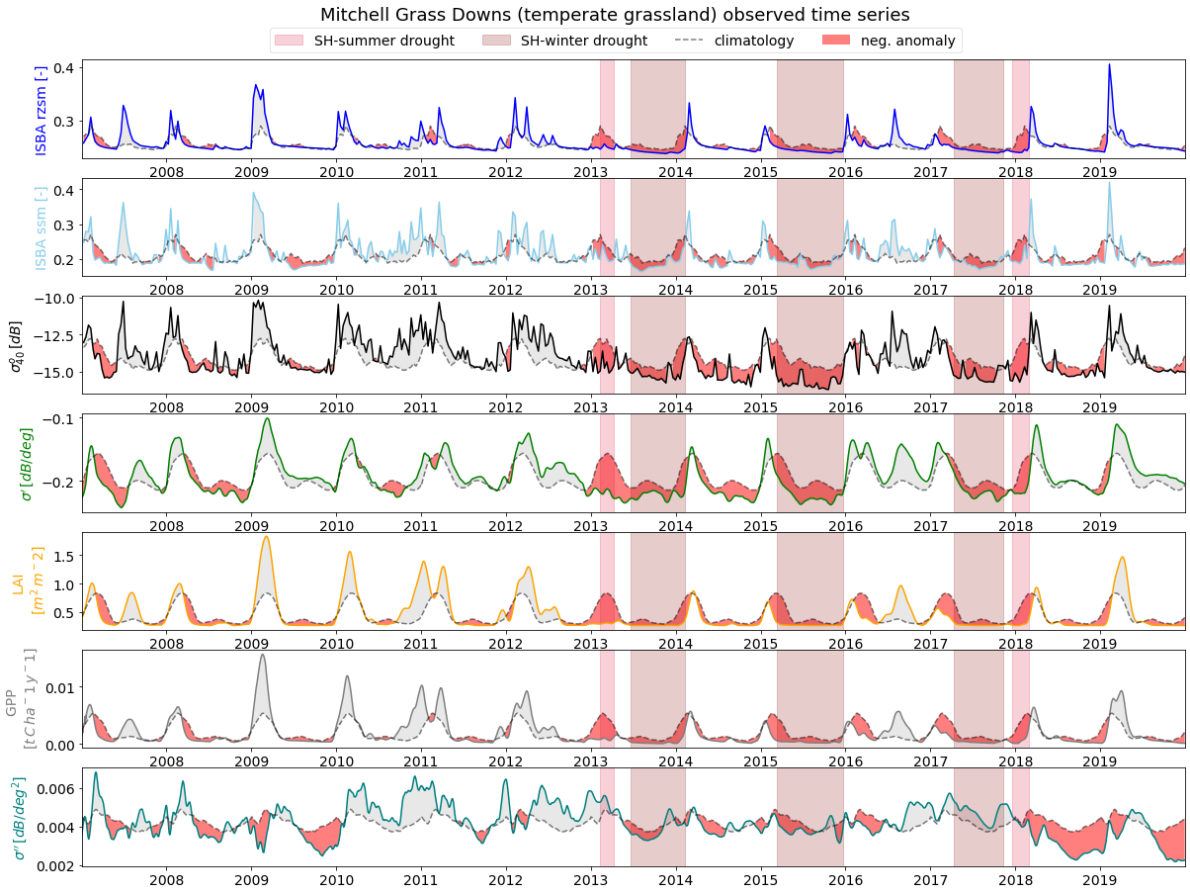

(a)

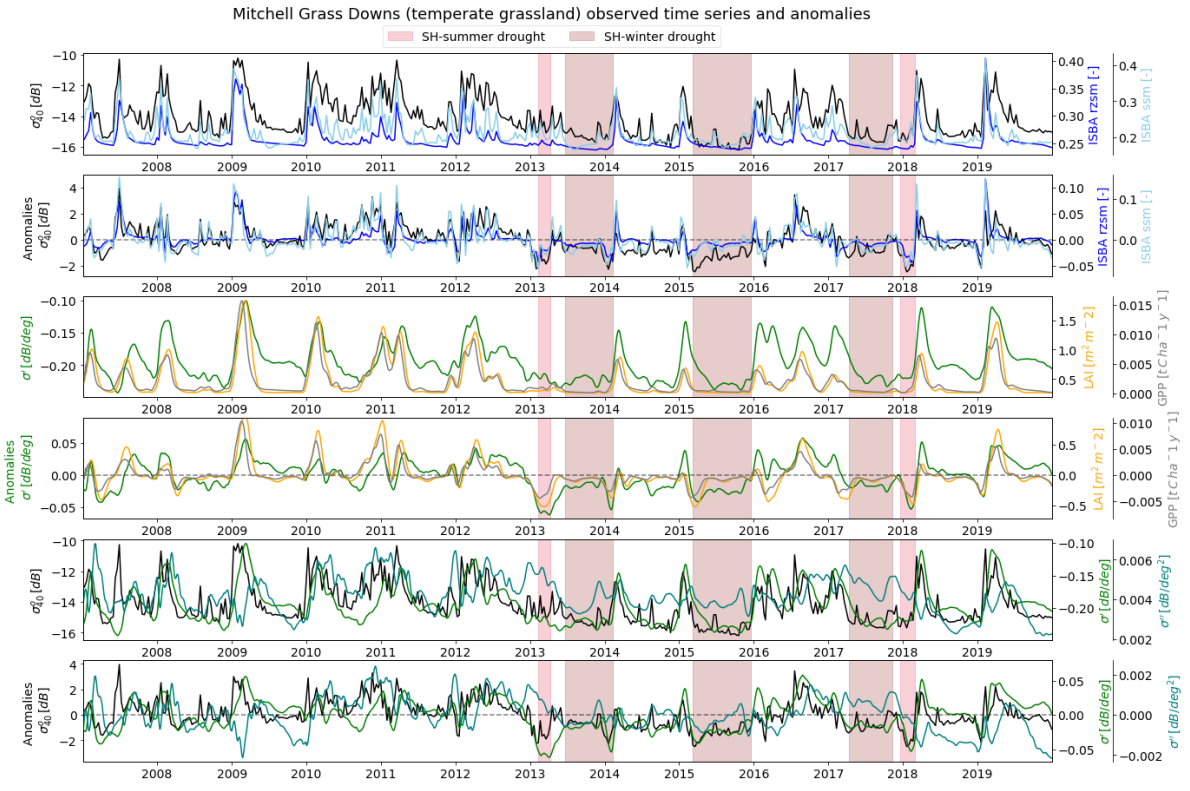

(b)

Figure 4.14: Mitchell Grass Downs (temperate grassland) time series with anomalies and droughts highlighted

4.3.5. Tropical grasslands

The Arnhem Plateau in northern Australia has a steady monsoonal climate with a very distinct wet season in an otherwise dry year. This makes that the defined drought periods occur frequently due to delayed onset or shorter length of the wet season.

The time series for this ROI have been detrended again because of a clear long term trend in slope (see fig. C.7a in appendix C). Looking at the trends in figure 4.16 all variables, except for the slope, have a similar trend (opposite sign for curvature). Comparing the anomalies of σ^o_{40} and σ'' in figure 4.15b and their long term trend shows that in both cases they are the exact opposite of each. The curvature has a really stable seasonal cycle, unlike in any other vegetation type, and appears to be strongly driven by σ^o_{40} . This means that sensitivity to soil moisture is high at almost all incidence angles and dominates changes in the σ^o - θ curve, irregardless of the season. This is plausible since vegetation density as observed in the slope is high but fairly constant throughout the year, typical for tropical climates. Remembering the climatological σ^o - θ relation in section 4.2 this translates to a change from a slightly concave to convex curve for low to high σ^o values.

Though there is a clear seasonal cycle in the slope, figure 4.15a shows that it is largely dominated by short term fluctuations. It is difficult to say whether these fluctuations, like in the South Eastern Highlands (evergreen forest), are a result of unsurpressed measurement noise due to not enough local slope values being averaged within the kernel window (Steele-Dunne et al., 2021). It could also be that these are actually due to short term changes in vegetation dynamics, since the typical short term fluctuations do follow changes in σ^o_{40} and are less apparent in curvature. Both the mean and the range of the σ' time series in figure 4.15a indicate tree cover, though it is known the understory is largely made up of grasses (see section 3.2.1). This could explain the rapid response to small pulses of increased moisture content.
The abundance of both trees and grasses in tropical grassland ROIs make it difficult to interpret the signal in ASCAT parameters. Within ISBA it is also recognized that the heterogeneity of this vegetation type makes it difficult to precisely calculate the vegetation fractions, which could explain the discrepancy between the simulated ISBA and observed ASCAT vegetation parameters (Moigne, 2018). The curvature is relatively similar for all tropical grassland ROIs(see also appendix C), but the timing of the slope peak, and how broad the peak is, varies considerably. And though the range in slope time series is small, the variations are highly dynamic. This indicates that the differences in vegetation primarily manifest themselves in vegetation density and above ground wet biomass, but are small enough to not greatly affect the relative importance of surface, volume, or multiple scattering effects on total backscatter.
Looking at the time series in figure 4.15a again this means that the vegetation water content in the canopy decreases near the end of the dry season, and even more so if the wet season is delayed, leading to a slightly higher sensitivity to underlying soil and grass understory.

Although the deviating long term trend in slope adds to the difficulty of comparing anomalies, it is an interesting feature. This type of interannual variation is typically a feature that can be observed using dynamically calculated σ' values, in contrast to using only climatological σ' values (Steele-Dunne et al., 2021). Such a long term trend could perhaps indicate a change in the dominance of certain vegetation cover, though this would have to be confirmed with more detailed (ground) observations.

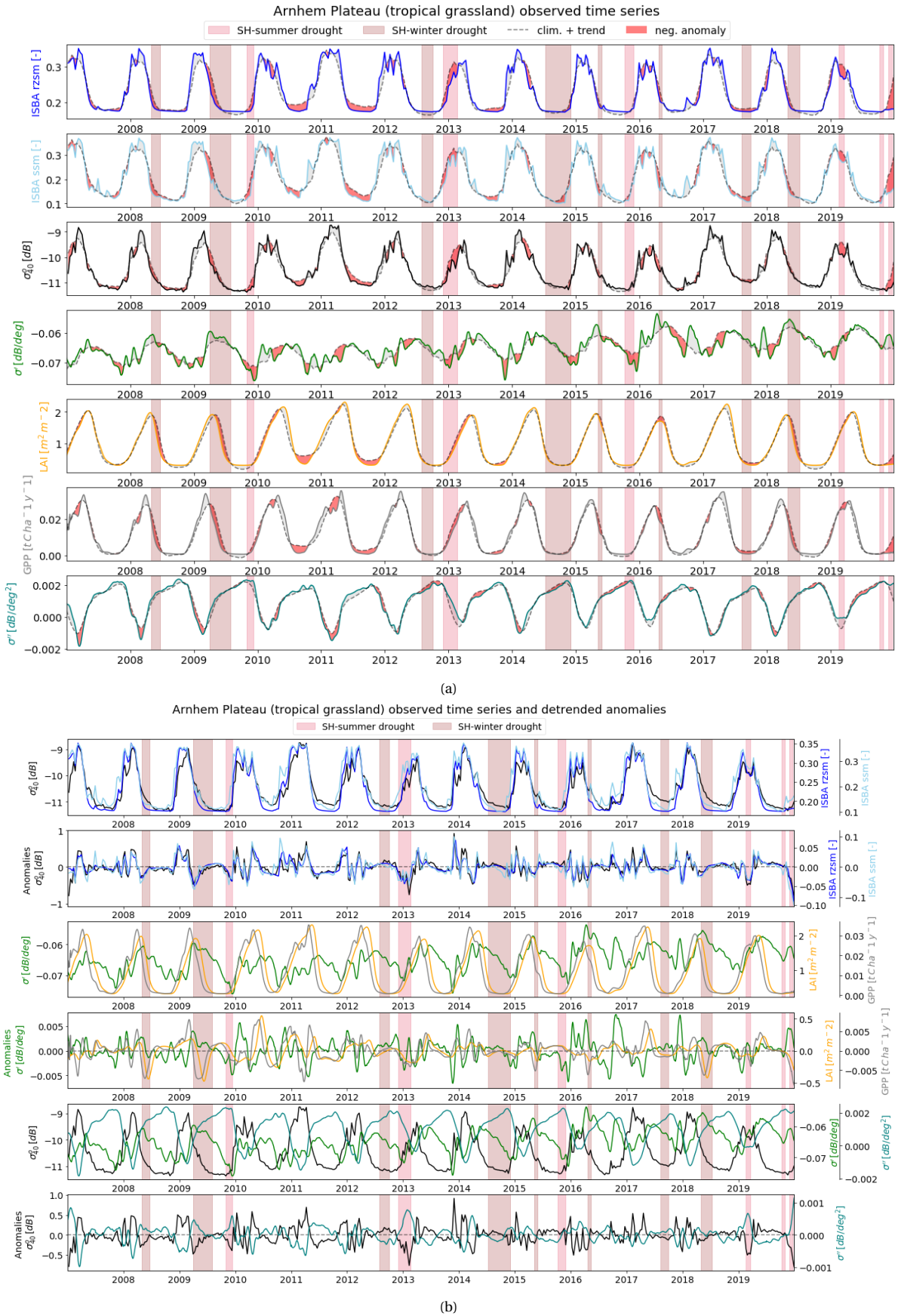

Figure 4.15: Arnhem Plateau (tropical grasslands) time series with the long term trend removed from the anomalies and added to the seasonal cycle

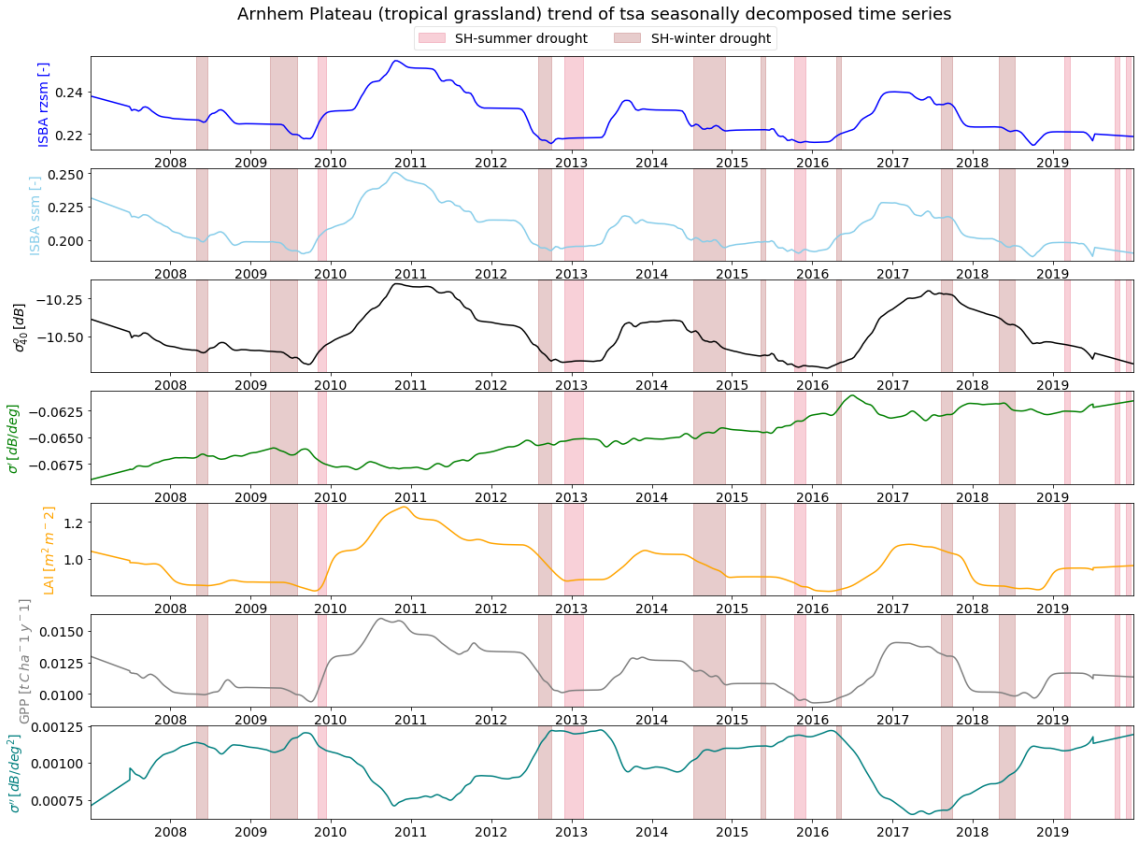

Figure 4.16: Arnhem Plateau (tropical grasslands) long term trend

4.3.6. Bare soil

The time series in figure 4.17 is made up of two extended periods of positive anomalies, interchanged with three prolonged negative anomalies. It is clear from this that the seasonality shown in section 4.2 is actually a construct of the interannual variation, as the seasonal cycle is negligible compared to the magnitude of the anomalies.

Sandy deserts are often problematic for accurate retrieval of σ' values due to the high variance in local slope (Hahn et al., 2017). However, in this case the slope appears to adequately capture the response of vegetation to a sudden increase in soil moisture content. This occasional sprouting out of vegetation in the Simpson desert as a result of heavy rainfall and flash floods to the north is a well known phenomenon. It is also in line with the observations of Vreugdenhil et al. (2017) that found good agreement between σ' and VOD across bare soil and sparsely vegetated areas in Australia.
The reason this region is marked as bare soil is because the LAI and GPP are practically zero. It could be that due to the highly variable nature of the vegetation in these arid regions the ECOCLIMAP database under estimates the vegetation content. Therein lies perhaps an opportunity to use ASCAT dynamic vegetation parameters to calibrate land surface models.

The particular bare soil ROIs investigated here resemble a very arid form of grasslands. Looking at the reaction of ASCAT parameters in and around drought periods it is very similar to the Mitchell Grass Downs. The σ' rises almost instantaneously due to increased σ^o_{40} values, and the σ'', when viewed in combination with σ', gives insight into the vegetation dynamics and the contribution of surface or multiple scattering effects.

As can be seen in appendix D the time series can easily be divided into a clear 'step-wise' long term trend which is far more important in this region than any short term fluctuations. Hence for sparsely vegetated regions the current calculation of ASCAT dynamic vegetation parameters appears to allow for sufficiently good monitoring of vegetation anomalies.

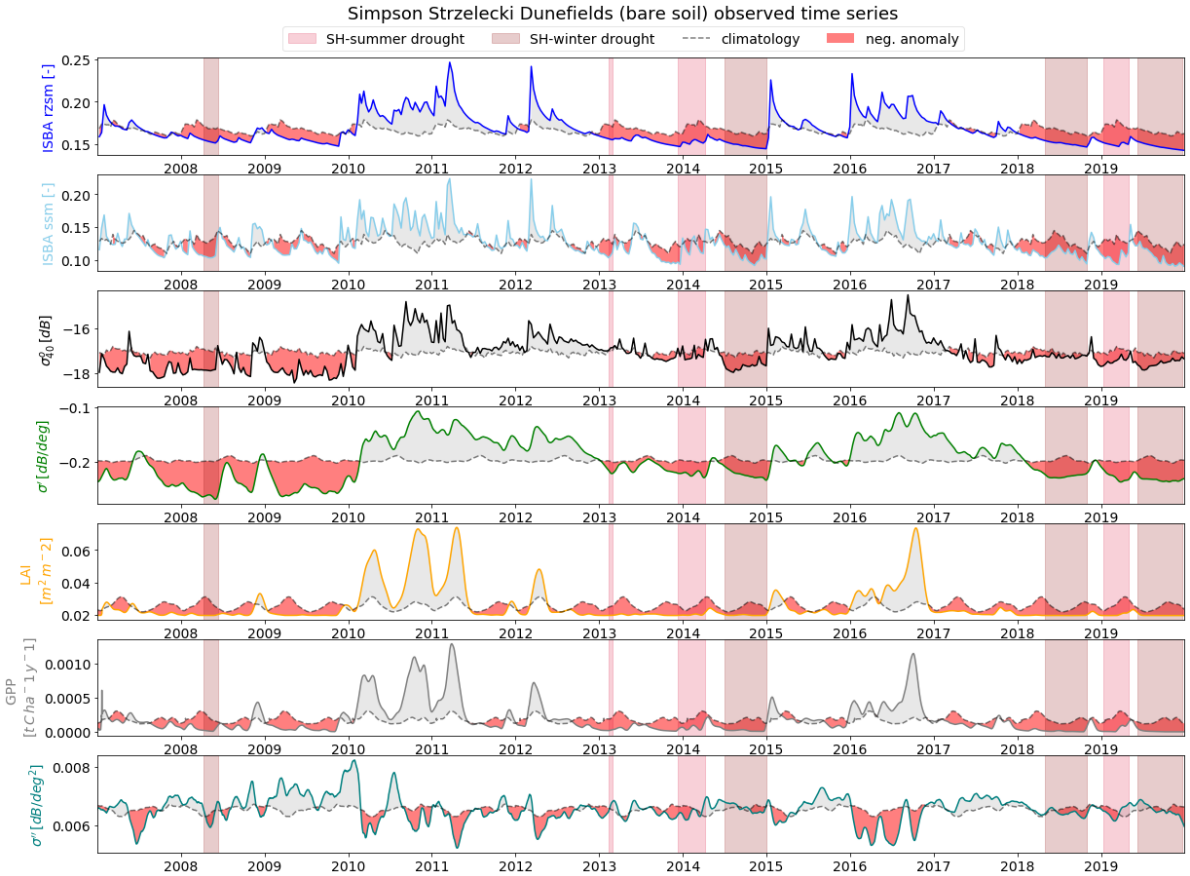

Figure 4.17: Simpson Strzelecki Dunefields (bare soil) time series with anomalies and droughts highlighted

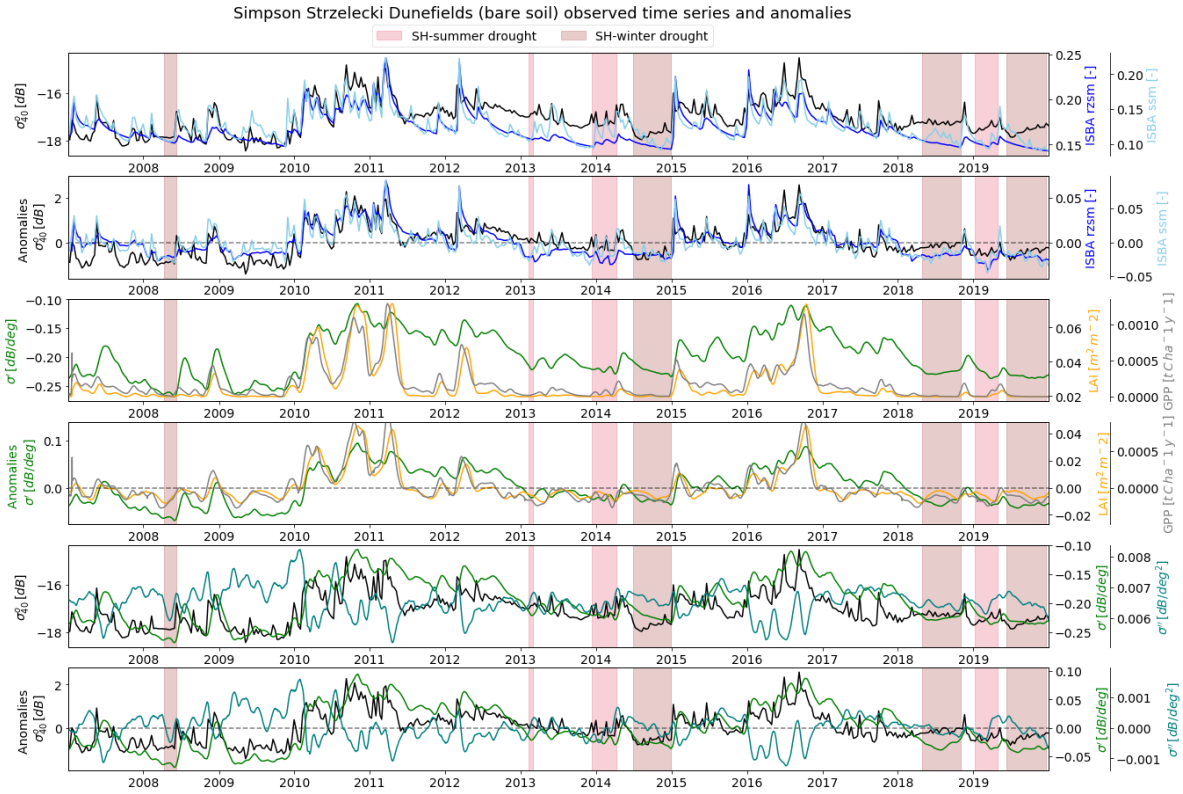

Figure 4.18: Simpson Strzelecki Dunefields (bare soil) observed time series and anomalies with droughts highlighted

4.4. Burnt area detection

This section briefly explores the possibility of using the dynamic vegetation parameters in identifying areas affected by bush fires, one of the most frequently experienced natural hazards in Australia (Sharples et al., 2016). Bush fires generally occur after prolonged periods of drought, in part due to the drying out of vegetation (Yebra et al., 2018).

Burnt areas are, however, typically not as spatially extensive as droughts. Hence, averaging over all grid points in an ROI, especially when these grid points are non-adjacent, will suppress the burn signal. Therefore, the analysis is carried out for some individual grid points. Hypothetically, if the bushfire covered enough of the 25km x 25km grid point, this should result in a considerable change in scattering mechanism over an otherwise vegetated surface, especially if it involves a change from a dense forest to bare soil.

As an example the time series of ASCAT parameters for one of the grid points in Victoria, southeast Australia, that was affected by the Black Saturday fires in February 2009, is shown in 4.20. It clearly shows unprecedented low slope and high curvature values in the season following the burn. This is consistent with the effect a fire would have on vegetation water dynamics in a forest; the above ground wet biomass plummets leading to the relative dominance of direct surface scattering and ground bounce terms over volume scattering.

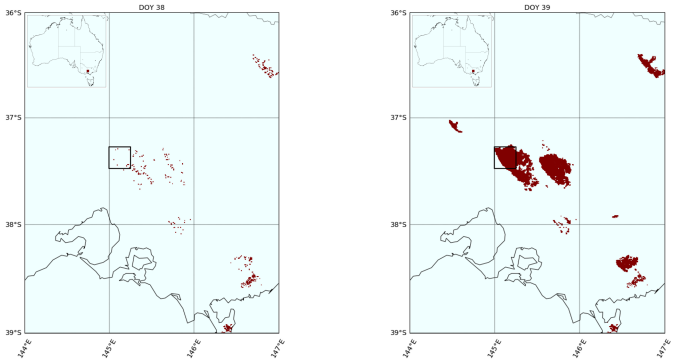

Figure 4.19: Difference in burnt area between Feb. 7th and 8th (Black Saturday) 2009 for a gridpoint dominated by evergreen forest in the state of Victoria

When zooming in on the actual burn date, it shows that exactly 21 days prior to this day σ'' starts to rise and σ' starts to drop. This corresponds to the edge of the 42 day kernel window centred around the burn date. Thus the premature rise and fall in σ'' and σ', respectively, can be attributed to the kernel smoother used. It is, however, encouraging that such a big sudden change in vegetation dynamics is visible, even at the edge of the kernel window.
In σ^o_{40} the burn is not clearly detectable because of its sensitivity to soil moisture which would already change at the slightest rainfall event after the fire, especially with the forest canopy gone. Hence, it is really the dynamic vegetation parameters σ' and σ'' that allow to detect burnt areas.

Currently, for a burn to be detected as an anomaly in the time series a region must not experience bushfires on a regular basis, the σ' and σ'' signal across the vegetation type must differ considerably from bare soil, and a large enough area of the grid point has to be affected by the bushfire, otherwise the burn signal is not visible in the time series. Though much further detailed analysis is needed, ASCAT has a potential to be used in the monitoring of burnt areas, for example complementary to visible or infrared products, which often have a higher spatial resolution but can be hampered by cloud cover.

The Fuel Moisture Content (FMC) strongly influences key components of flammability (Yebra et al., 2018). In theory the high sensitivity of σ' and σ'' to vegetation water dynamics could be used to give early warnings of high FMC. However, to be of added value in prediction of bush fires, and take advantage of the high temporal resolution of ASCAT, the dynamic calculation for daily values of σ' and σ'' would have to be strongly improved so that short term fluctuations are picked up, but measurement noise is still suppressed.

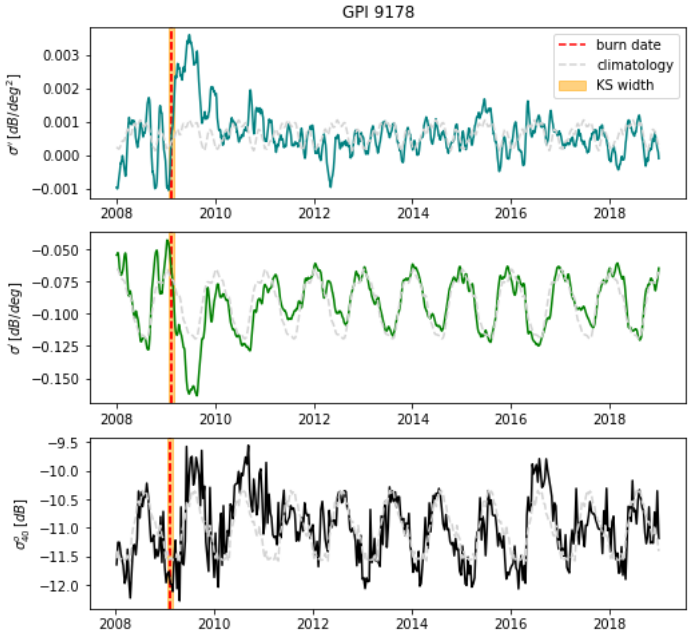

Figure 4.20: Time series of ASCAT parameters for a grid point in evergreen forest in Victoria

5

Discussion

This chapter discusses the results, reflects on some of the limitations of this study, and points to possible improvements for future studies.

Spatial variability
The findings of this study are in agreement with previous studies that backscatter from scatterometers can be used to differentiate between main vegetation regions, most notable between translucent (grasses and crops) and nontransparent (forest and shrubs) vegetation (Wagner et al., 1999). With the addition of slope and curvature considerably more information can be gained from the vegetated surface. For example, the spatial distribution of mean slope clearly followed the delineation of some bioregions in Australia, something that was less visible in the σ^o_{40} map. In addition, the slope allowed to identify differences in vegetation density between C3 crops and temperate grasslands, which otherwise have similar backscatter values. In tropical grasslands the lower range in slope indicated that the range in σ^o_{40} was due to changes in soil moisture rather than phenology. Thus when combined with backscatter data, slope and curvature can be used to discriminate further between main vegetation regions based on soil moisture and land cover features.

Seasonal climatology
Despite its coarse resolution, the seasonal vegetation dynamics can be captured quite accurately with ASCAT's dynamic vegetation parameters. This is especially apparent in C3 croplands, which in the Australian wheat-sheep zone is largely dominated by wheat. The seasonal cycle of slope and curvature, particularly when viewed in the σ^o - θ relation, is able to neatly explain the growth stages of wheat. This is primarily thanks to the numerous studies, like Veloso et al. (2017) and Mattia et al. (2003), that have studied scattering mechanisms with high resolution from wheat fields in experimental sites, or with more detailed Sentinel satellite data. Understanding the vegetation-ground interaction, the vertical distribution of water content, and the difference in scattering mechanisms before and after heading is vital in an accurate interpretation of slope and curvature across wheat fields.
The ability to monitor the seasonal cycle of vegetation at this spatial resolution with such detail should be an encouragement for future studies investigating the σ^o - θ relation across other vegetation types. An improved understanding of the influence that vegetation structure, water content distribution, and biomass density have on scattering mechanisms in certain grasslands or woodlands could lead to greatly improved interpretations of the slope and curvature signals there too.

It must be said that in this study the ROIs were defined based on grid points with highly uniform ISBA vegetation type fractions (>80% for crops and forests; >70% for grasses). In croplands, where a land cover fraction of 100% crops is not unusual, this makes the interpretation of the ASCAT signal significantly easier. In contrast, the tropical grasslands vegetation type is heterogeneous by nature. The mix of grasses and trees make it difficult to exactly attribute changes in scattering mechanisms to phenology. Similarly Pfeil et al. (2020) found that for grid points dominated by crops in Austria,

even a small fraction of deciduous broadleaved forest could already result in a 'spring-peak' in slope, caused by scattering from bare trees. Thus for a solid interpretation of the seasonal cycle of slope and curvature in terms of vegetation dynamics, it is desirable to have grid points with highly uniform vegetation, or a detailed knowledge of the land cover.

In general the seasonal cycle of backscatter agrees well with surface soil moisture from ISBA, with the exception of evergreen forest ROIs. This poor relation between backscatter and soil moisture as a result of signal attenuation in the canopy is also problematic in the TUW SMR (Wagner et al., 2013).

Drought response

To adequately capture the propagation of drought, and the highly dynamic and often non-linear relation between soil moisture and vegetation the entire time series are studied. The drought events themselves are not analyzed in detail in this study, they primarily serve to identify periods with the lowest root zone soil moisture, even though a datarecord of 13 years is relatively short to define droughts.

Based on the results from this study, ASCAT parameters are most suitable to monitor droughts in fairly dry semi-arid regions, like the temperate grasslands. The anomalies in ASCAT parameters match the anomalies in their ISBA equivalent well, and there is practically no lag between anomalies in soil moisture and vegetation parameters, which makes interpretation of the propagation of drought a lot simpler. This is in line with earlier conclusions of Wagner et al. (2013) who showed particularly strong correlations between SWI derived from ASCAT backscatter, and NDVI time series across semi-arid regions of Africa.
Steele-Dunne et al. (2019) found clear anomalies in slope and curvature over the arid Nebraska Sand Hills that lagged behind negative σ^o_{40} anomalies. In this study, across temperate grasslands, the onset and duration of anomalies in slope neatly followed σ^o_{40} . The curvature was more difficult to interpret and seemed to have no consistent relation with slope. Looking at the σ^o - θ relation in such cases really helps to link the slope and curvature time series. It allows to unravel whether scattering is dominated by surface scattering from dry or wet soils, and what contribution, if any, is made by volume scattering from vegetation.

Over the bare soil ROIs the ASCAT parameters respond in much the same way as they would over a dry, sparsely vegetated grassland, because in Australian deserts vegetation growth can come as a rapid response to rare heavy precipitation events. This has also been observed by Vreugdenhil et al. (2017), who found good correlation between VOD from ASCAT backscatter, and satellite derived LAI. However, these prolonged positive slope anomalies are not reflected in the simulated LAI and GPP, as a result of how the vegetation fraction is defined in ISBA. Potentially, ASCAT parameters, and particularly slope, could be exploited for monitoring land cover changes, and be used to calibrate the vegetation fraction in land surface models dynamically. This could improve the critical contribution of land-atmosphere feedback interactions in drought monitoring (Herrera Estrada et al., 2017).

The vegetation dynamics in times of water stress over croplands also seemed to be adequately captured by slope and curvature time series, mostly because the seasonal cycle could be interpreted so well. However, it was difficult to compare this to simulated LAI and GPP, primarily because ISBA doesn't take into account anthropogenic influences like irrigation or sowing and harvesting dates. Over croplands this resulted in early onset of biomass peak compared to slope.
One of the limitations of using simulated LAI and GPP is that they are largely driven by climate. LAI does not explicitly simulate phenology but the onset of leaf growth simply follows a carbon balance. Moreover, a single optimum temperature for photosynthesis is used for each vegetation type across the globe (Gibelin et al., 2006). Whereas the simulated LAI performs better in dry periods compared to observations, the opposite is true for GPP (Albergel et al., 2010; Brut et al., 2009). The simulated GPP is also highly sensitive to temperature, and the optimum temperature is often overestimated in ISBA. Furthermore, GPP is in part dependent on LAI, because respiration takes place through photosynthesis (Albergel et al., 2010).
Although each dataset, simulated or remotely sensed, has its own advantage and disadvantages it would be good for a future study that compares vegetation variables directly to slope and curvature

to use satellite derived data. Especially over croplands where phenology can be highly dynamic, observed optical or NIR vegetation indices would be worth comparing too. It would also be interesting because in this study the LAI peak preceded the slope but indicated a lower vegetation density, whereas in validation studies the simulated LAI in ISBA was often higher and delayed compared to satellite derived products (Brut et al., 2009).

Across evergreen forests monitoring the propagation of drought from a soil moisture anomaly to a vegetation anomaly was more challenging because of mismatch in timing between the two. One of the reasons is likely that the root zone soil moisture depth in this version of ISBA is limited to 1m, whereas the rooting depth of Eucalyptus trees are known to easily extend to 10m depth (Robinson et al., 2006). It has been recognized that the plant extractable water capacity of soils and the rooting depth are rather uncertain parameters in ISBA (Brut et al., 2009). Using prescribed rooting profiles, which in reality are highly dynamic and actively respond to environmental stress, is a short coming in many land surface models (Sivandran and Bras, 2013). The fact that the simulated anomalies in root zone soil moisture corresponded so neatly with backscatter, which across evergreen forests is more influenced by vegetation and interception than actual soil moisture, also raises some flags. This could explain why soil moisture deficits and simulated vegetation anomalies on the one hand, and the observed anomalies in slope and curvature on the other, react on different time scales.
Another aspect in the different responses to soil moisture deficits is that, though for most parts of Australia vegetation growth is moisture driven, across the high rainfall zones like the evergreen forests it is radiation driven (Nemani et al., 2003). (Petchiappan, 2019) found that across the Amazon the seasonal cycle of slope was closely related to the radiation cycle. This would be useful to consider in future studies when comparing slope from wet forest regions with relatively shallow simulated root zone soil moisture.

Differences in long term trends, potentially as a result of the above mentioned limitations in ISBA, have also made it difficult to asses the accuracy with which vegetation water stress can be captured by slope and curvature. These differences were mostly in regions with high stable slope values, i.e. evergreen forests and tropical grasslands. Whereas the long term trends themselves were suitable to explain the interannual variability from a physical point of view, the remaining anomalies were small high frequency fluctuations in the time series. A recent study by Steele-Dunne et al. (2021) found that these short term variations increased with shorter kernel smoother windows. This makes it difficult to determine whether these anomalies that remain after the trend is removed are a result of short term vegetation dynamics, or unsurpressed measurement noise. Their preliminary conclusion is that smooth dynamic vegetation parameters lead to better soil moisture retrieval, i.e. better representation of vegetation effects. In this study that would be feasible to apply since the interannual variation can be adequately captured in the smoother long term trend. However, much can be gained from a calculation of a short kernel window that still leads to robust slope and curvature values. This is a big challenge, also for the soil moisture retrieval algorithm, that needs to be further investigated.

6

Conclusions

This study investigates if ASCAT could be used as a self-contained dataset in drought monitoring. The spatial variability, the seasonal cycle, and the drought response of backscatter, slope and curvature across different vegetation types is assessed. More specifically, it is examined whether the ability of the dynamic vegetation parameters, slope and curvature, to adequately describe vegetation water dynamics also holds during periods of water stress. Simulated soil moisture, LAI and GPP from ISBA are used to aid in the interpretation of the ASCAT signal.

The ability of ASCAT to be used as a self-contained dataset in drought monitoring largely depends on the vegetation type. Across dry semi-arid regions with grasses (or crops), the good correlation between both moisture and vegetation related variables from ASCAT and ISBA indicate that ASCAT performs at least as well as the land surface model, and could thus be used alone in monitoring droughts over these regions. This could start to fill the gap in the need of near-real-time satellite-based monitoring of vegetation for successful drought monitoring. Particularly good insights into the vegetation dynamics of the grasses and crops in times of drought can be gained from the σ^o - θ relationship. This is because the scattering mechanisms from the structure and moisture distribution in these types of vegetation is better understood.

The vegetation's response to a drought in forests or a mix of grasses and trees showed more inconsistencies regarding the propagation of a soil moisture anomaly into a vegetation anomaly. For more accurate retrieval of soil moisture over these regions, more knowledge is needed of the relationship between backscatter measurements and scattering from these types of vegetation. It is further recommended to also compare ASCAT dynamic vegetation parameters over forests and mixed vegetation to other observed (remote sensing) vegetation indices as these can be better at capturing the real vegetation phenology than simulated variables.

The results of this study are particularly promising for monitoring droughts with ASCAT over extended croplands, which from an economic point of view is the most valuable vegetation type. The dynamic vegetation parameters have shown, qualitatively, to adequately capture the vegetation anomalies in wheatfields. The sensitivity to vegetation structure and density, to the water content and distribution, and to ground conditions could greatly complement optical or NIR indices that primarily provide measures of photosynthetic leaf area and vegetation greenness. The temporal stability of spatial patterns in vegetation would allow the coarse resolution, but high revisit time, of ASCAT to be used for local scale crop monitoring with these other indices.

For future studies in regions where using ASCAT as a self-contained dataset in drought monitoring is still too ambitious, it has a real potential to be used as calibration in land surface models. Considering the increasingly recognized role that land-atmosphere feedback mechanisms play in the propagation and persistence of droughts, and the often limited representation of vegetation responses in land surface models, points to the added value the dynamic vegetation parameters can have in drought monitoring. The high revisit times and low spatial resolution of ASCAT make it especially compatible with land surface models.

To conclude, this study confirms that the dynamic vegetation parameters yield valuable information of how vegetation dynamics change over time. The understanding of slope as a measure of vegetation density has been reinforced, and across woody vegetation has been specified to a measure of vegetation water content. The curvature as a measure of the relative dominance in scattering mechanisms related to vegetation structure and variations in phenology, and the ground contribution is also supported by the results. Depending on the land cover, the curvature can show a direct relation with the backscatter or slope signal. These interpretations of slope and curvature have been shown to hold in time of vegetation water stress. This should further encourage the development of the dynamic vegetation parameters in the TUW SMR algorithm. With future research into the the kernel smoothing technique to allow for a dynamic calculation of slope and curvature, the benefit of a high temporal signature of ASCAT backscatter can be exploited, and other applications like bushfire prediction can potentially be explored.

References

Albergel, C., Calvet, J.-C., Gibelin, A.-L., Lafont, S., Roujean, J.-L., Berne, C., Traullé, O., & Fritz, N. (2010). Observed and modelled ecosystem respiration and gross primary production of a grassland in southwestern France. *Biogeosciences*, *7*(5), 1657–1668. https://doi.org/10.5194/bg-7-1657-2010

Albergel, C., Rüdiger, C., Pellarin, T., Calvet, J.-C., Fritz, N., Froissard, F., Suquia, D., Petitpa, A., Piguet, B., & Martin, E. (2008). From near-surface to root-zone soil moisture using an exponential filter: An assessment of the method based on in-situ observations and model simulations. *Hydrology and Earth System Sciences*, *12*(6), 1323–1337. https://doi.org/10.5194/hess-12-1323-2008

Andreadis, K. M., Clark, E. A., Wood, A. W., Hamlet, A. F., & Lettenmaier, D. P. (2005). Twentieth-Century Drought in the Conterminous United States. *Journal of Hydrometeorology*, *6*(6), 985–1001. https://doi.org/10.1175/JHM450.1

Baik, J., Zohaib, M., Kim, U., Aadil, M., & Choi, M. (2019). Agricultural drought assessment based on multiple soil moisture products. *Journal of Arid Environments*, *167*, 43–55. https://doi.org/10.1016/j.jaridenv.2019.04.007

Bartalis, Z., Wagner, W., Naeimi, V., Hasenauer, S., Scipal, K., Bonekamp, H., Figa, J., & Anderson, C. (2007). Initial soil moisture retrievals from the METOP-A Advanced Scatterometer (ASCAT). *Geophysical Research Letters*, *34*(20). https://doi.org/10.1029/2007GL031088

Bastin, G. (2008, August). *Rangelands 2008 - Taking the pulse*. Australian Government Department of Agriculture, Water and the Environment. Retrieved December 30, 2020, from https://www.environment.gov.au/land/publications/acris-rangelands-2008-taking-pulse

Bioregion overviews. (2016). NSW Government. Retrieved December 30, 2020, from https://www.environment.nsw.gov.au/bioregions/BioregionOverviews.htm
Last Modified: 2016-04-26

BoM. (2021). *About Australian Climate*. Bureau of Meteorology. Retrieved February 8, 2021, from http://www.bom.gov.au/climate/about/australian-climate-influences.shtml

Borgomeo, E., Pflug, G., Hall, J. W., & Hochrainer Stigler, S. (2015). Assessing water resource system vulnerability to unprecedented hydrological drought using copulas to characterize drought duration and deficit. *Water Resources Research*, *51*(11), 8927–8948. https://doi.org/10.1002/2015WR017324

Brut, A., Rüdiger, C., Lafont, S., Roujean, J.-L., Calvet, J.-C., Jarlan, L., Gibelin, A.-L., Albergel, C., Le Moigne, P., Soussana, J.-F., Klumpp, K., Guyon, D., Wigneron, J.-P., & Ceschia, E. (2009). Modelling LAI at a regional scale with ISBA-A-gs: Comparison with satellite-derived LAI over southwestern France. *Biogeosciences*, *6*(8), 1389–1404. https://doi.org/10.5194/bg-6-1389-2009

Bureau of meteorology - climate classifications maps. (2021). Bureau of Meteorology. Retrieved February 8, 2021, from http://www.bom.gov.au/jsp/ncc/climate_averages/climate-classifications/index.jsp?maptype=kpn#maps

Calvet, J.-C., & Noilhan, J. (2000). From Near-Surface to Root-Zone Soil Moisture Using Year-Round Data. *Journal of Hydrometeorology*, *1*(5), 393–411. https://doi.org/10.1175/1525-7541(2000)001<0393:FNSTRZ>2.0.CO;2

Carrão, H., Russo, S., Sepulcre-Canto, G., & Barbosa, P. (2016). An empirical standardized soil moisture index for agricultural drought assessment from remotely sensed data. *International Journal*

of Applied Earth Observation and Geoinformation, *48*, 74–84. https://doi.org/10.1016/j.jag.2015.06.011

Crocetti, L., Forkel, M., Fischer, M., Jure ka, F., Grlj, A., Salentinig, A., Trnka, M., Anderson, M., Ng, W.-T., Kokalj, Ž., Bucur, A., & Dorigo, W. (2020). Earth Observation for agricultural drought monitoring in the Pannonian Basin (southeastern Europe): Current state and future directions. *Regional Environmental Change*, *20*(4), 123. https://doi.org/10.1007/s10113-020-01710-w

Dai, A. (2011). Drought under global warming: A review. *WIREs Climate Change*, *2*(1), 45–65. https://doi.org/10.1002/wcc.81

Dracup, J. A., Lee, K. S., & Paulson, E. G. (1980). On the definition of droughts. *Water Resources Research*, *16*(2), 297–302. https://doi.org/10.1029/WR016i002p00297

Figa-Saldaña, J., Wilson, J. J. W., Attema, E., Gelsthorpe, R., Drinkwater, M. R., & Stoffelen, A. (2002). The advanced scatterometer (ASCAT) on the meteorological operational (MetOp) platform: A follow on for European wind scatterometers. *Canadian Journal of Remote Sensing*, *28*(3), 404–412. https://doi.org/10.5589/m02-035

Fleig, A. K., Tallaksen, L. M., Hisdal, H., Hisdal, H., Demuth, S., & Demuth, S. (2006). *A global evaluation of streamflow drought characteristics*. Hydrology and Earth System Sciences. Retrieved February 8, 2021, from https://doaj.org

Frison, P. L., & Mougin, E. (1996). Monitoring global vegetation dynamics with ERS-1 wind scatterometer data. *International Journal of Remote Sensing*, *17*(16), 3201–3218. https://doi.org/10.1080/01431169608949139

Frison, P.-L., Jarlan, L., & Mougin, E. (2016). Using satellite scatterometers to monitor continental surfaces (N. Baghdadi & M. Zribi, Eds.). In N. Baghdadi & M. Zribi (Eds.), *Land Surface Remote Sensing in Continental Hydrology*. London, ISTE Press Ltd. https://doi.org/10.1016/B978-1-78548-104-8.50003-6

Gibelin, A.-L., Calvet, J.-C., Roujean, J.-L., Jarlan, L., & Los, S. O. (2006). Ability of the land surface model ISBA-A-gs to simulate leaf area index at the global scale: Comparison with satellites products. *Journal of Geophysical Research: Atmospheres*, *111*(D18). https://doi.org/10.1029/2005JD006691

Gouveia, C., Trigo, R. M., & DaCamara, C. C. (2009). Drought and vegetation stress monitoring in Portugal using satellite data. *Natural Hazards and Earth System Sciences*, *9*(1), 185–195. https://doi.org/10.5194/nhess-9-185-2009

Hahn, S., Reimer, C., Vreugdenhil, M., Melzer, T., & Wagner, W. (2017). Dynamic Characterization of the Incidence Angle Dependence of Backscatter Using Metop ASCAT. *IEEE Journal of Selected Topics in Applied Earth Observations and Remote Sensing*, *10*(5), 2348–2359. https://doi.org/10.1109/JSTARS.2016.2628523

Heberger, M. (2012). Australia's Millennium Drought: Impacts and Responses (P. H. Gleick, Ed.). In P. H. Gleick (Ed.), *The World's Water*. Washington, DC, Island Press/Center for Resource Economics. https://doi.org/10.5822/978-1-59726-228-6_5

Heim, R. R. (2002). A Review of Twentieth-Century Drought Indices Used in the United States. *Bulletin of the American Meteorological Society*, *83*(8), 1149–1166. https://doi.org/10.1175/1520-0477-83.8.1149

Herrera Estrada, J. E., Satoh, Y., & Sheffield, J. (2017). Spatiotemporal dynamics of global drought. *Geophysical Research Letters*, *44*(5), 2254–2263. https://doi.org/10.1002/2016GL071768

Hisdal, E. H., & Tallaksen, L. M. (2000). *Drought Event Definition* (Technical report No. 6). University of Oslo.

Hisdal, H., Tallaksen, L. M., Clausen, B., Peters, E., & Gustard, A. (2004). Hydrological Drought Characteristics, In *Hydrological Drought: Processes and Estimation Methods for Streamflow and Groundwater*. Amsterdam, Elsevier.

Jones, M. O., Kimball, J. S., Jones, L. A., & McDonald, K. C. (2012). Satellite passive microwave detection of North America start of season. *Remote Sensing of Environment*, *123*, 324–333. https://doi.org/10.1016/j.rse.2012.03.025

Keyantash, J., & Dracup, J. A. (2002). The Quantification of Drought: An Evaluation of Drought Indices. *Bulletin of the American Meteorological Society*, *83*(8), 1167–1180. https://doi.org/10.1175/1520-0477-83.8.1167

Kiem, A. S., Johnson, F., Westra, S., van Dijk, A., Evans, J. P., O'Donnell, A., Rouillard, A., Barr, C., Tyler, J., Thyer, M., Jakob, D., Woldemeskel, F., Sivakumar, B., & Mehrotra, R. (2016). Natural hazards in Australia: Droughts. *Climatic Change*, *139*(1), 37–54. https://doi.org/10.1007/s10584-016-1798-7

Konings, A. G., Rao, K., & Steele Dunne, S. C. (2019). Macro to micro: Microwave remote sensing of plant water content for physiology and ecology. *New Phytologist*, *223*(3), 1166–1172. https://doi.org/10.1111/nph.15808

Liu, X., Zhu, X., Pan, Y., Li, S., Liu, Y., & Ma, Y. (2016). Agricultural drought monitoring: Progress, challenges, and prospects. *Journal of Geographical Sciences*, *26*(6), 750–767. https://doi.org/10.1007/s11442-016-1297-9

Martínez-Fernández, J., González-Zamora, A., Sánchez, N., & Gumuzzio, A. (2015). A soil water based index as a suitable agricultural drought indicator. *Journal of Hydrology*, *522*, 265–273. https://doi.org/10.1016/j.jhydrol.2014.12.051

Mattia, F., Toan, T. L., Picard, G., Posa, F. I., D'Alessio, A., Notarnicola, C., Gatti, A. M., Rinaldi, M., Satalino, G., & Pasquariello, G. (2003). Multitemporal C-band radar measurements on wheat fields. *IEEE Transactions on Geoscience and Remote Sensing*, *41*(7), 1551–1560. https://doi.org/10.1109/TGRS.2003.813531

Melzer, T. (2013). Vegetation modelling in WARP 6.0, In *Proc EUMETSAT*. Meteorological Satellite Conference, Vienna, Austria.

Mishra, A. K., & Singh, V. P. (2010). A review of drought concepts. *Journal of Hydrology*, *391*(1), 202–216. https://doi.org/10.1016/j.jhydrol.2010.07.012

Moigne, P. L. (2018). *SURFEX SCIENTIFIC DOCUMENTATION*.

Naeimi, V., Scipal, K., Bartalis, Z., Hasenauer, S., & Wagner, W. (2009). An Improved Soil Moisture Retrieval Algorithm for ERS and METOP Scatterometer Observations. *IEEE Transactions on Geoscience and Remote Sensing*, *47*(7), 1999–2013. https://doi.org/10.1109/TGRS.2008.2011617

Nemani, R. R., Keeling, C. D., Hashimoto, H., Jolly, W. M., Piper, S. C., Tucker, C. J., Myneni, R. B., & Running, S. W. (2003). Climate-Driven Increases in Global Terrestrial Net Primary Production from 1982 to 1999. *Science*, *300*(5625), pmid 12791990, 1560–1563. https://doi.org/10.1126/science.1082750

Olson, D. M., Dinerstein, E., Wikramanayake, E. D., Burgess, N. D., Powell, G. V. N., Underwood, E. C., D'amico, J. A., Itoua, I., Strand, H. E., Morrison, J. C., Loucks, C. J., Allnutt, T. F., Ricketts, T. H., Kura, Y., Lamoreux, J. F., Wettengel, W. W., Hedao, P., & Kassem, K. R. (2001). Terrestrial Ecoregions of the World: A New Map of Life on Earth. *BioScience*, *51*(11), 933. https://doi.org/10.1641/0006-3568(2001)051[0933:TEOTWA]2.0.CO;2

Petchiappan, A. (2019). *Active microwave remote sensing of the Amazon forest region* (Master Thesis). TU Delft. Delft.

Pfeil, I., Wagner, W., Forkel, M., Dorigo, W., & Vreugdenhil, M. (2020). Does ASCAT observe the spring reactivation in temperate deciduous broadleaf forests? *Remote Sensing of Environment*, *250*, 112042. https://doi.org/10.1016/j.rse.2020.112042

Rees, G. (2013). *Physical principles of remote sensing* (3rd ed). Cambridge ; New York, Cambridge University Press.

Richards, L., Brew, N., & Smith, L. (2020). *2019–20 Australian bushfires—frequently asked questions: A quick guide* (Quick Guide). Parliamentary Library. https://www.aph.gov.au/About_Parliament/Parliamentary_Departments/Parliamentary_Library/pubs/rp/rp1920/Quick_Guides/AustralianBushfires

Robinson, N., Harper, R. J., & Smettem, K. R. J. (2006). Soil water depletion by Eucalyptus spp. integrated into dryland agricultural systems. *Plant and Soil*, *286*(1), 141–151. https://doi.org/10.1007/s11104-006-9032-4

Schroeder, R., McDonald, K. C., Azarderakhsh, M., & Zimmermann, R. (2016). ASCAT MetOp-A diurnal backscatter observations of recent vegetation drought patterns over the contiguous U.S.: An assessment of spatial extent and relationship with precipitation and crop yield. *Remote Sensing of Environment*, *177*, 153–159. https://doi.org/10.1016/j.rse.2016.01.008

Scipal, K., Wagner, W., Trommler, M., & Naumann, K. (2002). The global soil moisture archive 1992-2000 from ERS scatterometer data: First results, In *IEEE International Geoscience and Remote Sensing Symposium*. IEEE International Geoscience and Remote Sensing Symposium. IGARSS 2002, Toronto, Ont., Canada, IEEE. https://doi.org/10.1109/IGARSS.2002.1026129

Sharples, J. J., Cary, G. J., Fox-Hughes, P., Mooney, S., Evans, J. P., Fletcher, M.-S., Fromm, M., Grierson, P. F., McRae, R., & Baker, P. (2016). Natural hazards in Australia: Extreme bushfire. *Climatic Change*, *139*(1), 85–99. https://doi.org/10.1007/s10584-016-1811-1

Sheffield, J., Andreadis, K. M., Wood, E. F., & Lettenmaier, D. P. (2009). Global and Continental Drought in the Second Half of the Twentieth Century: Severity–Area–Duration Analysis and Temporal Variability of Large-Scale Events. *Journal of Climate*, *22*(8), 1962–1981. https://doi.org/10.1175/2008JCLI2722.1

Sheffield, J., Goteti, G., Wen, F., & Wood, E. F. (2004). A simulated soil moisture based drought analysis for the United States. *Journal of Geophysical Research: Atmospheres*, *109*(D24). https://doi.org/10.1029/2004JD005182

Sheffield, J., & Wood, E. F. (2011). *DROUGHT past problems and future scenarios*. Retrieved October 22, 2019, from https://ebookcentral-proquest-com.tudelft.idm.oclc.org/lib/delft/reader.action?docID=1046811

Sivandran, G., & Bras, R. L. (2013). Dynamic root distributions in ecohydrological modeling: A case study at Walnut Gulch Experimental Watershed. *Water Resources Research*, *49*(6), 3292–3305. https://doi.org/10.1002/wrcr.20245

Steele-Dunne, S. C., Hahn, S., Wagner, W., & Vreugdenhil, M. (2019). Investigating vegetation water dynamics and drought using Metop ASCAT over the North American Grasslands. *Remote Sensing of Environment*, *224*, 219–235. https://doi.org/10.1016/j.rse.2019.01.004

Steele-Dunne, S. C., Hahn, S., Wagner, W., & Vreugdenhil, M. (2021). Towards including Dynamic Vegetation Parameters in the ASCAT Soil Moisture Products. *Remote Sensing (Unpublished)*, 17.

Stiles, J. M., Sarabandi, K., & Ulaby, F. T. (2000). Electromagnetic scattering from grassland. II. Measurement and modeling results. *IEEE Transactions on Geoscience and Remote Sensing*, *38*(1), 349–356. https://doi.org/10.1109/36.823930

Tallaksen, L. M., & Van Lanen, H. A. J. (2004). *Hydrological Drought: Processes and Etimation Methods for Streamflow and Groundwater*. Amsterdam, Elsevier.

Ulaby, F., & Long, D. (2014). *Microwave Radar and Radiometric Remote Sensing*. University of Michigan Press. https://doi.org/10.3998/0472119356

Van Loon, A. F., Tijdeman, E., Wanders, N., Van Lanen, H. A. J., Teuling, A. J., & Uijlenhoet, R. (2014). How climate seasonality modifies drought duration and deficit. *Journal of Geophysical Research: Atmospheres*, *119*(8), 4640–4656. https://doi.org/10.1002/2013JD020383

Van Loon, A. F., & Van Lanen, H. A. J. (2012). A process-based typology of hydrological drought. *Hydrology and Earth System Sciences*, *16*(7), 1915–1946. https://doi.org/10.5194/hess-16-1915-2012

Van Loon, A. F. (2015). Hydrological drought explained: Hydrological drought explained. *Wiley Interdisciplinary Reviews: Water*, *2*(4), 359–392. https://doi.org/10.1002/wat2.1085

van Loon, A. F. (2013). *On the propagation of drought how climate and catchment characteristics influence hydrological drought development and recovery* (Doctoral dissertation). Wagening University. Wageningen. https://library.wur.nl/WebQuery/wurpubs/438510

Vegetation photos in the ANBG collection. (2012). Australian Plant Image Index. Retrieved December 30, 2020, from http://www.anbg.gov.au/photo/vegetation-search.html

Veloso, A., Mermoz, S., Bouvet, A., Le Toan, T., Planells, M., Dejoux, J.-F., & Ceschia, E. (2017). Understanding the temporal behavior of crops using Sentinel-1 and Sentinel-2-like data for agricultural applications. *Remote Sensing of Environment*, *199*, 415–426. https://doi.org/10.1016/j.rse.2017.07.015

Vidal, J.-P., Martin, E., Franchistéguy, L., Habets, F., Soubeyroux, J.-M., Blanchard, M., & Baillon, M. (2010). Multilevel and multiscale drought reanalysis over France with the Safran-Isba-Modcou hydrometeorological suite. *Hydrology and Earth System Sciences*, *14*(3), 459–478. https://doi.org/10.5194/hess-14-459-2010

Vreugdenhil, M., Dorigo, W. A., Wagner, W., de Jeu, R. A. M., Hahn, S., & van Marle, M. J. E. (2016). Analyzing the Vegetation Parameterization in the TU-Wien ASCAT Soil Moisture Retrieval. *IEEE Transactions on Geoscience and Remote Sensing*, *54*(6), 3513–3531. https://doi.org/10.1109/TGRS.2016.2519842

Vreugdenhil, M., Hahn, S., Melzer, T., Bauer-Marschallinger, B., Reimer, C., Dorigo, W. A., & Wagner, W. (2017). Assessing Vegetation Dynamics Over Mainland Australia With Metop ASCAT. *IEEE Journal of Selected Topics in Applied Earth Observations and Remote Sensing*, *10*(5), 2240–2248. https://doi.org/10.1109/JSTARS.2016.2618838

Wagner, W., Lemoine, G., Borgeaud, M., & Rott, H. (1999). A study of vegetation cover effects on ERS scatterometer data. *IEEE Transactions on Geoscience and Remote Sensing*, *37*(2), 938–948. https://doi.org/10.1109/36.752212

Wagner, W. (1998). *Soil moisture retrieval from ERS scatterometer data* (Doctoral dissertation). Vienna University of Technology. Wien, Austria. http://www.ipf.tuwien.ac.at/ww/home.htm

Wagner, W., Blöschl, G., Pampaloni, P., Calvet, J.-C., Bizzarri, B., Wigneron, J.-P., & Kerr, Y. (2007). Operational readiness of microwave remote sensing of soil moisture for hydrologic applications. *Hydrology Research*, *38*(1), 1–20. https://doi.org/10.2166/nh.2007.029

Wagner, W., Hahn, S., Kidd, R., Melzer, T., Bartalis, Z., Hasenauer, S., Figa-Saldaña, J., de Rosnay, P., Jann, A., Schneider, S., Komma, J., Kubu, G., Brugger, K., Aubrecht, C., Züger, J., Gangkofner, U., Kienberger, S., Brocca, L., Wang, Y., … Steinnocher, K. (2013). The ASCAT Soil Moisture Product: A Review of its Specifications, Validation Results, and Emerging Applications. *Meteorologische Zeitschrift*, 5–33. https://doi.org/10.1127/0941-2948/2013/0399

Wanders, N. (2010). *Indicators for drought characterization on a global scale* (Technical report No. 24). Wageningen.

West, H., Quinn, N., & Horswell, M. (2019). Remote sensing for drought monitoring & impact assessment: Progress, past challenges and future opportunities. *Remote Sensing of Environment*, *232*, 111291. https://doi.org/10.1016/j.rse.2019.111291

Wilhite, D. A. (2000). Drought as a Natural Hazard: Concepts and Definitions (D. A. Wilhite, Ed.). In D. A. Wilhite (Ed.), *Drought: A Global Assessment*. London, Routledge.

Woinarski, J., & Mockrin, M. (2020). *Terrestrial Ecoregions*. World Wildlife Fund. Retrieved December 30, 2020, from https://www.worldwildlife.org/biome-categories/terrestrial-ecoregions

Wood, E. F., Schubert, S. D., Wood, A. W., Peters-Lidard, C. D., Mo, K. C., Mariotti, A., & Pulwarty, R. S. (2015). Prospects for Advancing Drought Understanding, Monitoring, and Prediction. *Journal of Hydrometeorology*, *16*(4), 1636–1657. https://doi.org/10.1175/JHM-D-14-0164.1

Woodhouse, I. H. (2005). *Introduction to Microwave Remote Sensing*. Boca Raton, United States, Taylor & Francis Group. Retrieved June 23, 2020, from http://ebookcentral.proquest.com/lib/kb/detail.action?docID=5475678

Woodhouse, I., & Hoekman, D. (2000). Determining land-surface parameters from the ERS wind scatterometer. *IEEE Transactions on Geoscience and Remote Sensing*, *38*(1), 126–140. https://doi.org/10.1109/36.823907

Yebra, M., Quan, X., Riaño, D., Rozas Larraondo, P., van Dijk, A. I. J. M., & Cary, G. J. (2018). A fuel moisture content and flammability monitoring methodology for continental Australia based on optical remote sensing. *Remote Sensing of Environment*, *212*, 260–272. https://doi.org/10.1016/j.rse.2018.04.053

Yevjevich, V. (1969). An objective approach to definitions and investigations of continental hydrologic droughts. *Journal of Hydrology*, *7*(3), 353. https://doi.org/10.1016/0022-1694(69)90110-3

A

Sensitivity to threshold level parameters

Visual comparison of droughts

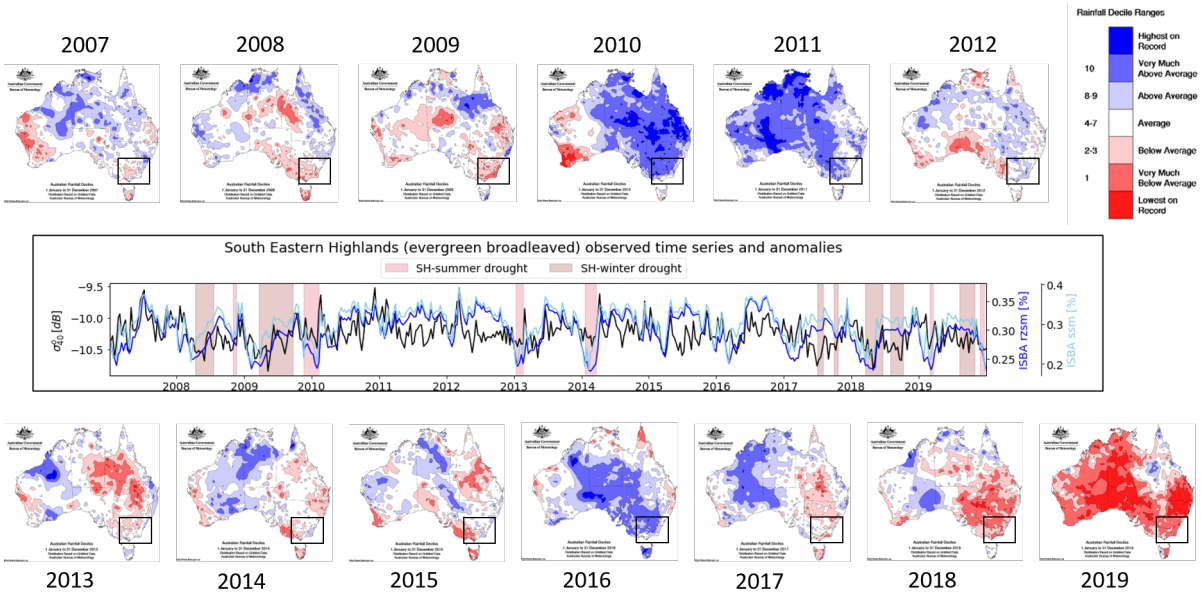

Figure A.1: Visual comparison of the droughts defined across the SEH in this study (middle panel), and the drought maps as defined by the BOM based on RD ranges. The ranges 'very much below average' and 'lowest on record' are considered droughts.

Figure A.1 show the visual comparison of droughts identified in this study for the South Eastern Highlands (SEH) and those identified by the BOM. Because the former is based on root zone soil moisture and the latter on rainfall deciles there won't be an exact match. Moreover, the drought maps from the Bureau of Meteorology (BOM) are yearly averages. There needn't be an exact match either because in this study the drought events are mostly as an indication of lowest soil moisture levels in the 13 years of data available. In studying the propagation of drought through the hydrological system the focus is just as much on the anomalies surrounding a drought, and not only on the drought characteristics of individual events. Hence, the idea of this comparison is to check whether there are no major droughts missing in the time series that could have significantly impacted the dynamic vegetation parameters.

Sensitivity to percentile monthly duration curve

The choice of the percentile of the monthly duration curve on which to base the threshold value has the largest influence on the distribution of drought characteristics. A threshold value between 70-95% of the monthly duration curve is common for perennial and intermittent streams (Fleig et al., 2006; Hisdal and Tallaksen, 2000). Figure A.2 shows the effect of the percentile of the monthly duration curve on the number of drought events, the mean duration, and the maximum deficit of drought events in one of the ROIs.

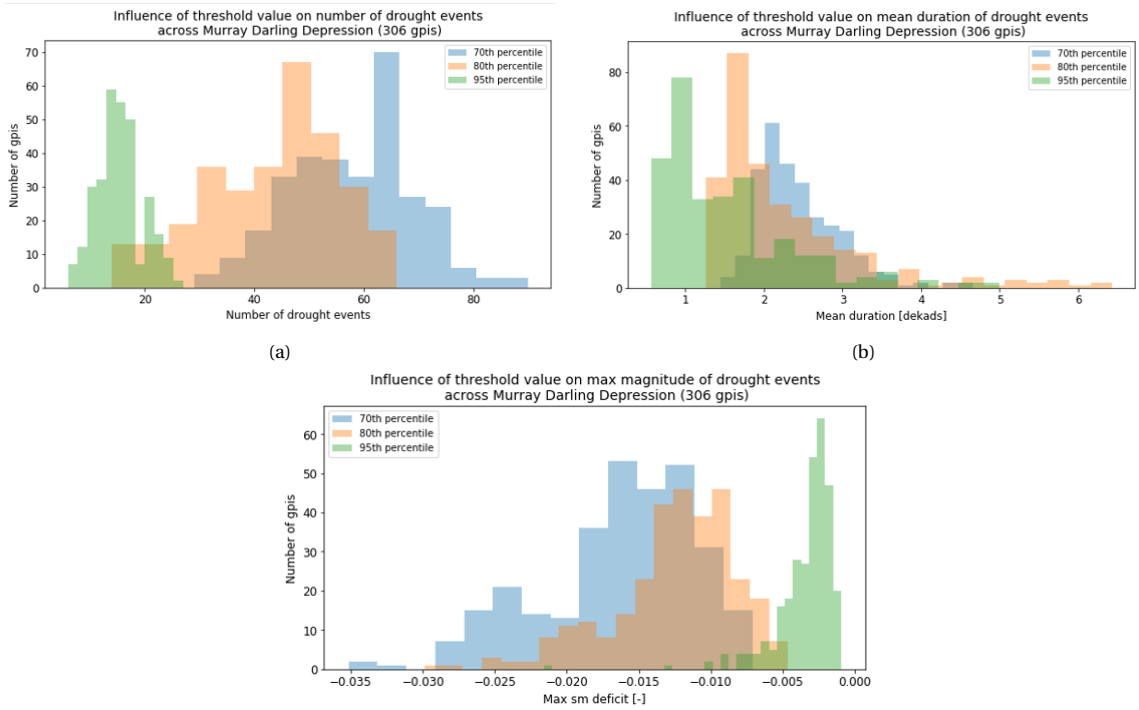

Figure A.2: Effect on the distribution of relevant drought characteristics across the Murray Darling Depression based on different threshold levels

Naturally, a lower threshold produces more and longer droughts, and the converse is true for a higher treshold. For soil moisture droughts the 80th percentile has been used before by van Loon (2013) and produces good results (see fig. A.1).

Sensitivity to inter-event time and minimum duration

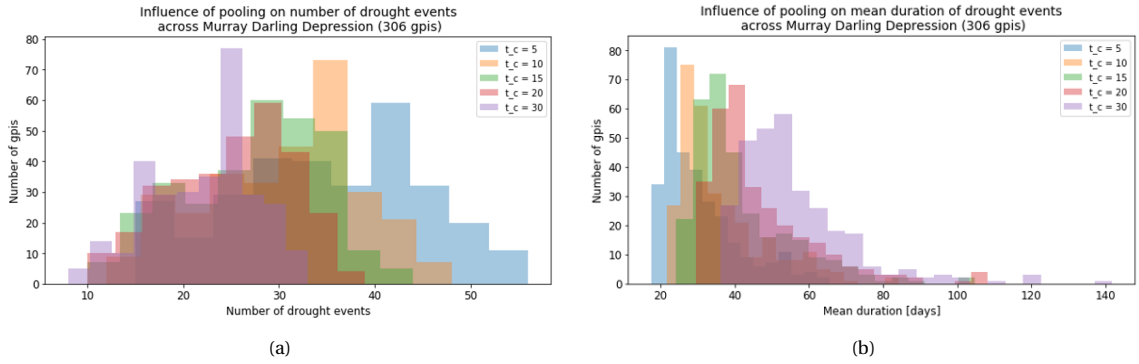

Figure A.3: Effect on the distribution of the number of drought events and their mean duration across the Murray Darling Depression based on different inter-event times

The inter-event time really only has an influence on the number of drought events (less droughts for

higher pooling number) and the duration (longer duration for higher pooling number). The maximum deficit, or magnitude, which is a measure of the severity of droughts for state variables such as soil moisture, is not affected because pooling only adds days with a positive soil moisture anomaly to the event.

The same is true for the sensitivity to the choice of minimum event duration. Naturally the number of drought events decreases, and the mean duration increases with increasing minimum duration. Once again though, this doesn't change the maximum magnitude of the drought events that remain.

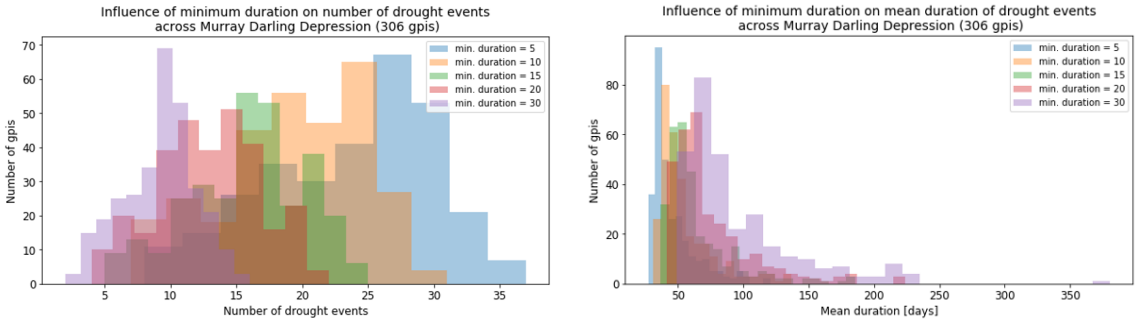

(a) (b)

Figure A.4: Effect on the distribution of the number of drought events and their mean duration across the Murray Darling Depression based on different minimum event durations

B

Seasonal climatologies of ROIs

C3 crops

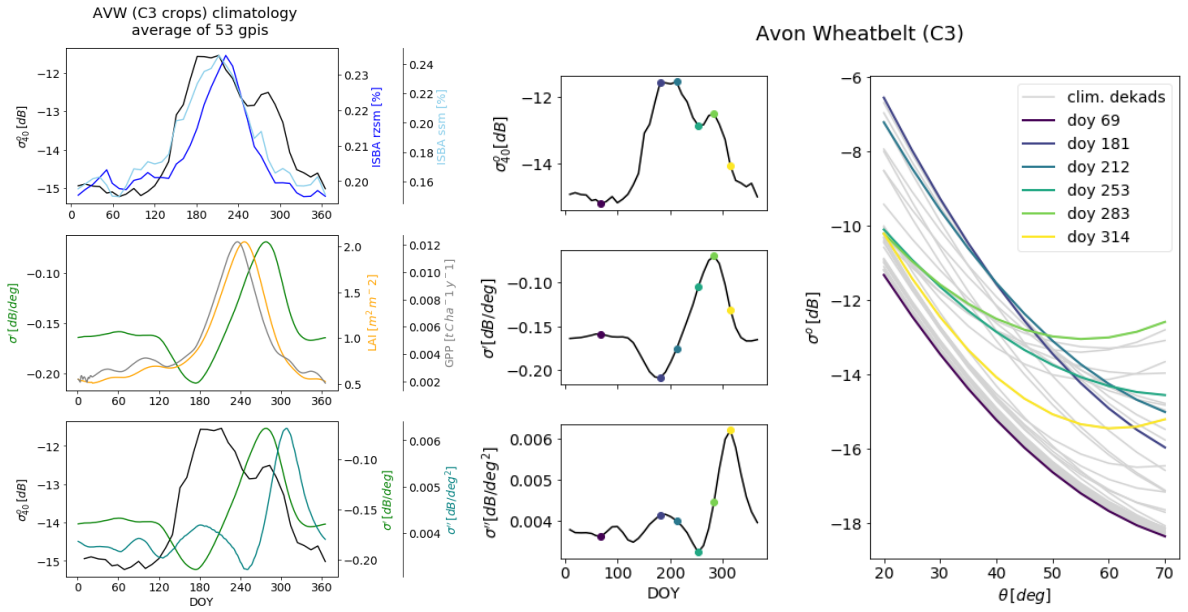

(a) Top panel: soil moisture related variables. Middle panel: vegetation related variables. Bottom panel: ASCAT parameters.

(b) Climatology of σ^o_{40} , σ' and σ'' with key dates highlighted in the σ^o - θ curve. Each line represents a dekad.

Figure B.1: Seasonal climatologies across the Avown Wheatbelt, one of the C3 cropland ROIs.

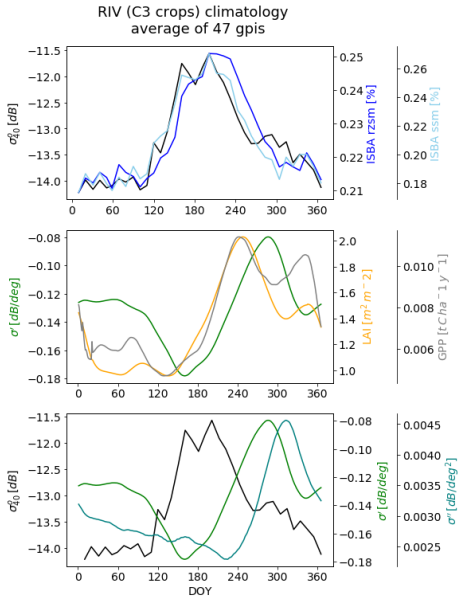

(a) Top panel: soil moisture related variables. Middle panel: vegetation related variables. Bottom panel: ASCAT parameters.

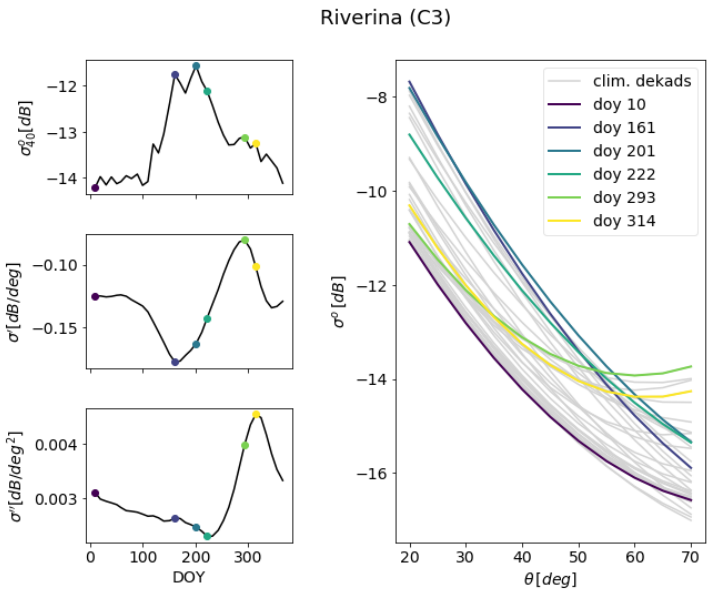

(b) Climatology of σ^o_{40} , σ' and σ'' with key dates highlighted in the σ^o - θ curve. Each line represents a dekad.

Figure B.2: Seasonal climatologies across the Riverina, one of the C3 cropland ROIs.

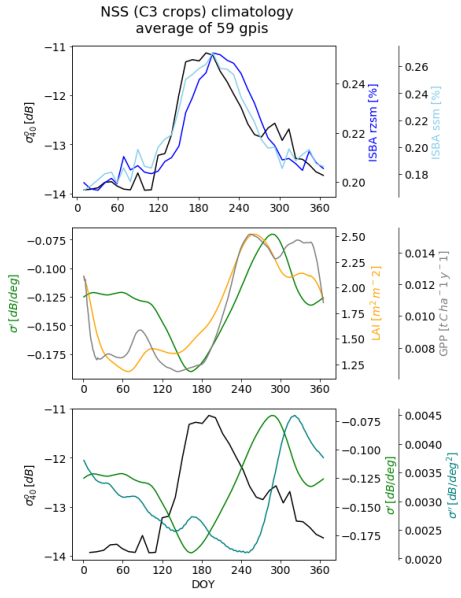

(a) Top panel: soil moisture related variables. Middle panel: vegetation related variables. Bottom panel: ASCAT parameters.

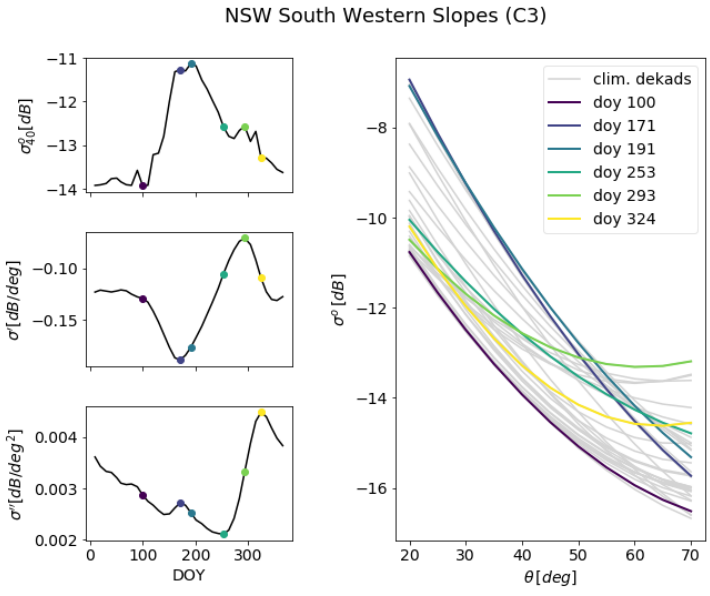

(b) Climatology of σ^o_{40} , σ' and σ'' with key dates highlighted in the σ^o - θ curve. Each line represents a dekad.

Figure B.3: Seasonal climatologies across the NSW Southern Slopes, one of the C3 cropland ROIs.

Evergreen broadleaved forests

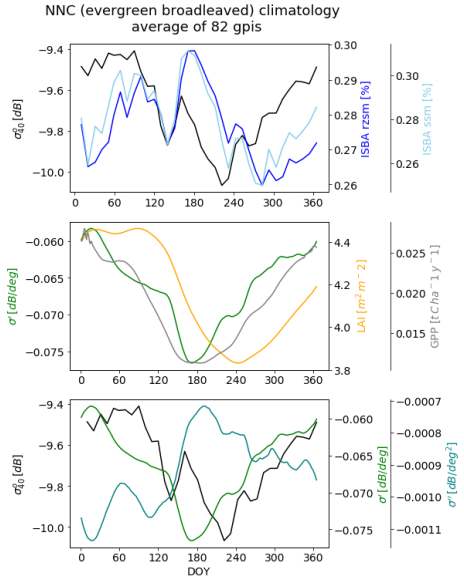

(a) Top panel: soil moisture related variables. Middle panel: vegetation related variables. Bottom panel: ASCAT parameters.

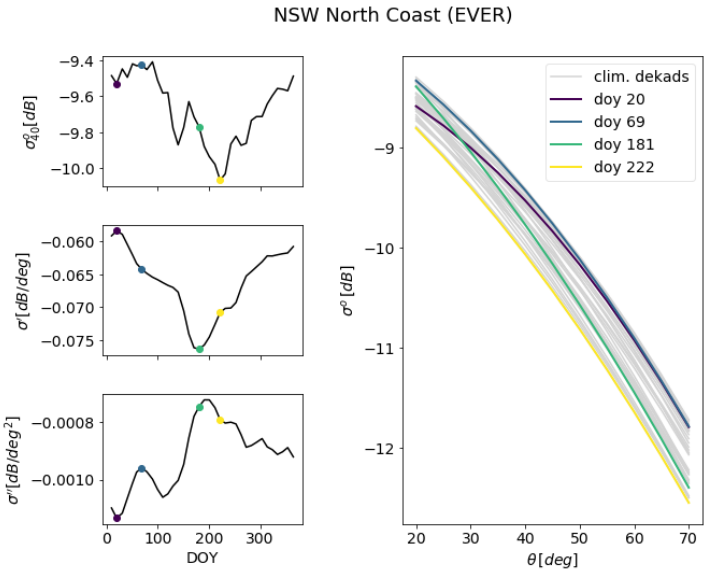

(b) Climatology of σ^o_{40} , σ' and σ'' with key dates highlighted in the σ^o - θ curve. Each line represents a dekad.

Figure B.4: Seasonal climatologies across the NSW Nort Coast, one of the evergreen broadleaf forest ROIs.

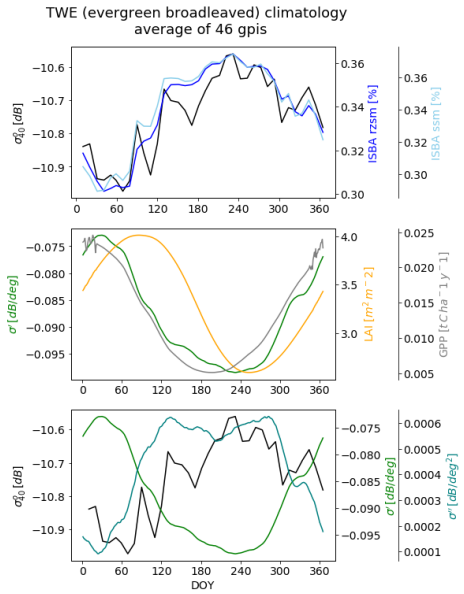

(a) Top panel: soil moisture related variables. Middle panel: vegetation related variables. Bottom panel: ASCAT parameters.

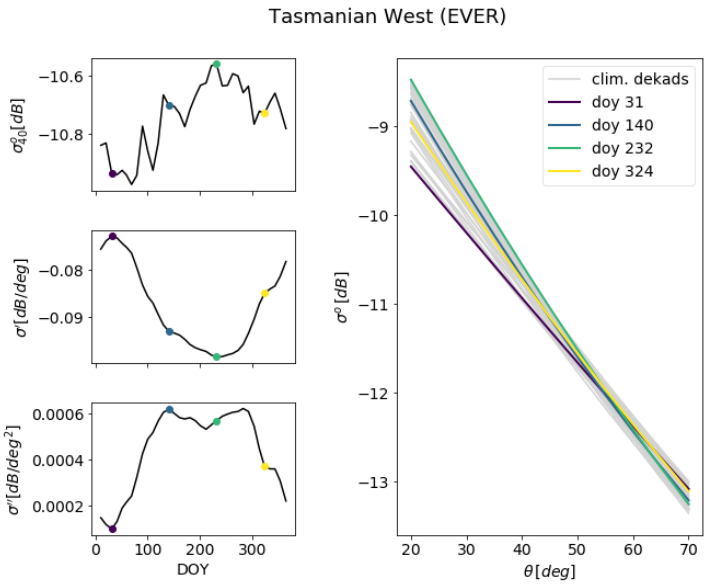

(b) Climatology of σ^o_{40} , σ' and σ'' with key dates highlighted in the σ^o - θ curve. Each line represents a dekad.

Figure B.5: Seasonal climatologies across the Tasmanian West, one of the evergreen broadleaf forest ROIs.

Tropical grasslands

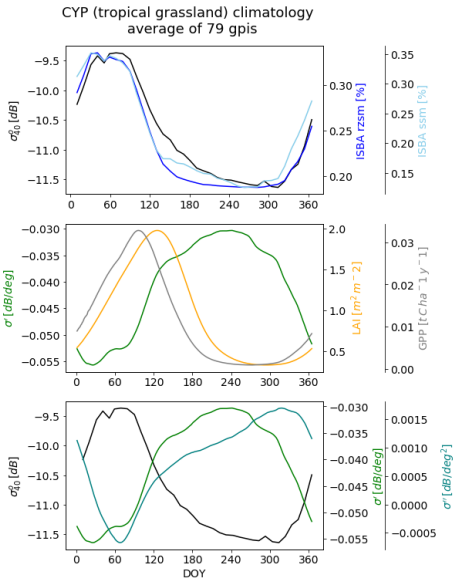

(a) Top panel: soil moisture related variables. Middle panel: vegetation related variables. Bottom panel: ASCAT parameters.

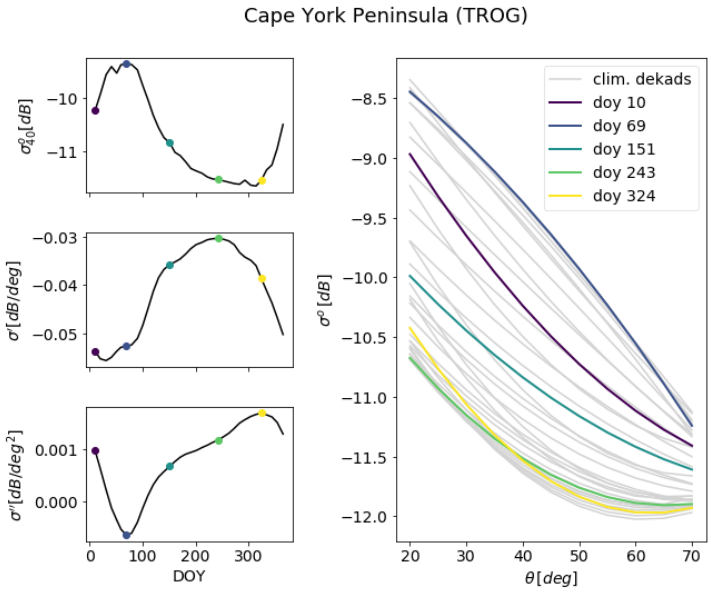

(b) Climatology of σ^o_{40} , σ' and σ'' with key dates highlighted in the σ^o - θ curve. Each line represents a dekad.

Figure B.6: Seasonal climatologies across the Cape York Peninsula, one of the tropical grassland ROIs.

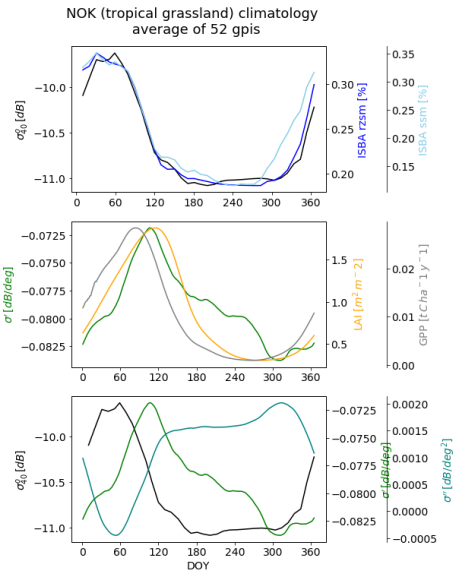

(a) Top panel: soil moisture related variables. Middle panel: vegetation related variables. Bottom panel: ASCAT parameters.

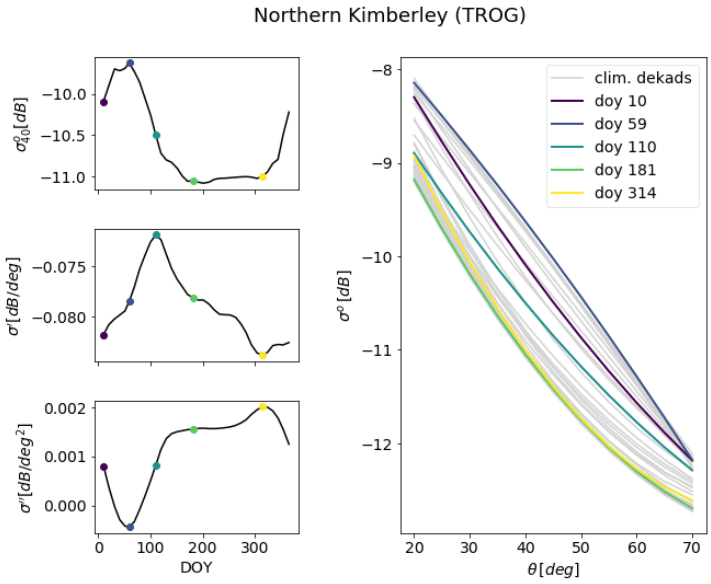

(b) Climatology of σ^o_{40} , σ' and σ'' with key dates highlighted in the σ^o - θ curve. Each line represents a dekad.

Figure B.7: Seasonal climatologies across the Northern Kimberley, one of the tropical grassland ROIs.

Bare soil

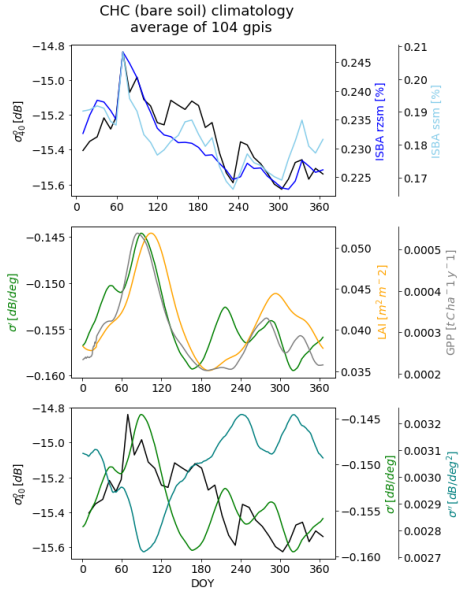

(a) Top panel: soil moisture related variables. Middle panel: vegetation related variables. Bottom panel: ASCAT parameters.

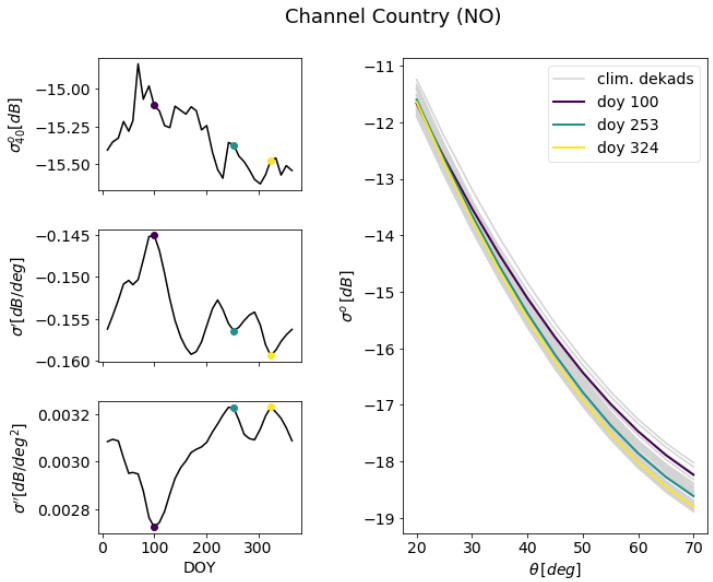

(b) Climatology of σ^o_{40} , σ' and σ'' with key dates highlighted in the σ^o - θ curve. Each line represents a dekad.

Figure B.8: Seasonal climatologies across the Channel Country, one of the bare soil ROIs.

C

Time series of ROIs for drought analysis

C3 crops

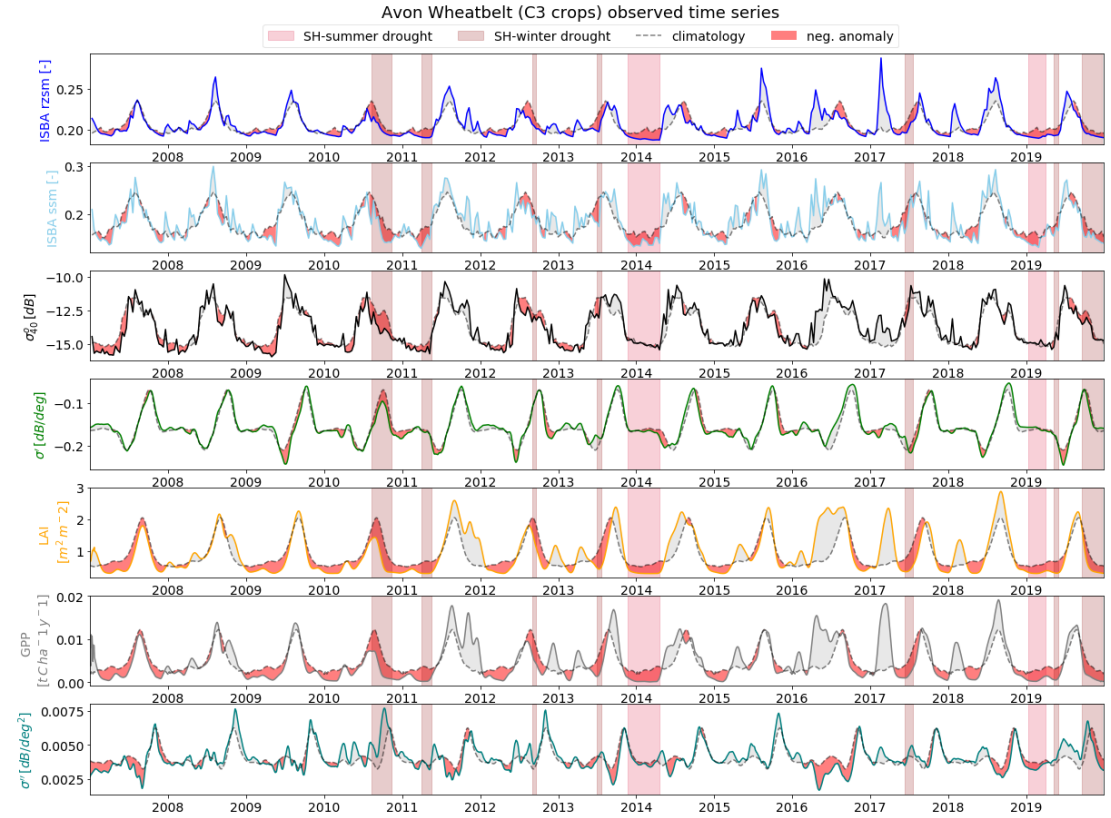

(a)

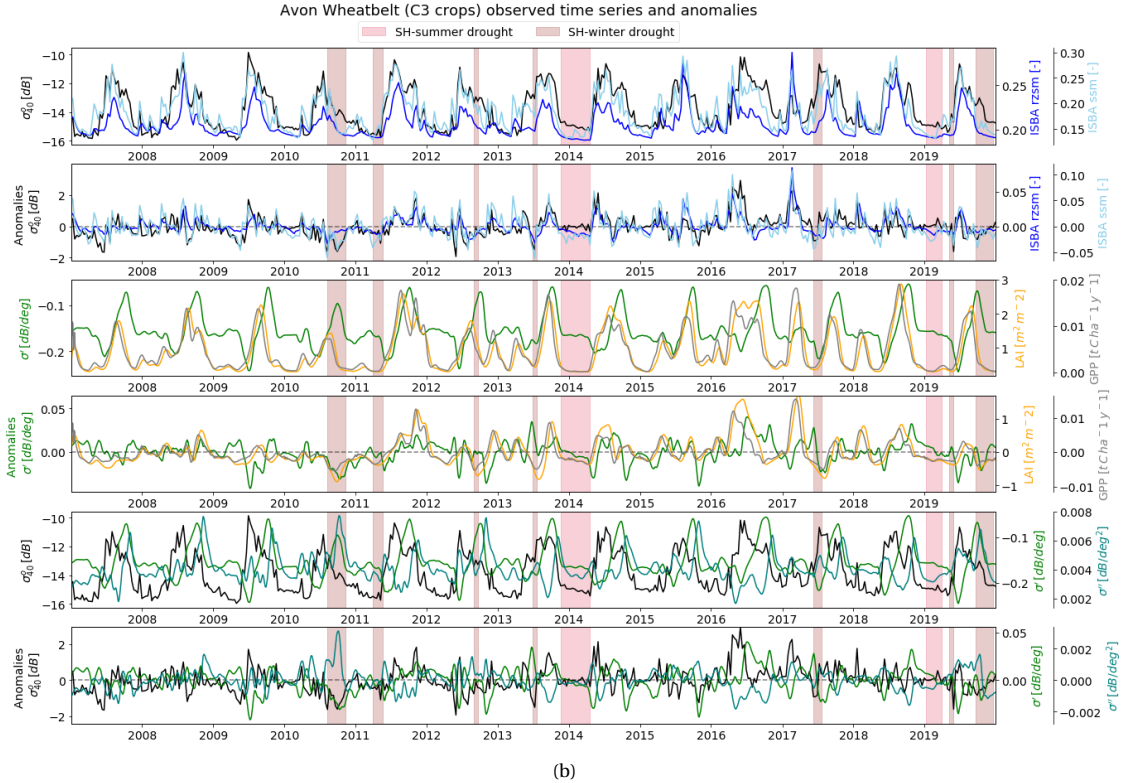

(b)

Figure C.1: Avon Wheatbelt (C3 crops) time series with anomalies and droughts highlighted

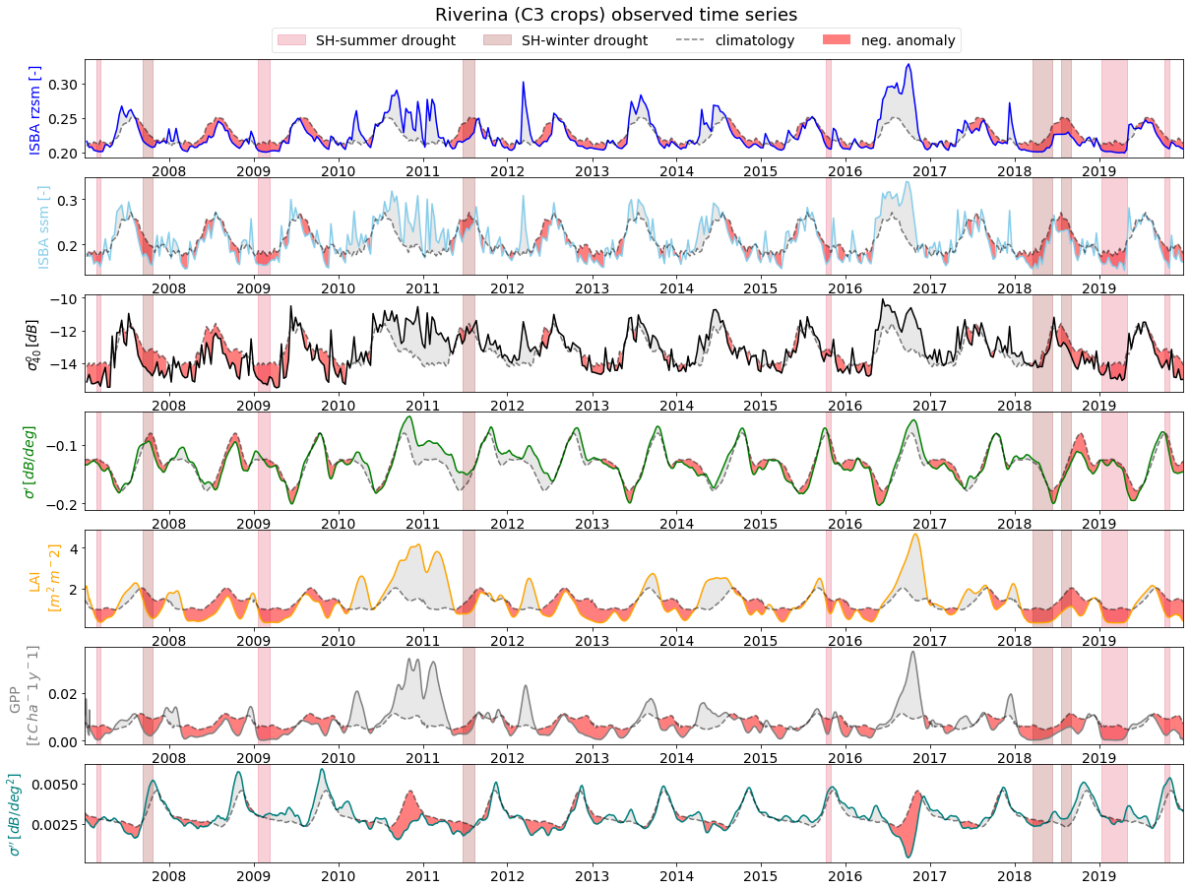

(a)

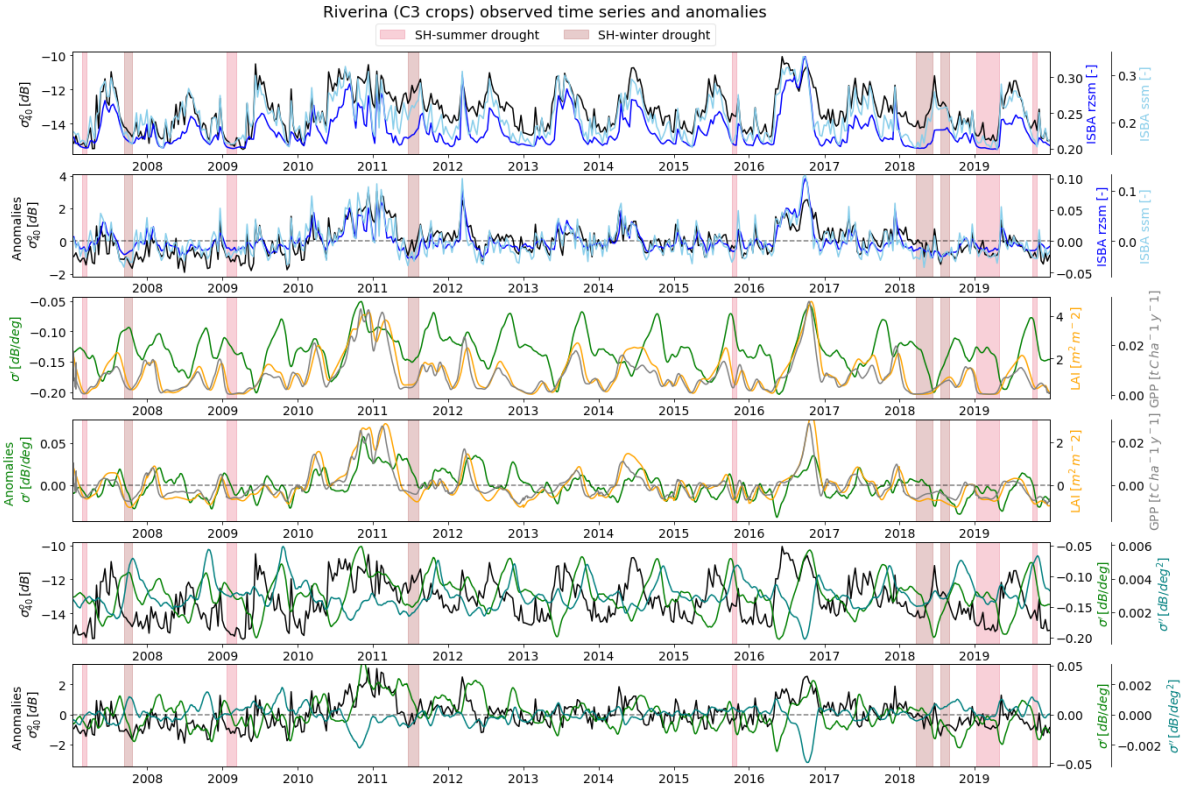

(b)

Figure C.2: Riverina (C3 crops) time series with anomalies and droughts highlighted

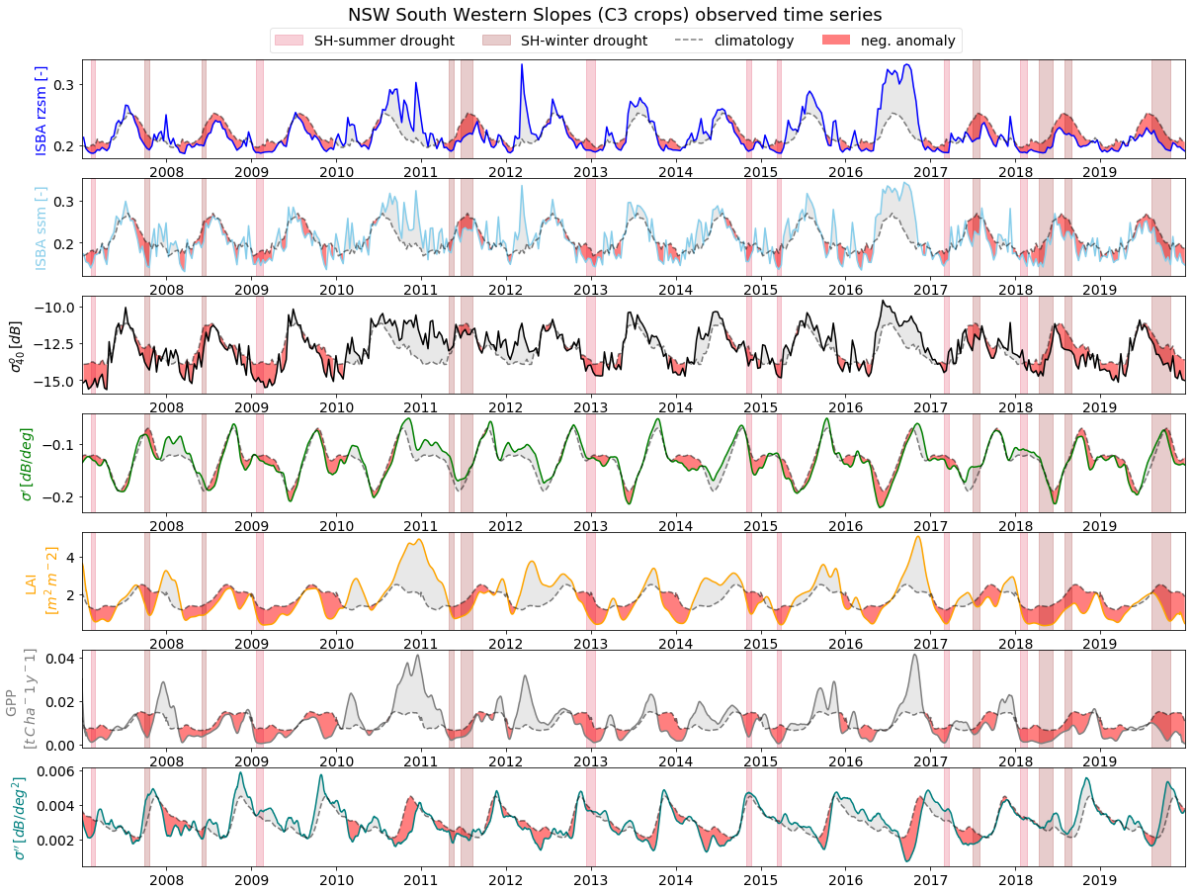

(a)

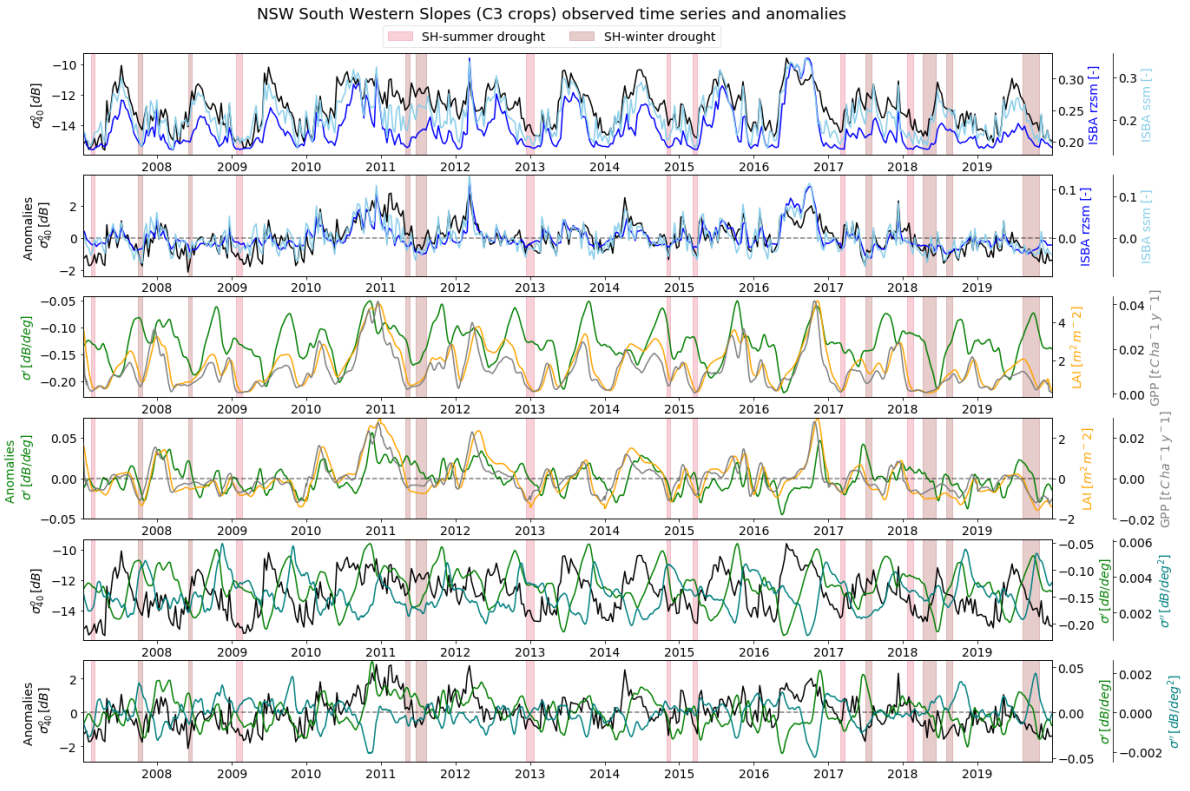

(b)

Figure C.3: NSW Southern Slopes (C3 crops) time series with anomalies and droughts highlighted

Evergreen broadleaved forests

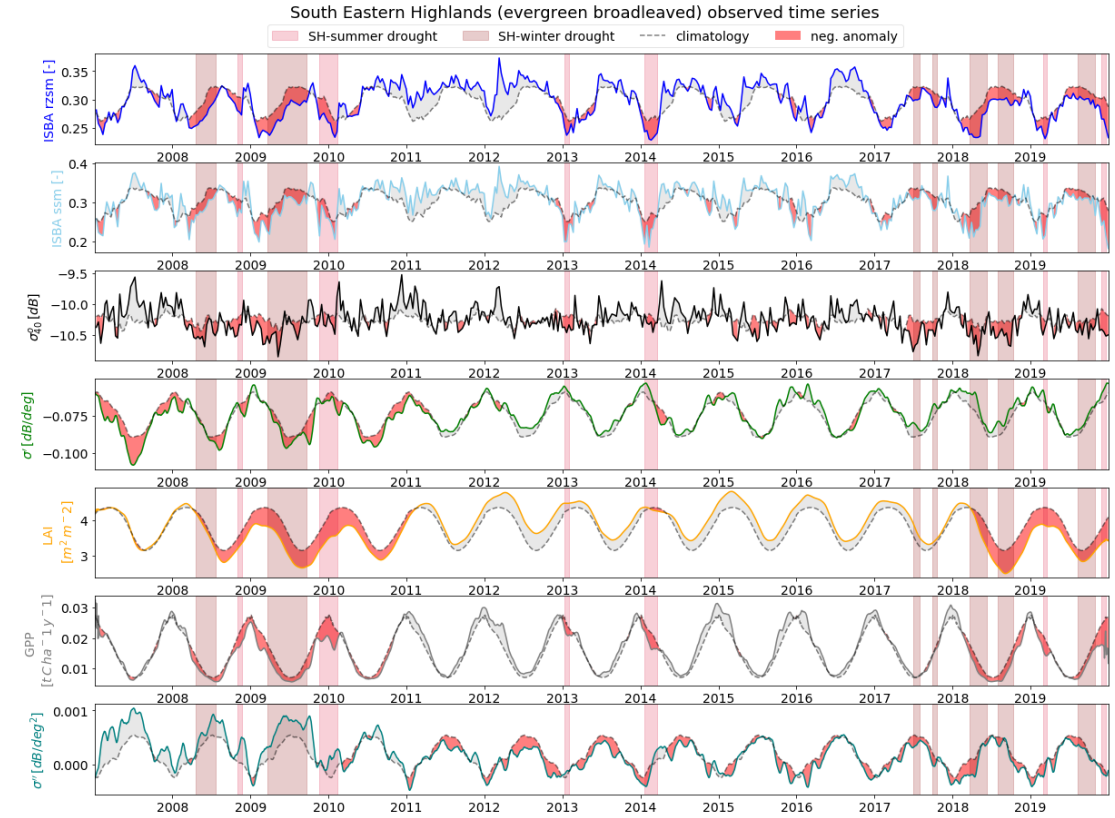

(a)

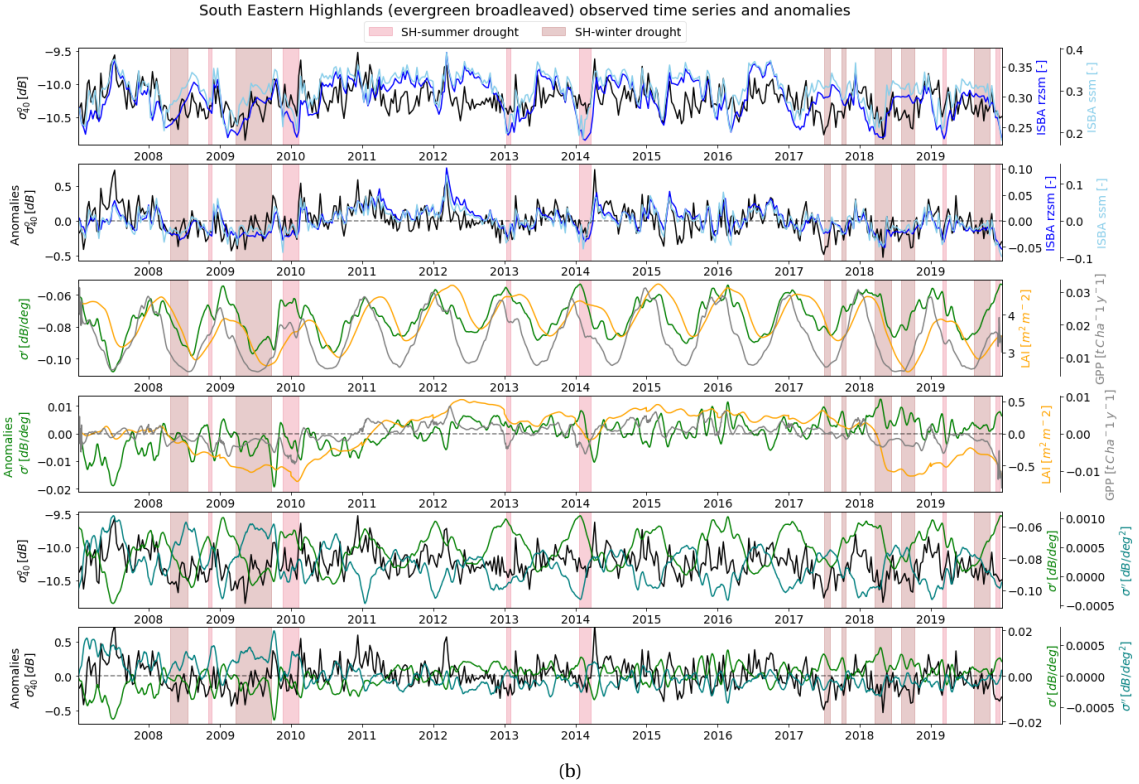

(b)

Figure C.4: South Eastern Highlands (evergreen broadleaved forests) time series with anomalies and droughts highlighted

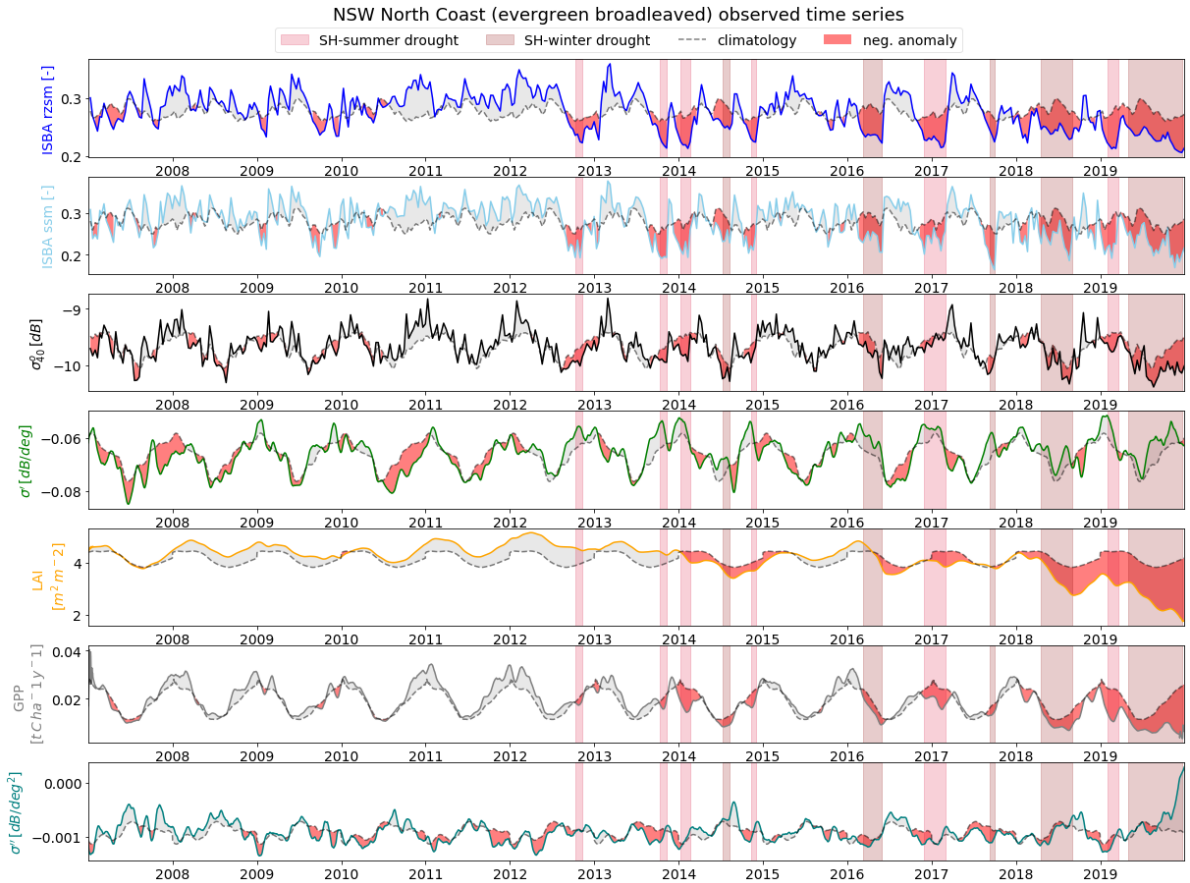

(a)

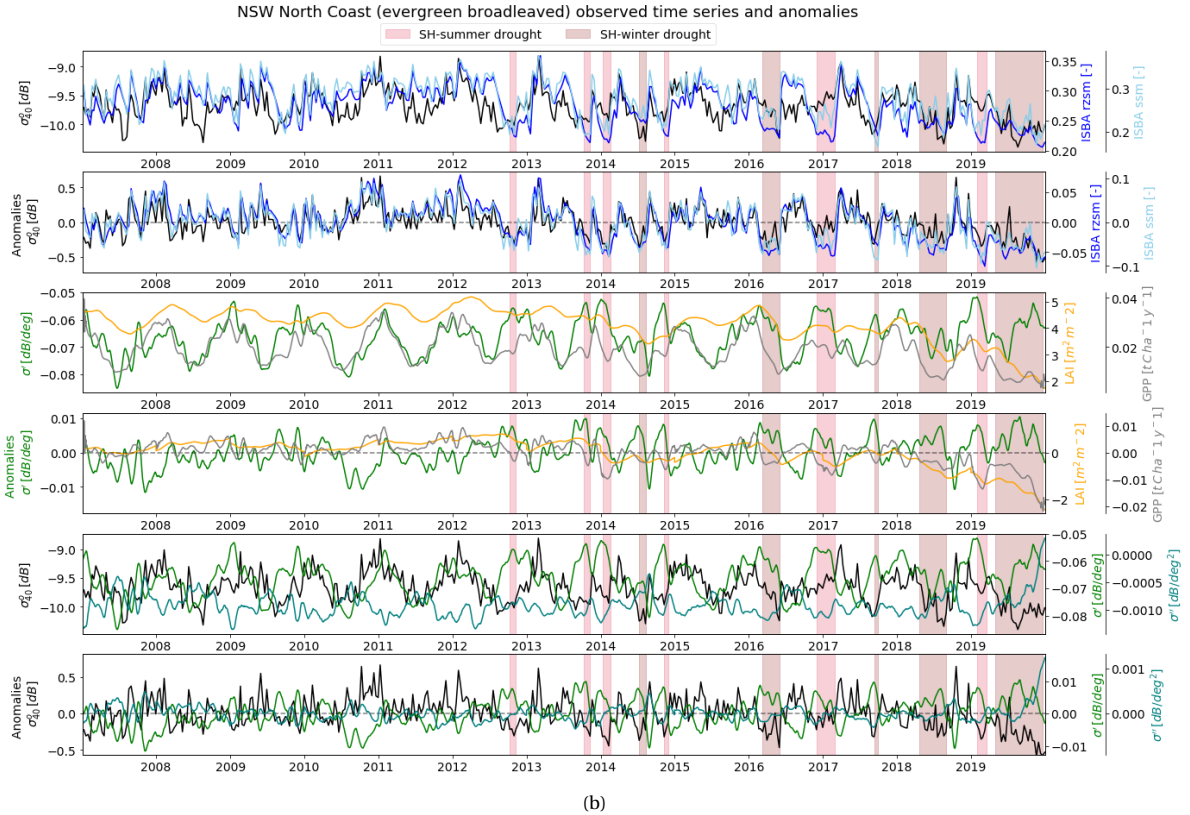

(b)

Figure C.5: NSW Northern Coast (evergreen broadleaved forests) time series with anomalies and droughts highlighted

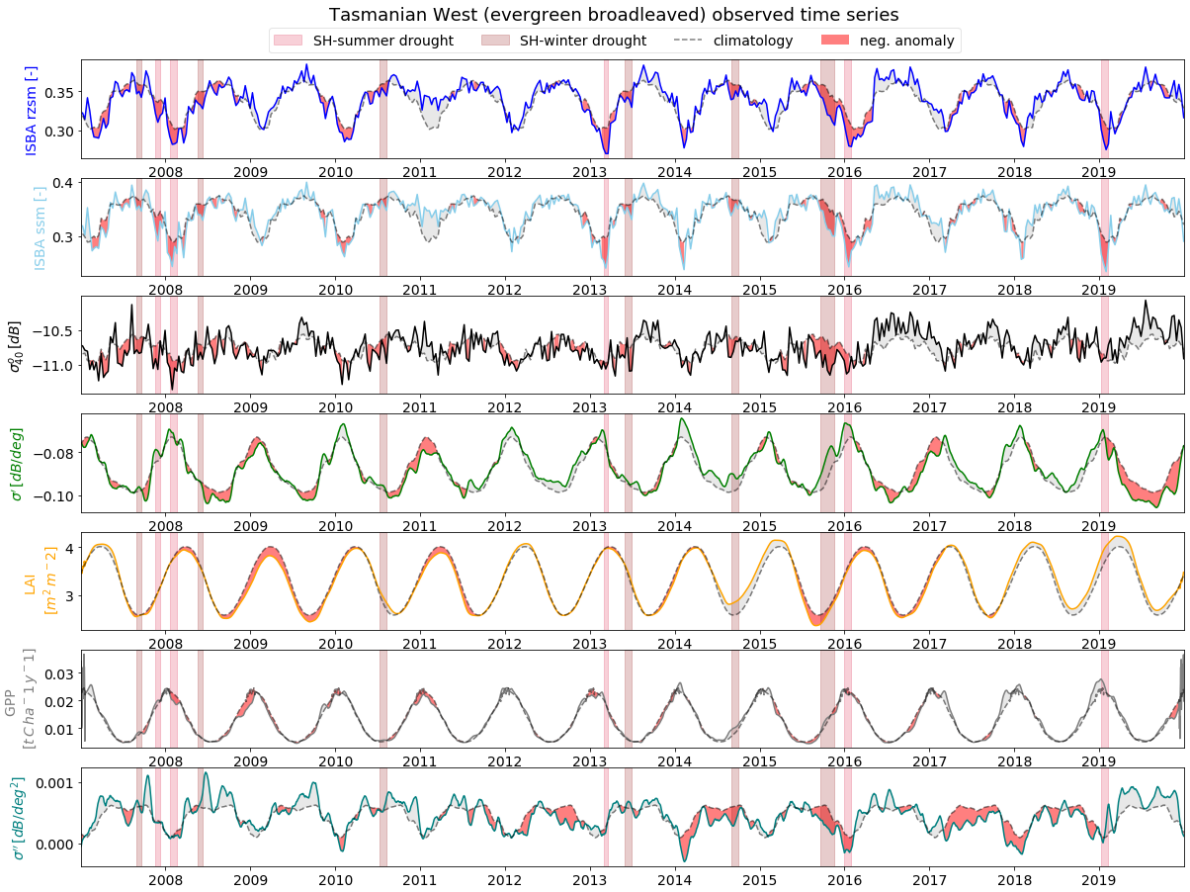

(a)

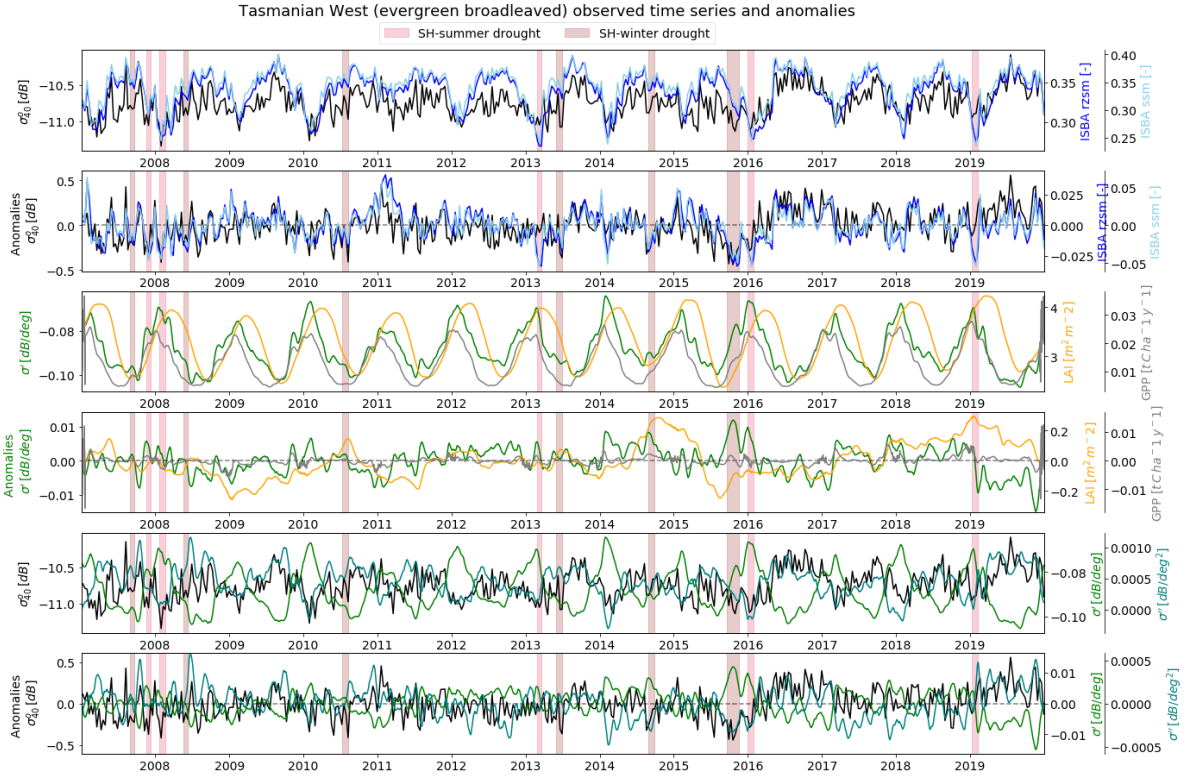

(b)

Figure C.6: Tasmanian West (evergreen broadleaved forests) time series with anomalies and droughts highlighted

Tropical grasslands

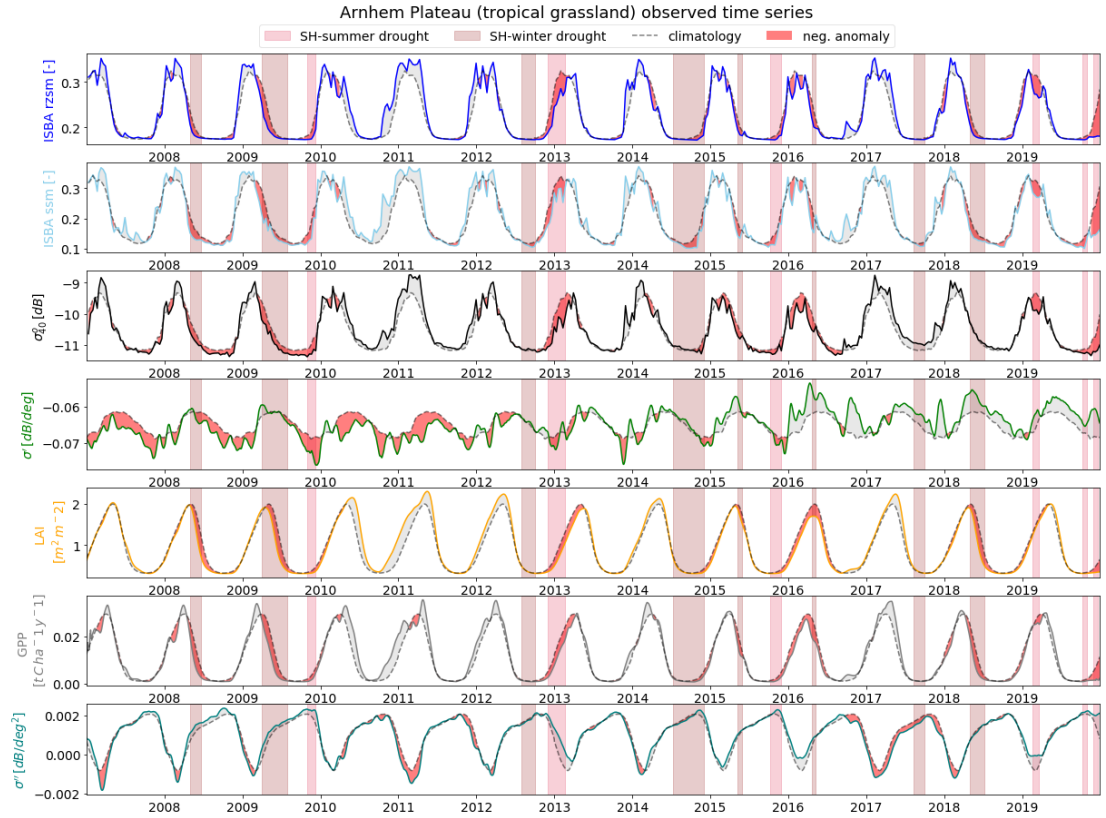

(a)

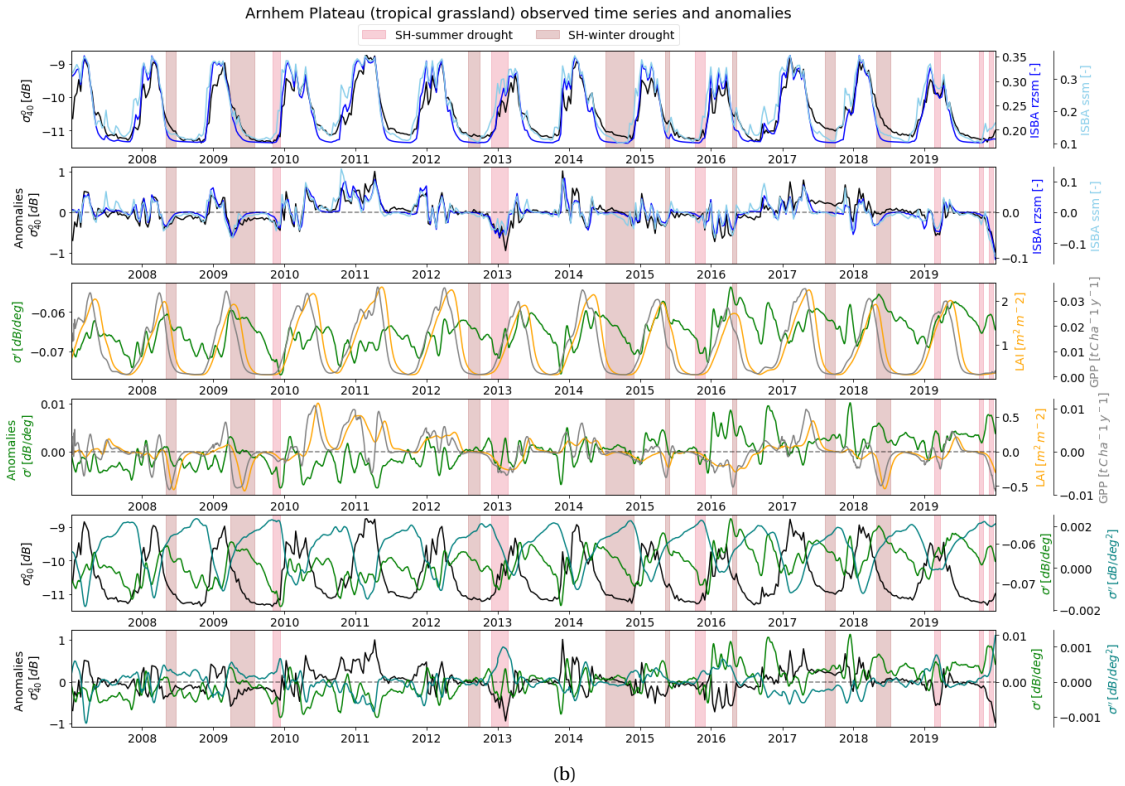

(b)

Figure C.7: Arnhem Plateau (tropical grasslands) time series with anomalies and droughts highlighted

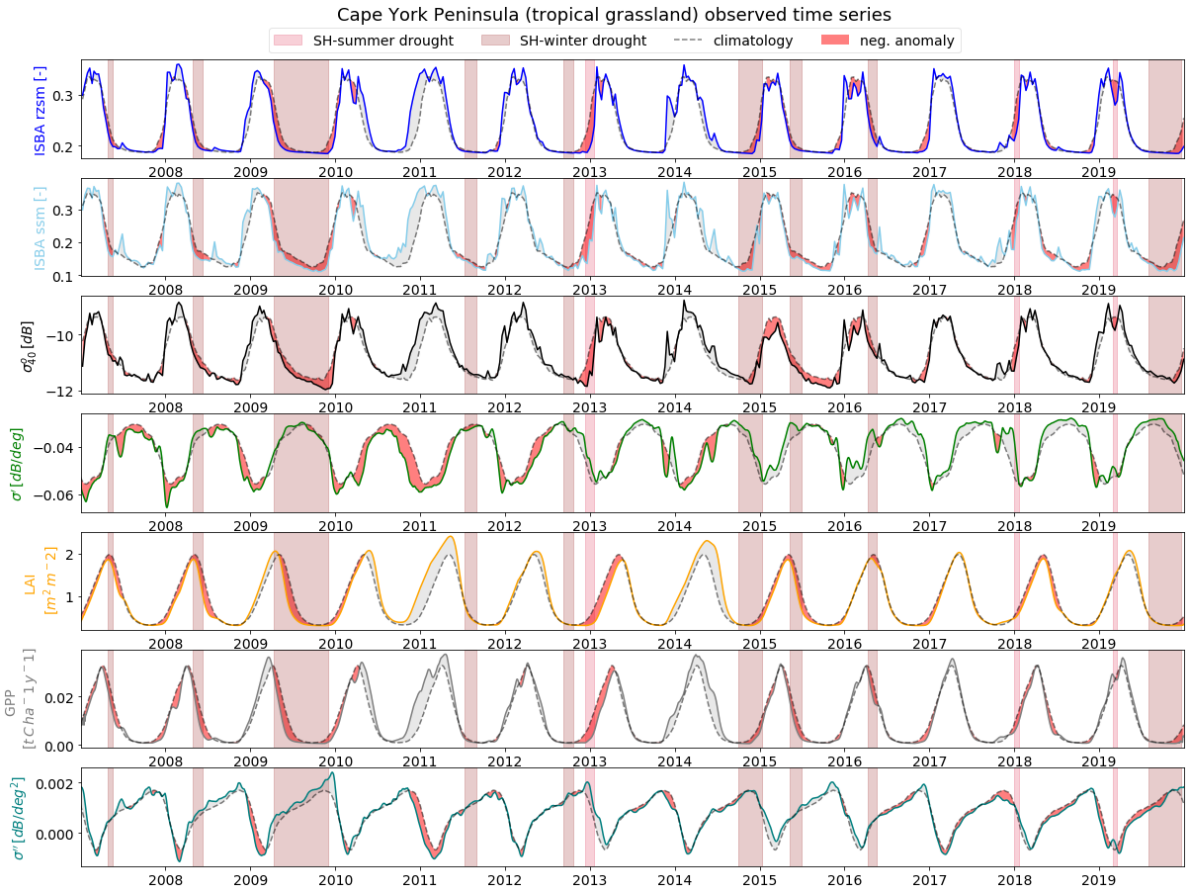

(a)

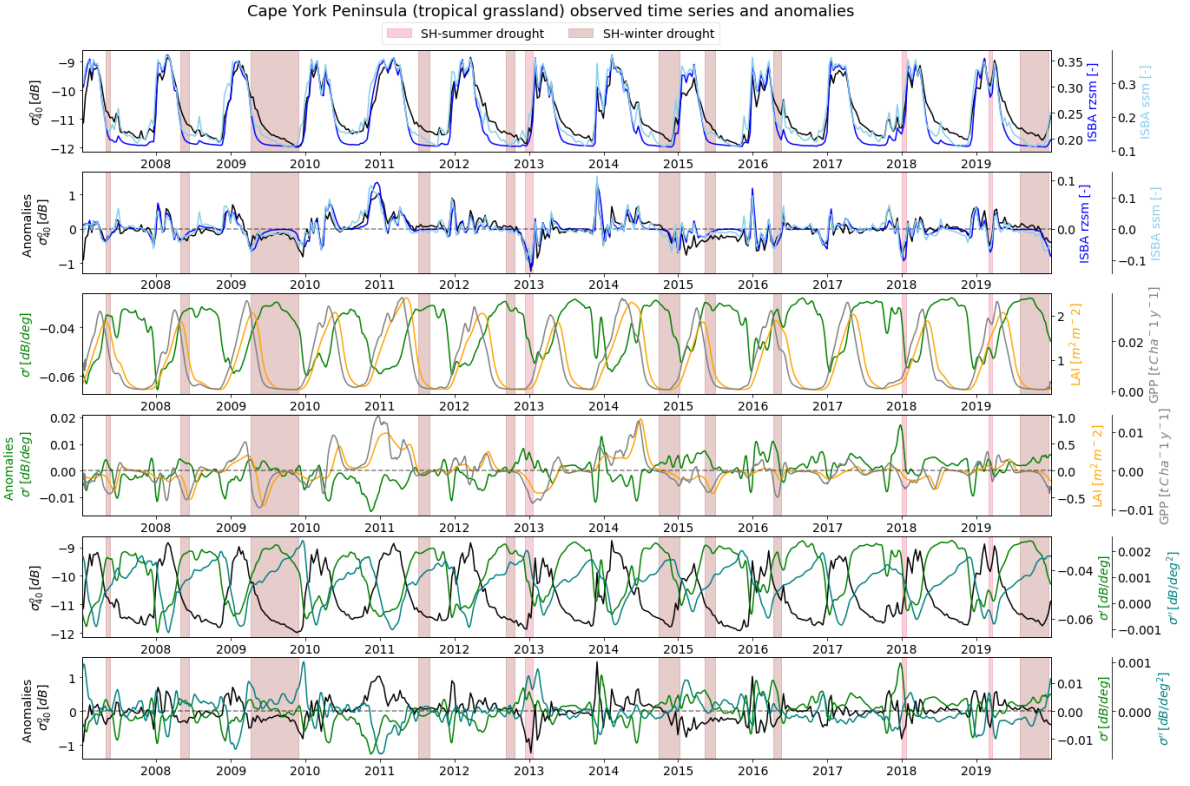

(b)

Figure C.8: Cape York Peninsula (tropical grasslands) time series with anomalies and droughts highlighted

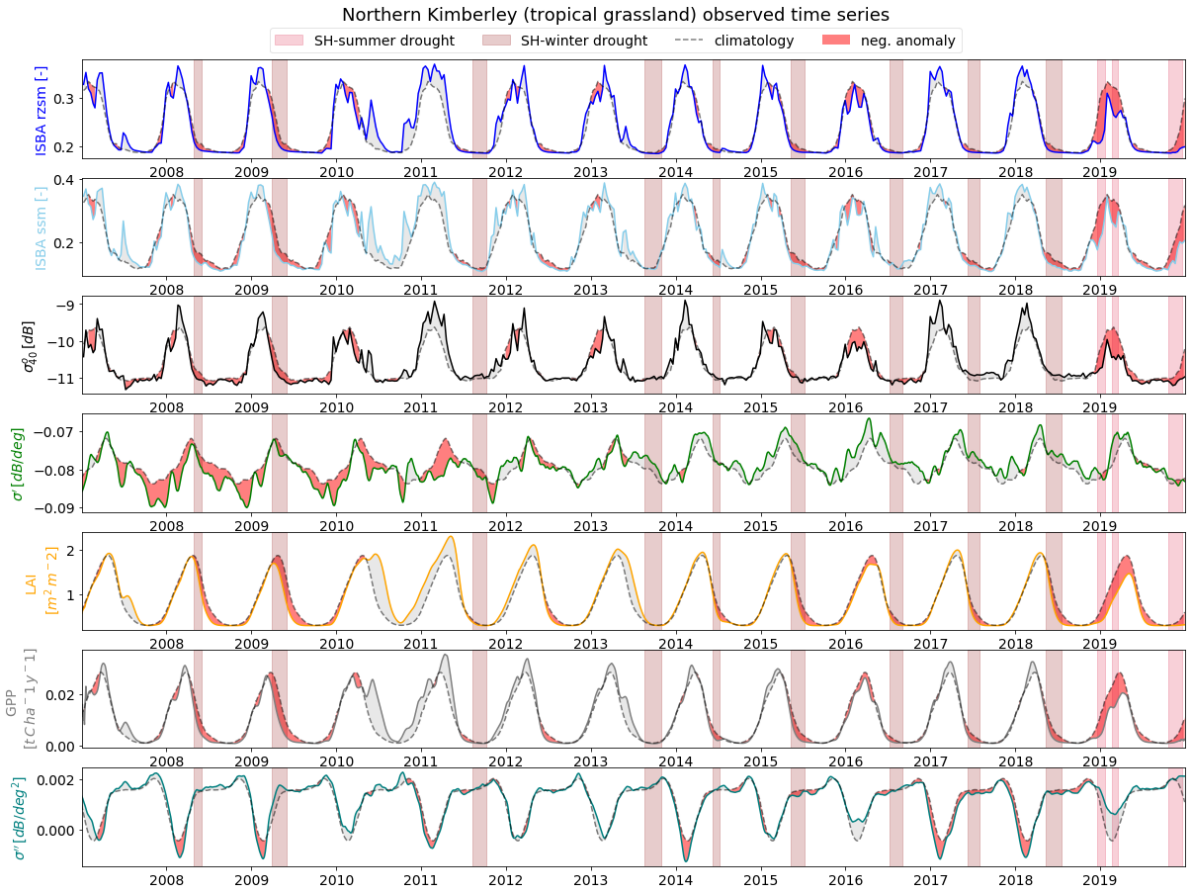

(a)

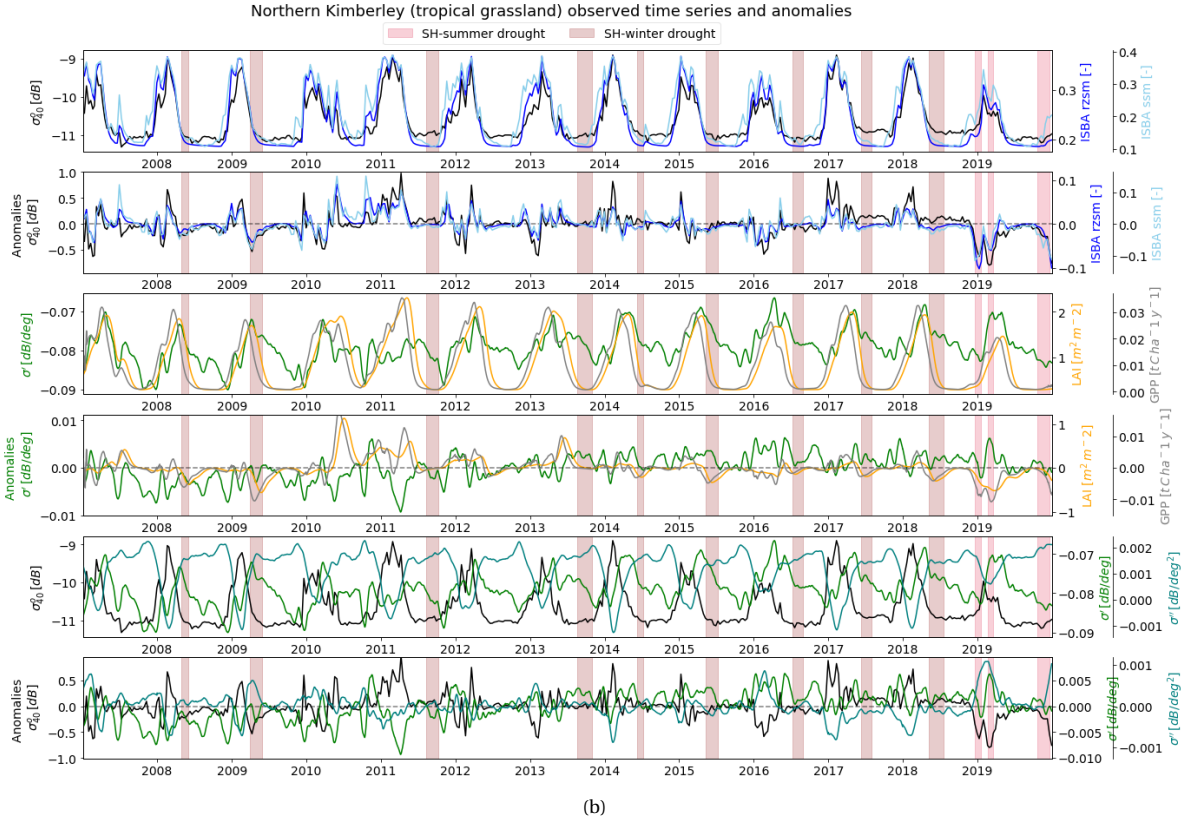

(b)

Figure C.9: Northern Kimberley (tropical grasslands) time series with anomalies and droughts highlighted

Bare soil

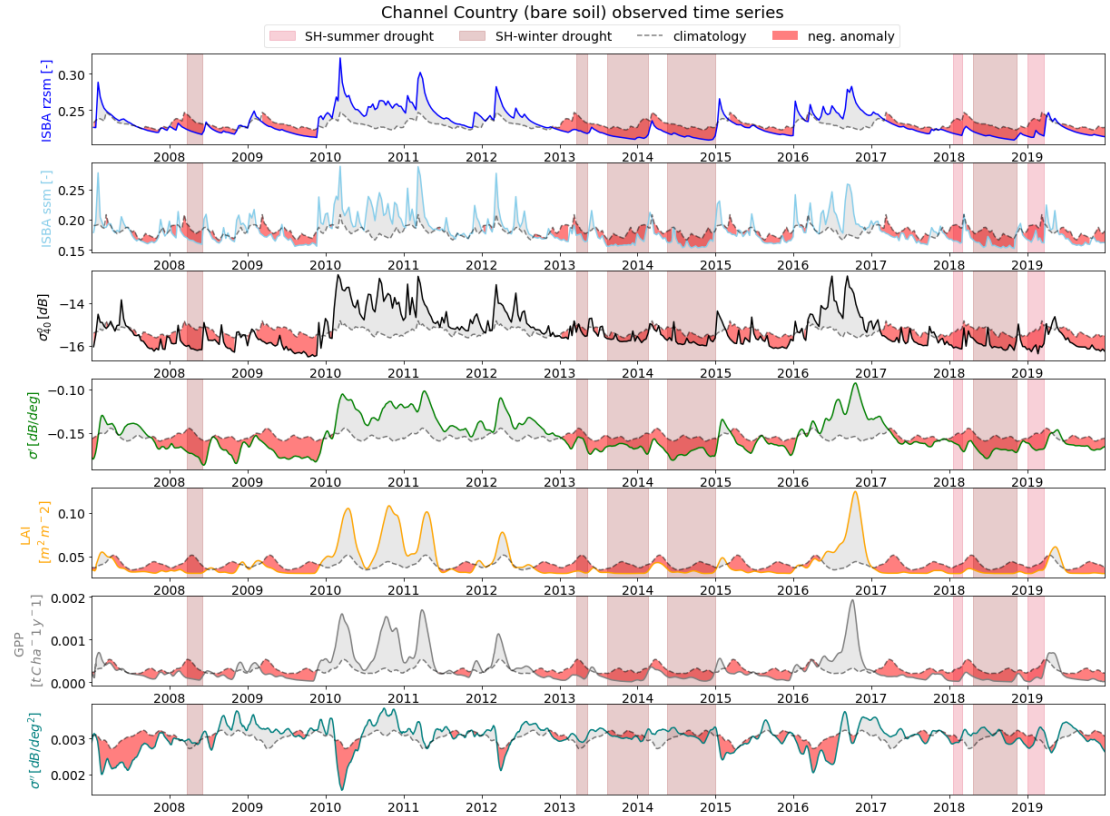

(a)

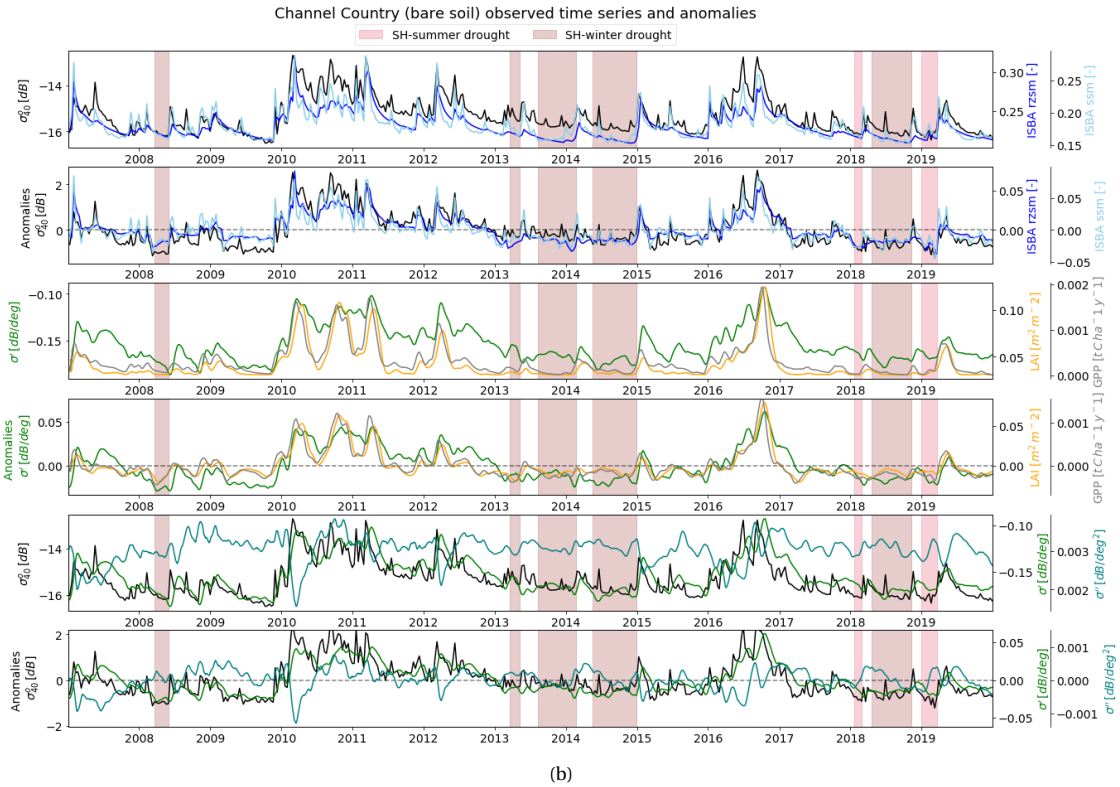

(b)

Figure C.10: Channel Country (bare soil) time series with anomalies and droughts highlighted

D

Detrended time series of ROIs with clear long term trends

Evergreen broadleaved forests

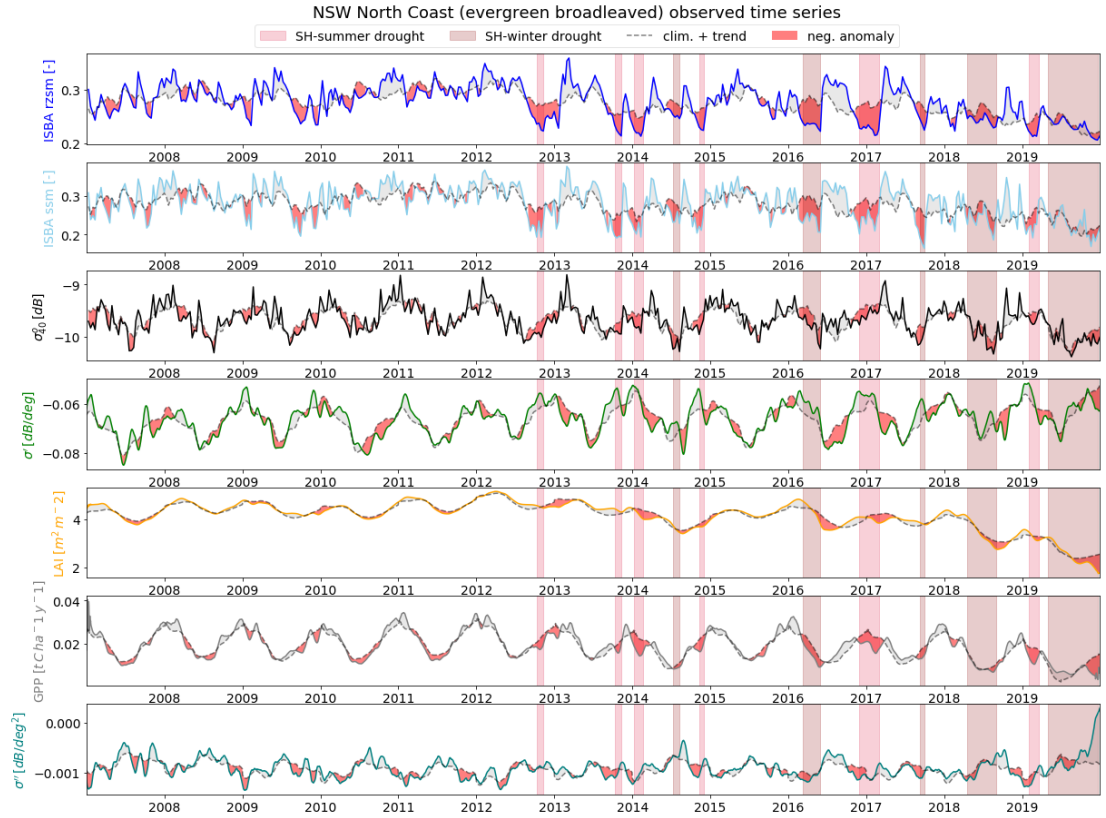

(a)

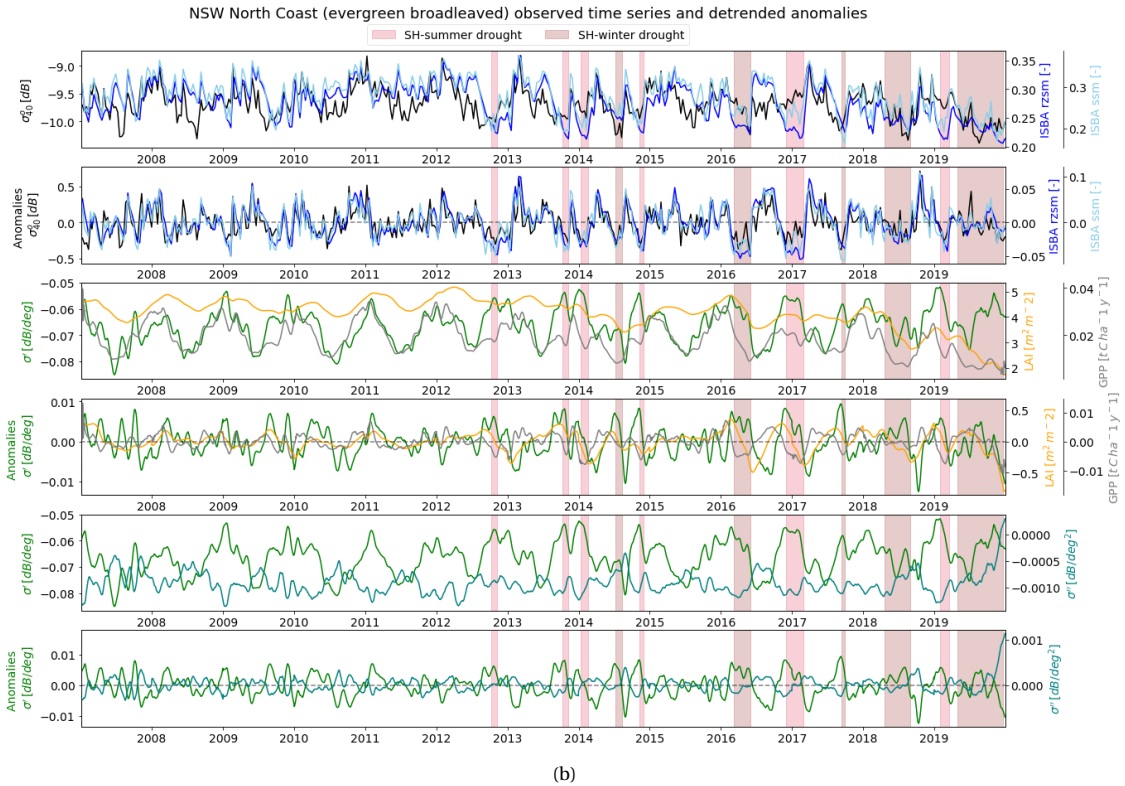

(b)

Figure D.1: NSW North Coast (evergreen broadleaved forests) time series with the long term trend removed from the anomalies and added to the seasonal cycle

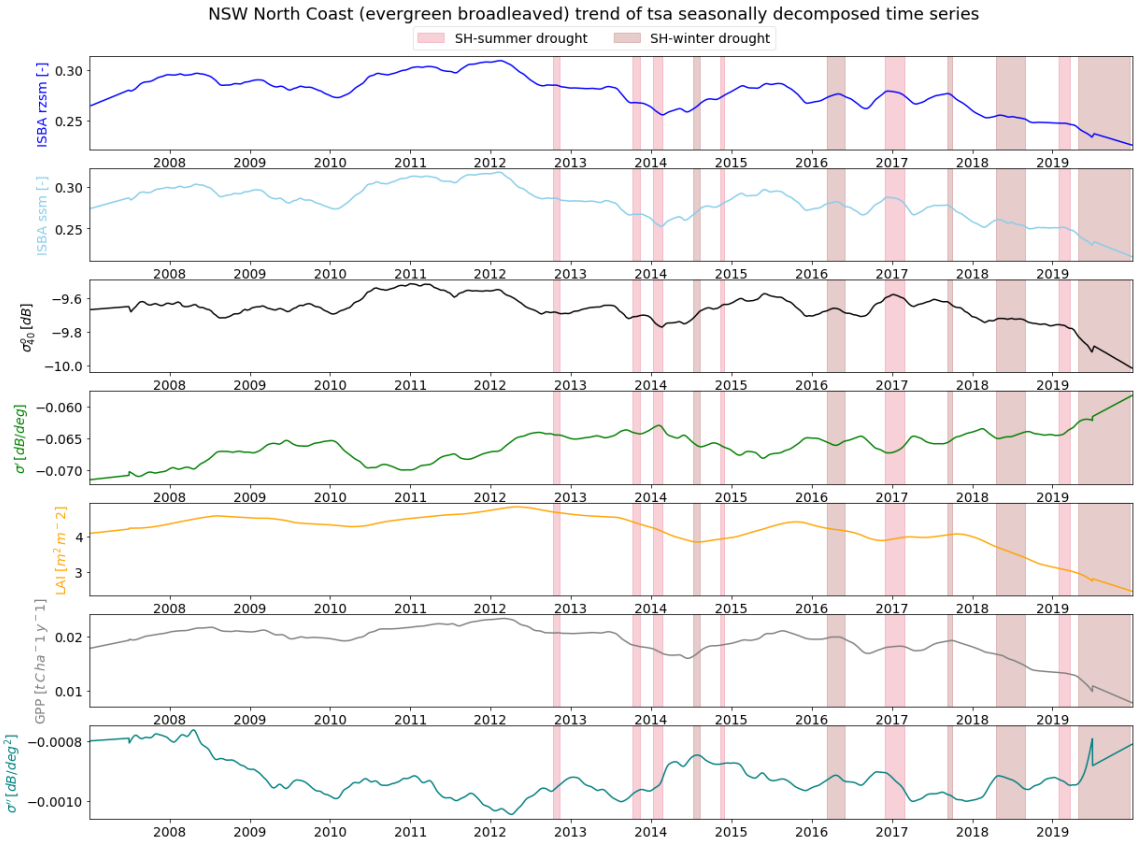

Figure D.2: NSW North Coast (evergreen broadleaved forests) long term trend

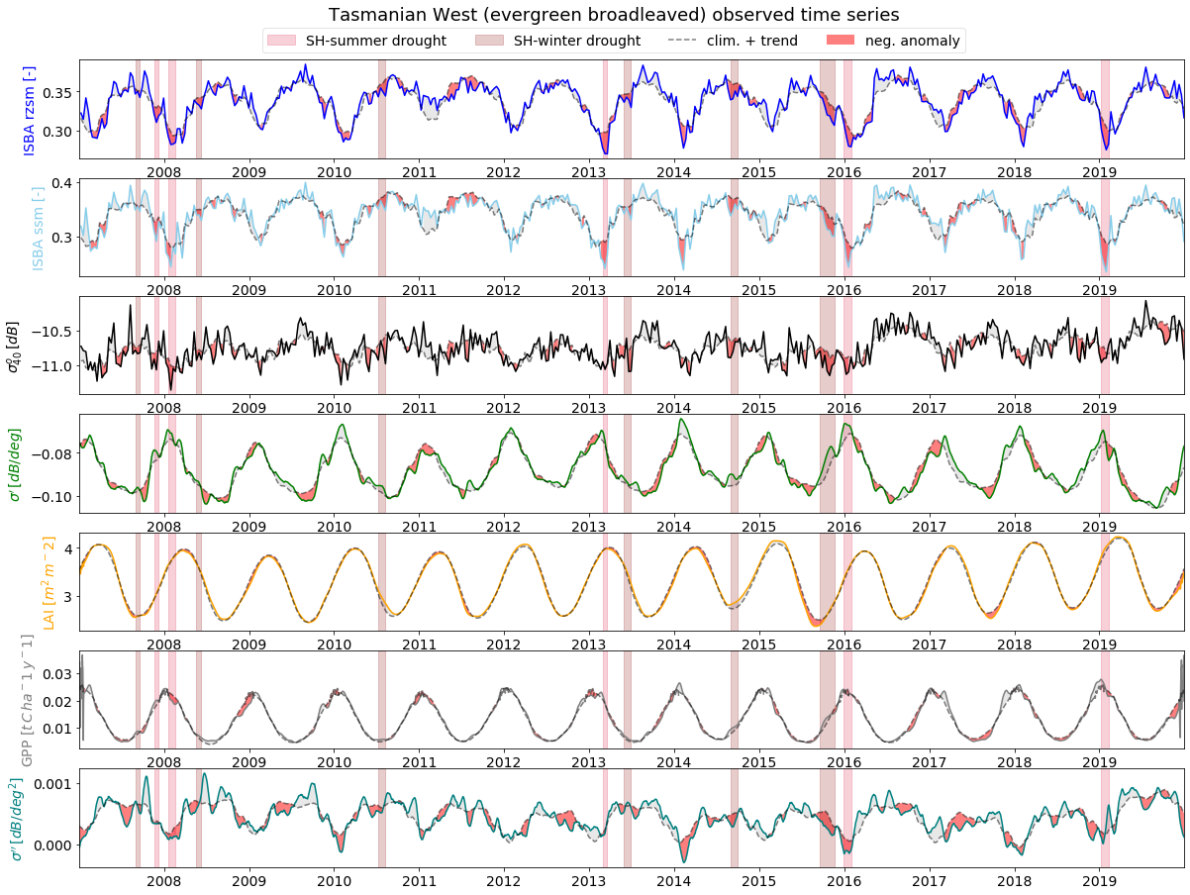

(a)

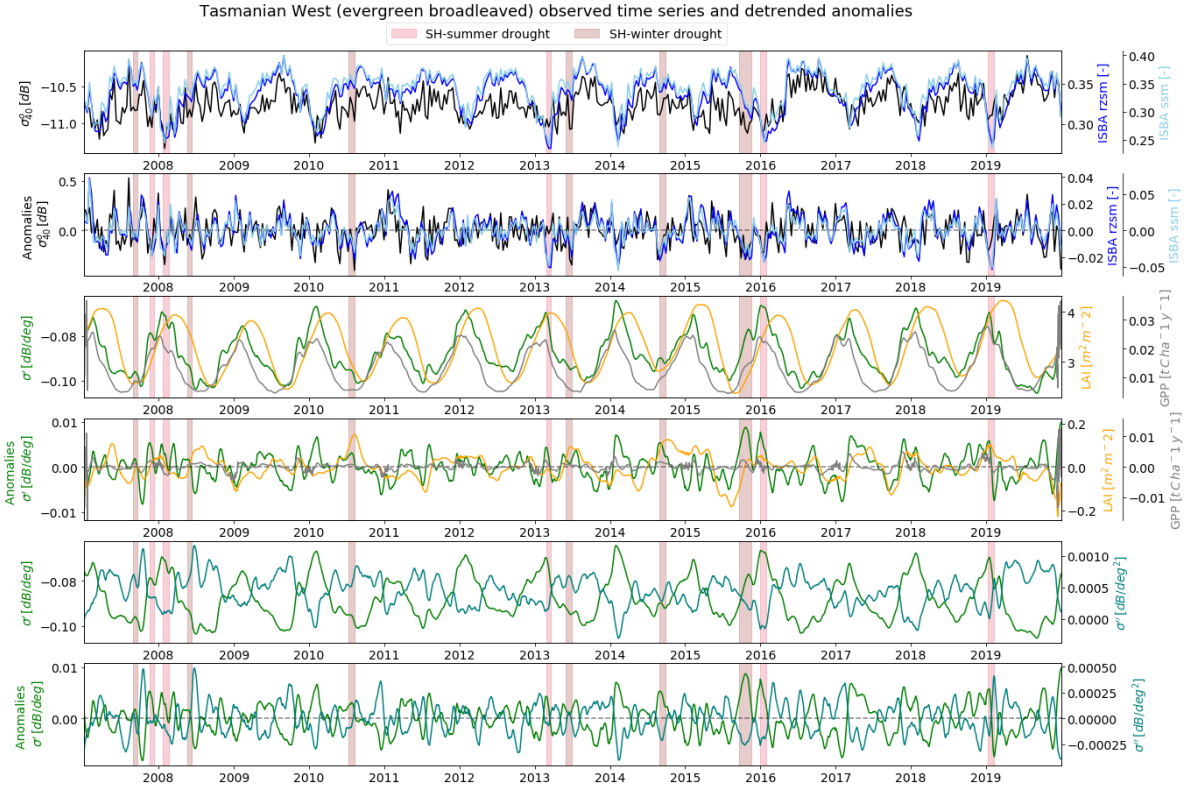

(b)

Figure D.3: Tasmanian West (evergreen broadleaved forests) time series with the long term trend removed from the anomalies and added to the seasonal cycle

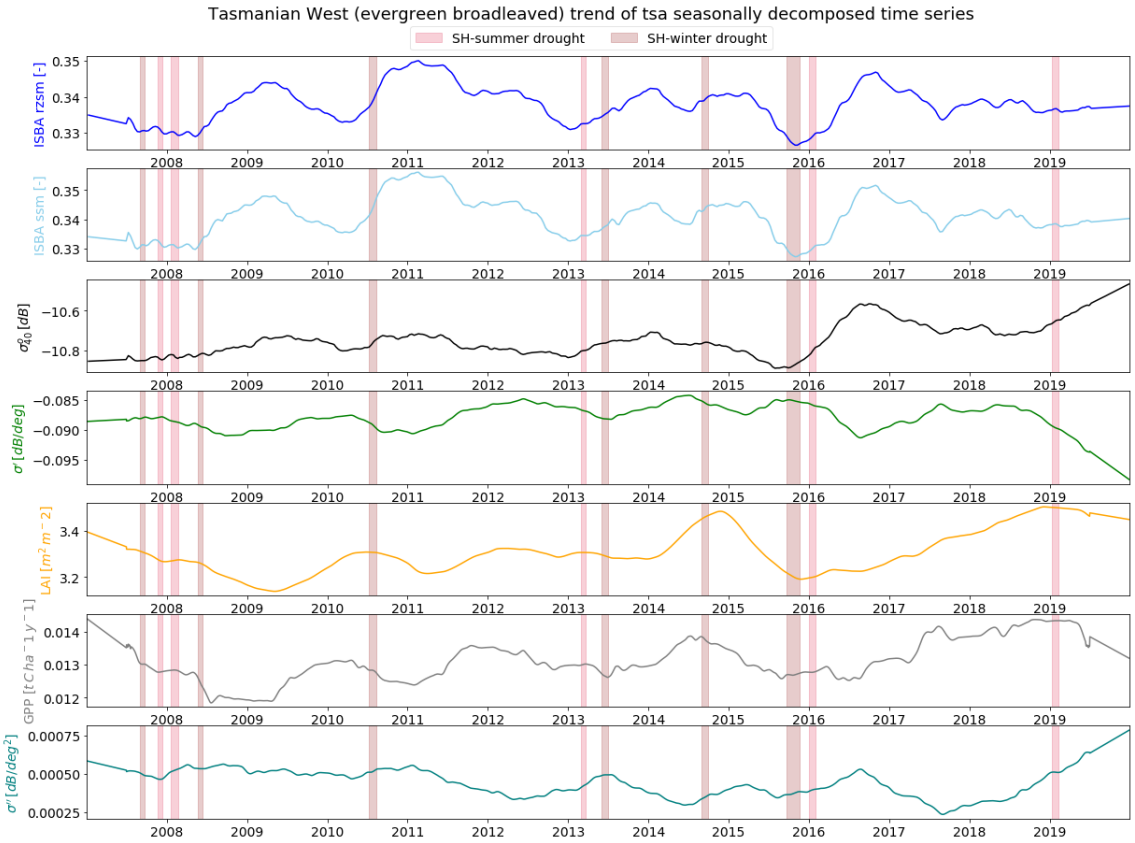

Figure D.4: Tasmanian West (evergreen broadleaved forests) long term trend

Tropical grasslands

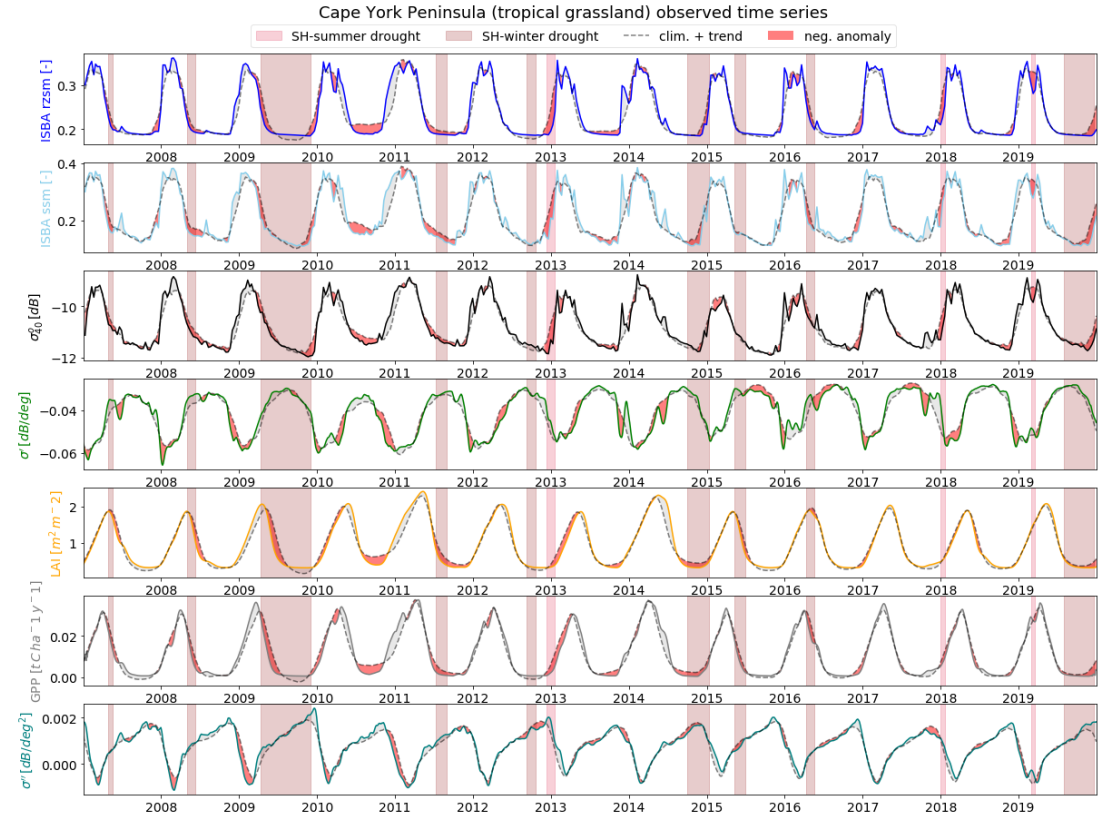

(a)

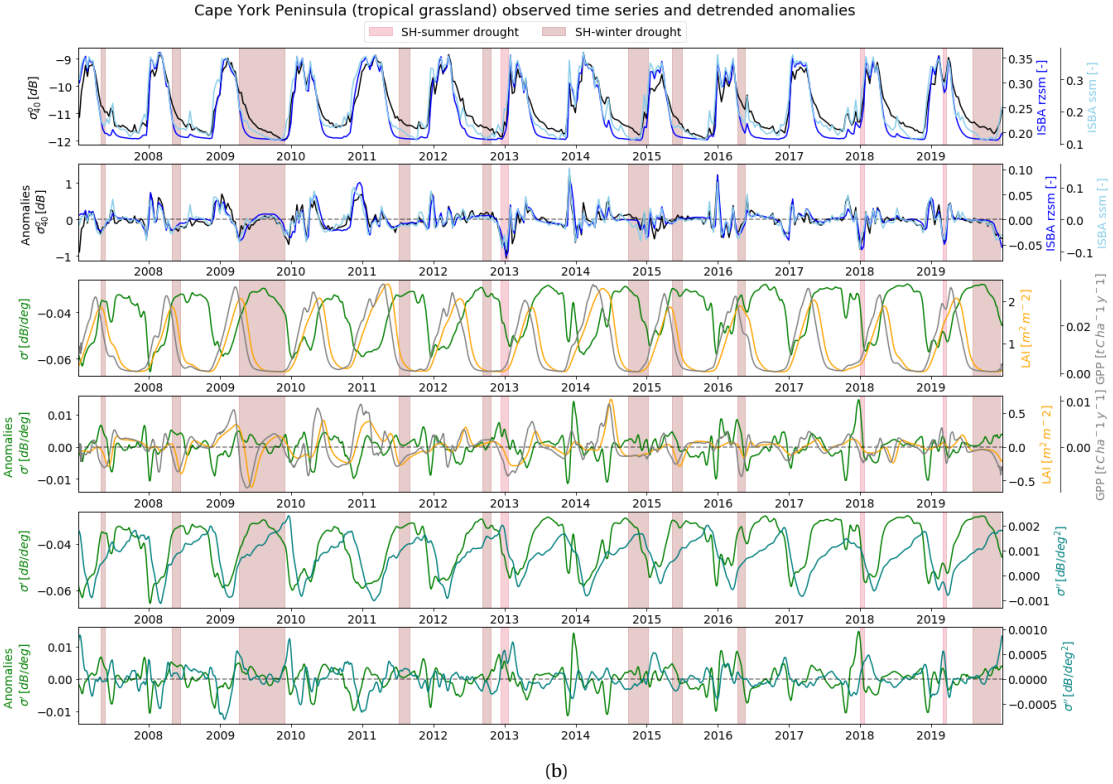

(b)

Figure D.5: Cape York Peninsula (tropical grasslands) time series with the long term trend removed from the anomalies and added to the seasonal cycle

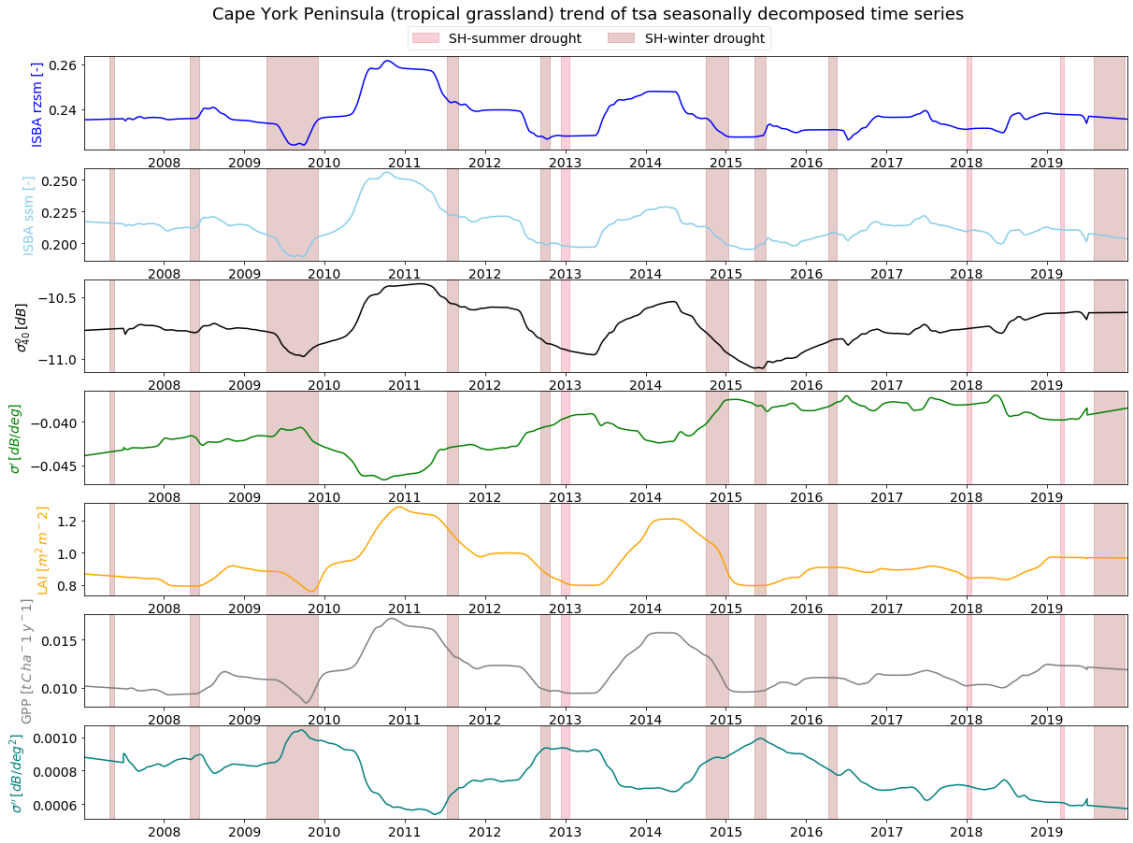

Figure D.6: Cape York Peninsula (tropical grasslands) long term trend

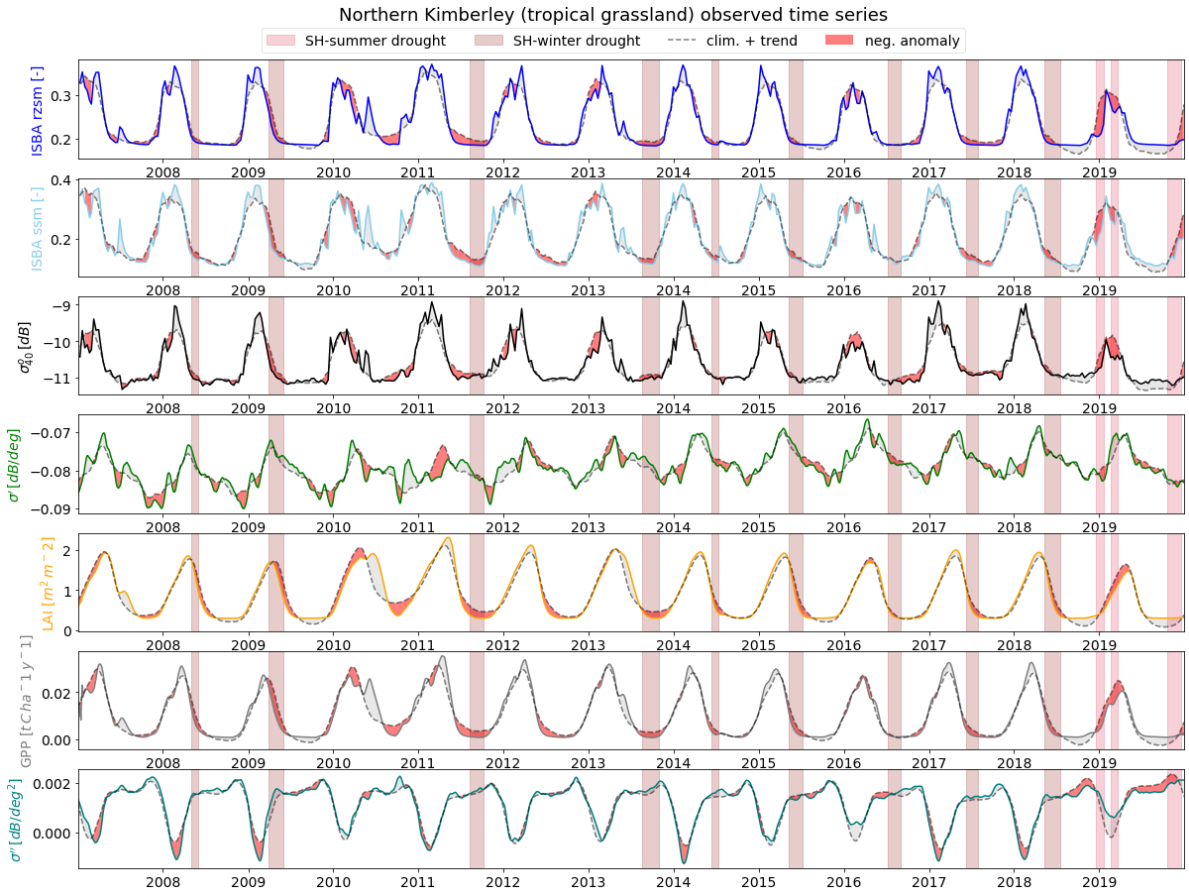

(a)

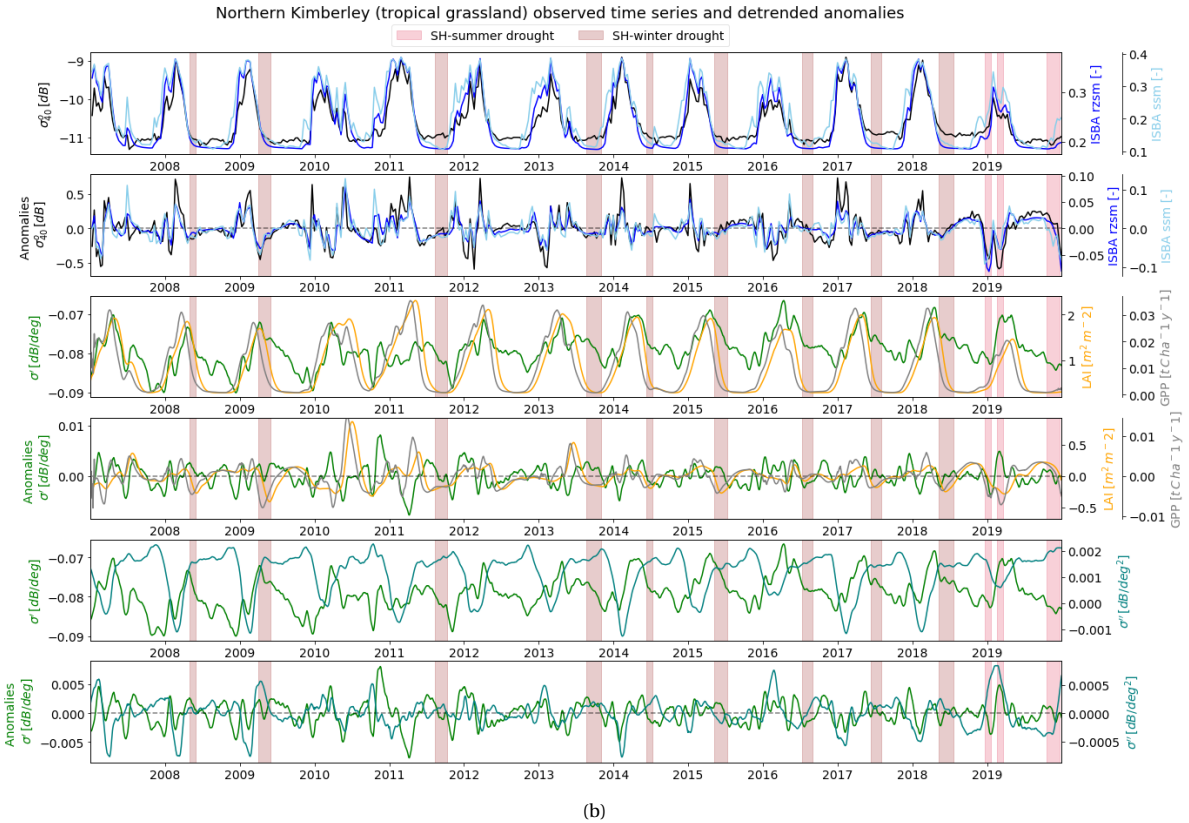

(b)

Figure D.7: Northern Kimberley (tropical grasslands) time series with the long term trend removed from the anomalies and added to the seasonal cycle

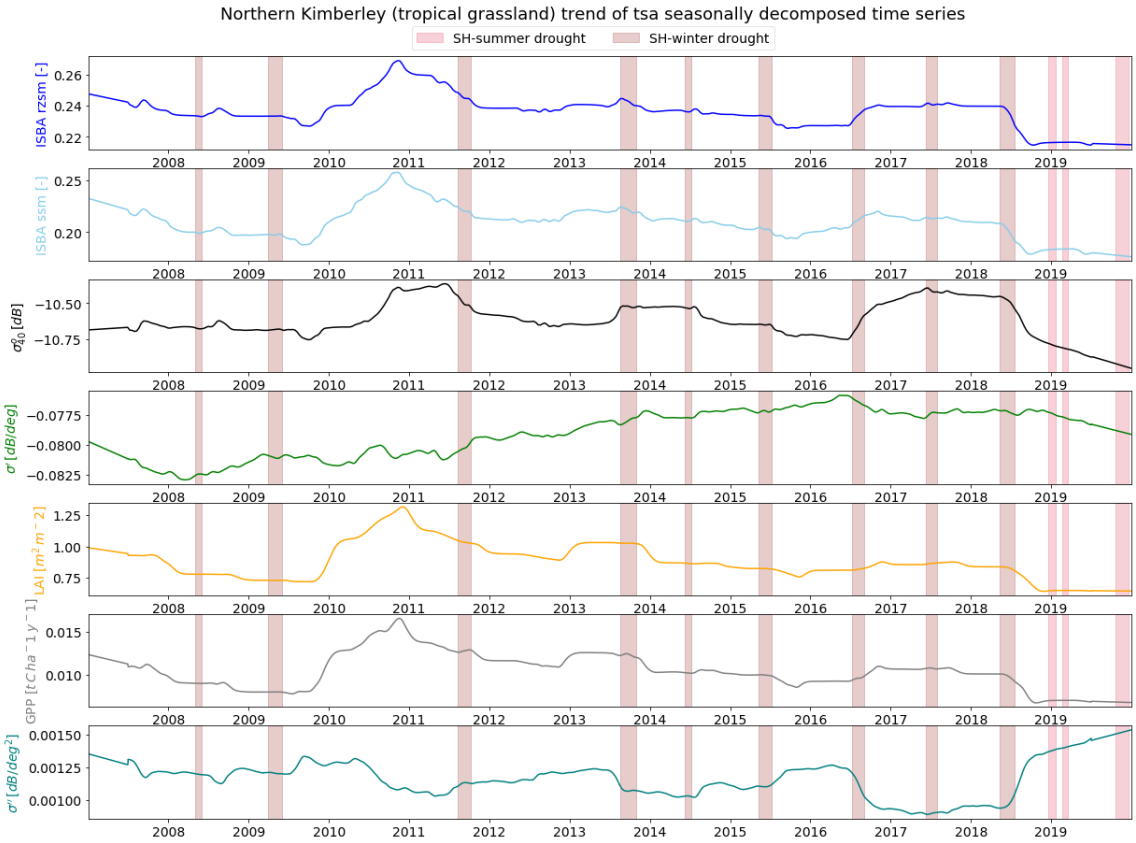

Figure D.8: Northern Kimberley (tropical grasslands) long term trend

Bare soil

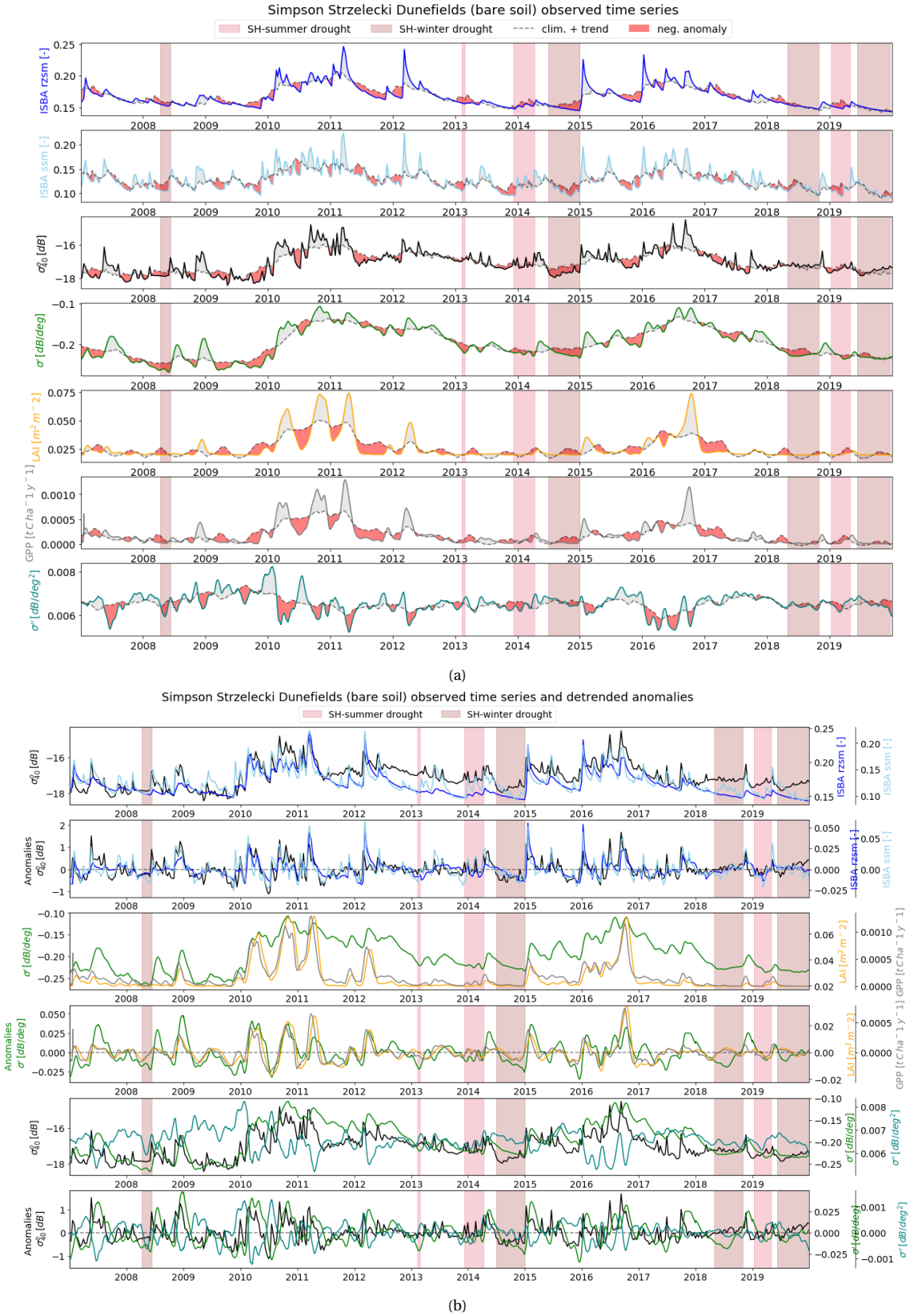

Figure D.9: Simpson Strzelecki Dunefields (bare soil) time series with the long term trend removed from the anomalies and added to the seasonal cycle

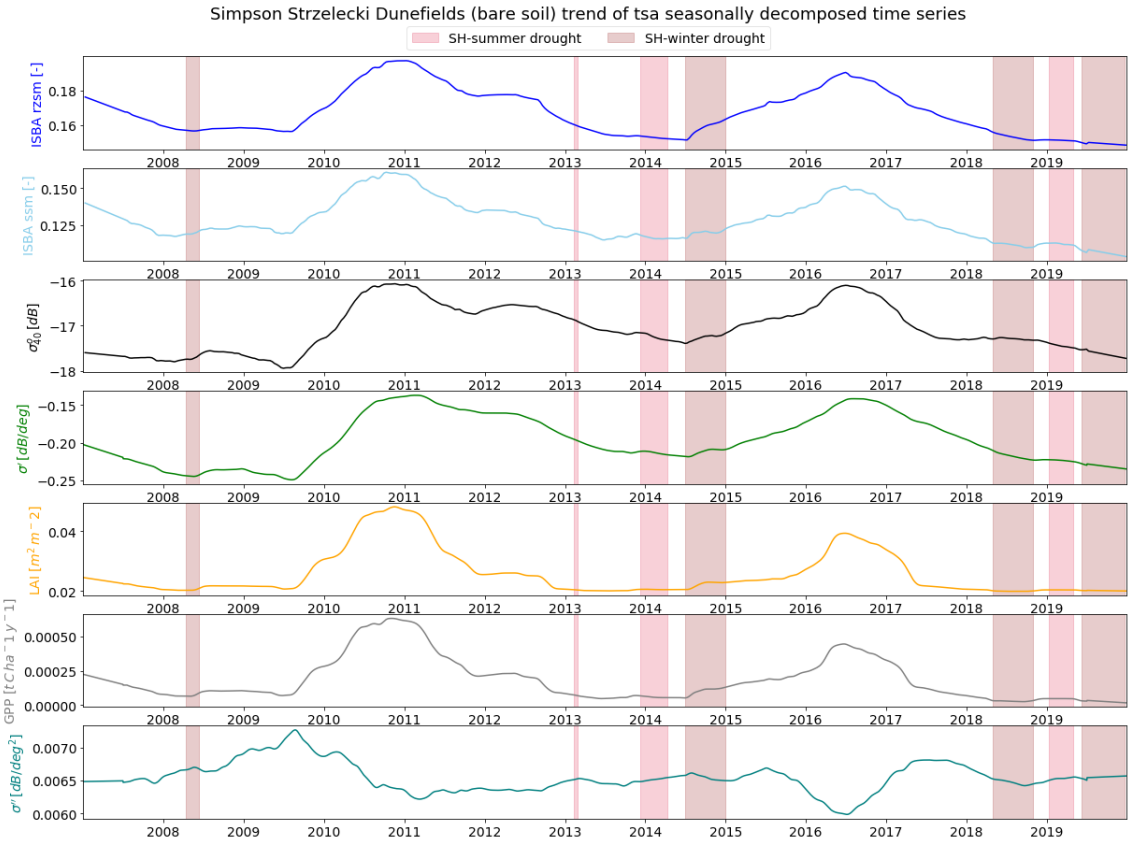

Figure D.10: Simpson Strzelecki Dunefields (bare soil) long term trend

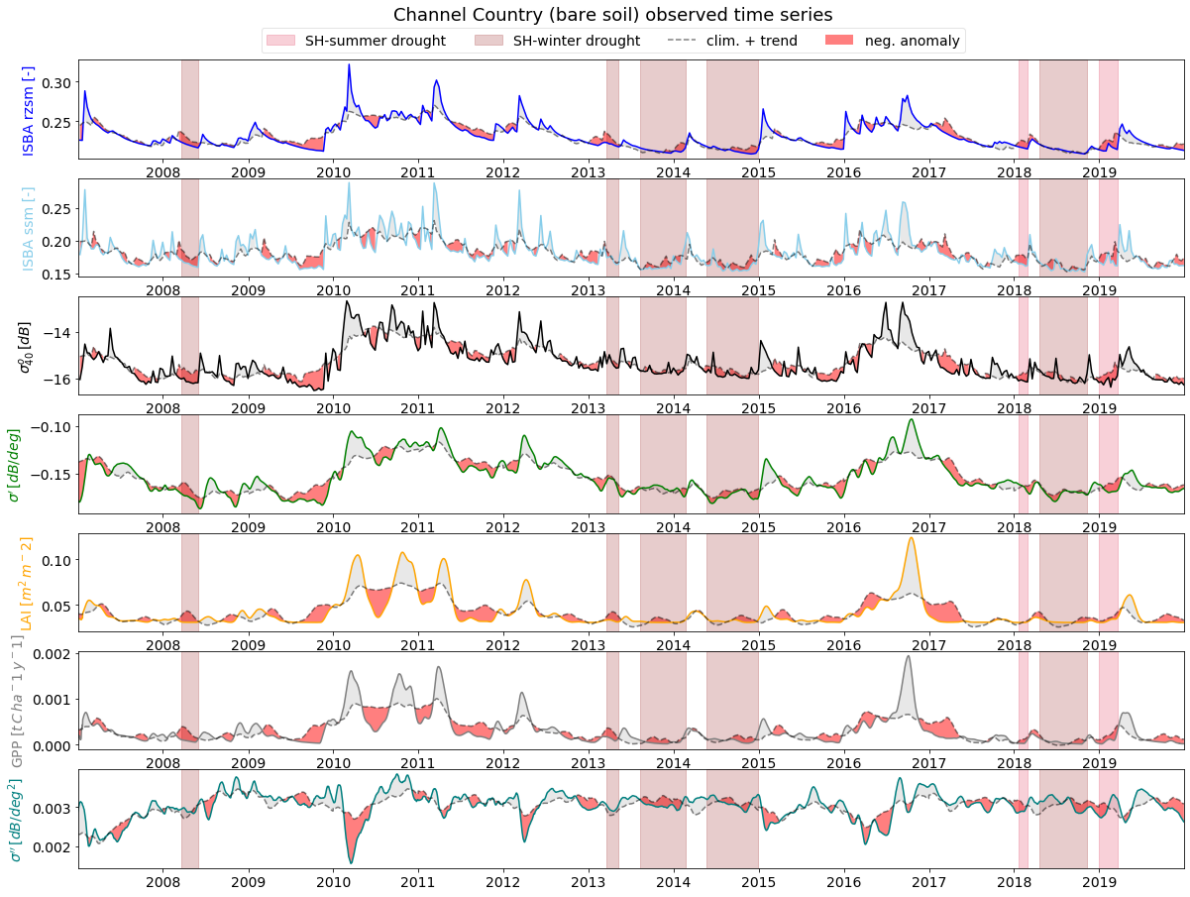

(a)

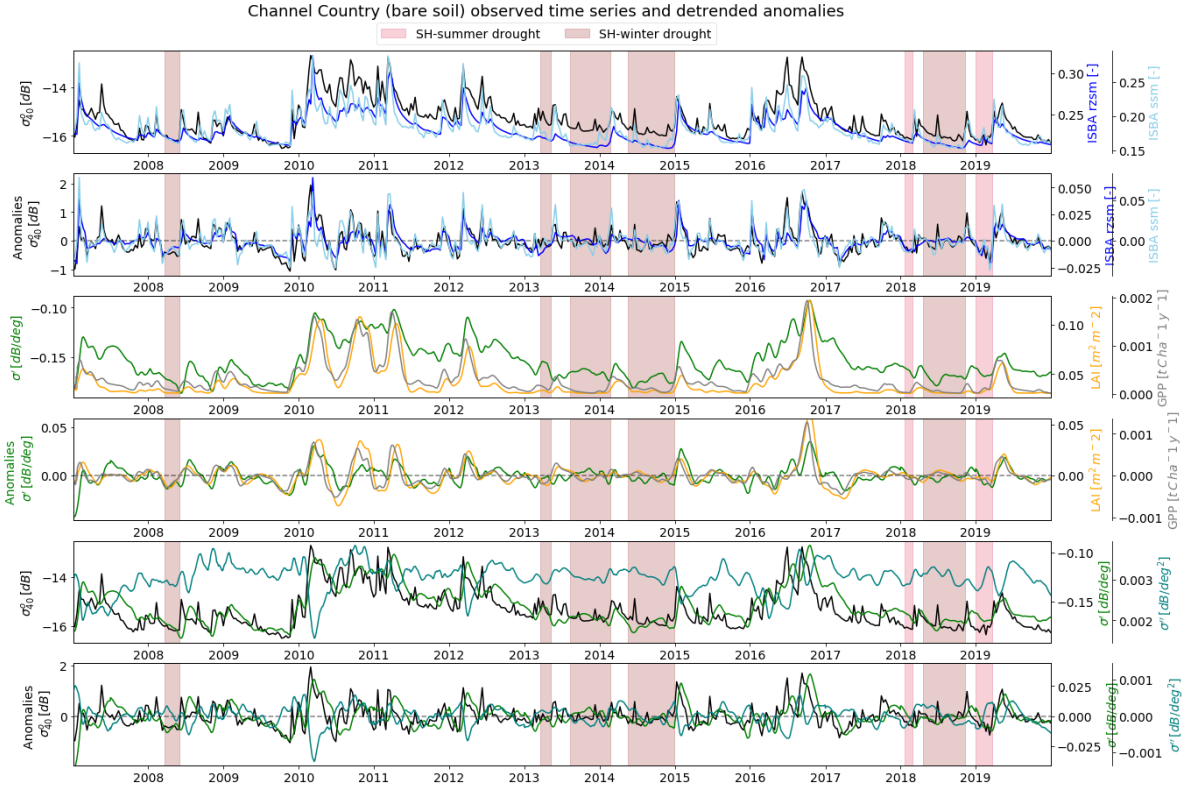

(b)

Figure D.11: Channel Country (bare soil) time series with the long term trend removed from the anomalies and added to the seasonal cycle

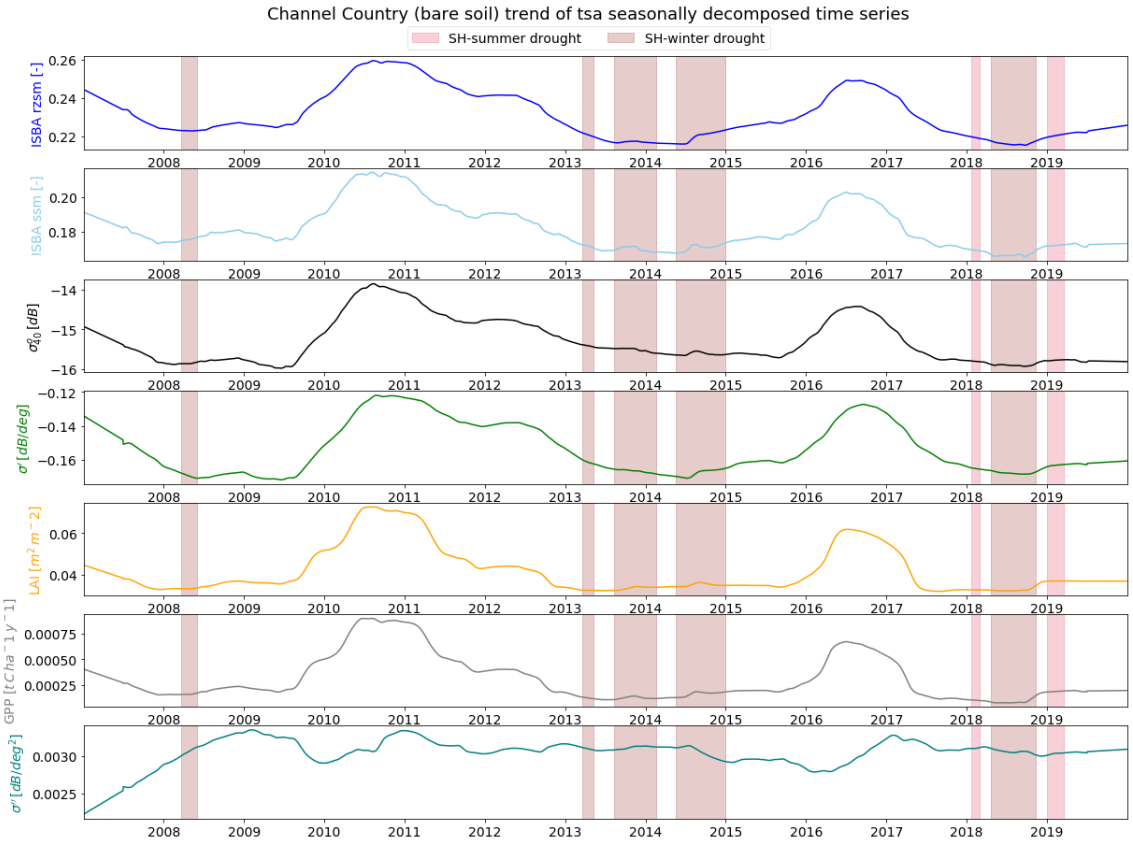

Figure D.12: Channel Country (bare soil) long term trend